

UNIVERSIDADE ESTADUAL DE MARINGÁ
CENTRO DE CIÊNCIAS BIOLÓGICAS
PROGRAMA DE PÓS-GRADUAÇÃO EM CIÊNCIAS BIOLÓGICAS
ÁREA DE CONCENTRAÇÃO EM BIOLOGIA CELULAR E MOLECULAR

RENAN FALCIONI

**Effects of light on plant growth and development and its spectral signature
contribution to leaf optical properties**

MARINGÁ

2020

RENAN FALCIONI

**Effects of light on plant growth and development and its spectral signature
contribution to leaf optical properties**

Tese apresentada ao Programa de Pós-Graduação em Ciências Biológicas (área de concentração – Biologia Celular e Molecular), da Universidade Estadual de Maringá para a obtenção do grau de Doutor em Ciências Biológicas – Biologia Celular e Molecular.

Orientador: Prof. Dr. Wanderley Dantas dos Santos

Coorientador: Prof. Dr. Werner Camargos Antunes

Maringá

2020

Dados Internacionais de Catalogação-na-Publicação (CIP)
(Biblioteca Central - UEM, Maringá - PR, Brasil)

F178e

Falcioni, Renan

Effects of light on plant growth and development and its spectral signature contribution to leaf optical properties / Renan Falcioni. -- Maringá, PR, 2020.
82 f.: il. color., figs., tabs.

Orientador: Prof. Dr. Wanderley Dantas dos Santos.

Coorientador: Prof. Dr. Werner Camargos Antunes.

Tese (Doutorado) - Universidade Estadual de Maringá, Centro de Ciências Biológicas, Departamento de Biologia, Programa de Pós-Graduação em Ciências Biológicas (Biologia Celular), 2020.

1. Plantas - Desenvolvimento e crescimento. 2. Propriedades ópticas foliares. 3. Microfibrilas. 4. Qualidade da luz. I. Santos, Wanderley Dantas dos, orient. II. Antunes, Werner Camargos, coorient. III. Universidade Estadual de Maringá. Centro de Ciências Biológicas. Departamento de Biologia. Programa de Pós-Graduação em Ciências Biológicas (Biologia Celular). IV. Título.

CDD 23.ed. 581.3

RENAN FALCIONI

**Effects of light on plant growth and development and its spectral signature
contribution to leaf optical properties**

Tese apresentada ao Programa de Pós-Graduação em Ciências Biológicas (área de concentração – Biologia Celular e Molecular), da Universidade Estadual de Maringá para a obtenção do grau de Doutor em Ciências Biológicas – Biologia Celular e Molecular.

Aprovado em: 16 / 07 / 2020

BANCA EXAMINADORA

Prof. Dr. Max Jean de Ornelas Toledo
Presidente da Banca – PBC/UEM
Universidade Estadual de Maringá

Prof. Dr. Halley Caixeta de Oliveira
Membro – BAV/UEL
Universidade Estadual de Londrina

Prof. Dr. Luiz Antônio de Souza
Membro – PGB/UEM
Universidade Estadual de Maringá

Prof. Dr. Carlos Moacir Bonato
Membro – DBI/UEM
Universidade Estadual de Maringá

Prof. Dr. Marcos Rafael Nanni
Membro – DAG/UEM
Universidade Estadual de Maringá

Local da Defesa: Remoto – Google–Meet – na data de 16 de Julho de 2020

BIOGRAPHY

RENAN FALCIONI, son of Sidnei Falcioni and Rosangela Maria Batista Falcioni, was born in Maringá, Paraná, Brazil in November 22th of 1991. He was undergraduated in Biological Sciences (Licenciate and Bachelor's degree) by State University of Maringá. On 2016 started his second undergraduated in Agronomy. On 2016 he obtained his *Specialist* degree in Plant Biology by Cândido Mendes University. On 2017 he obtained his *Master Scientiae* degree in Agronomy (Crop Production) by State University of Maringá. On 2017 he started his doctoral studies in Biological Science (Cellular and Molecular Biology) program also at State University of Maringá. In July of 2020 was finished some works being here show.

"If it wasn't for your love

Don't know where I'd be

Don't know what I'd do"

Forevermore – Whitesnake

DEDICATION

Rosangela, Sidnei e Thaise.
Em meus pensamentos e eternamente
no meu coração!!!

Dedico.

ACKNOWLEDGMENTS

Agradeço a Deus, por sempre abrir tantas portas quanto forem necessárias.

Aos meus Pais, Sidnei Falcioni e Rosangela Maria Batista Falcioni, por todo amor, apoio e carinho. Sem vocês não chegaria até aqui!!!

Thaise Moriwaki, my partner, my friend, my dear.... My sweet darling dear!!! Forevermore...

A Universidade Estadual de Maringá e ao Programa de Pós-Graduação em Ciências Biológicas.

Ao Conselho Nacional de Desenvolvimento e Pesquisa (CNPq) pela bolsa concedida.

Aos distintos **Professores**, dessa Universidade, que sempre propiciaram orientações, aconselhamentos, ensinamentos e acima de tudo à confiança depositada, muitas vezes sem esperar nada em contrapartida.

Aos **Professores**, **Colaboradores** e **Parceiros** de Instituições Nacionais e Internacionais, na qual acreditaram nas ideias e fizeram o possível para que estes e outros trabalhos fossem realizados, publicados, assim como aqueles que ainda estão por vir.

A todos que direta ou indiretamente contribuíram não somente para a realização deste trabalho, mas ao longo dos últimos 9 anos compartilharam o seu tempo, conhecimentos, experiências, histórias, laboratórios, parcerias, trocas de ideias, enfim... Seria injusto nomear alguns, sendo que muitos participaram, participam e agregaram experiências à minha vida.

Meu mais profundo agradecimento e carinho por todo o conhecimento, ensinamentos e experiências compartilhadas.

O meu respeito e admiração por todos vocês!!!

THANK YOU VERY MUCH!!!

RESUMO

Entre os fatores ambientais a luz exerce papel fundamental no crescimento e desenvolvimento das plantas. As vias de sinalização do crescimento e diferenciação celular, crosstalk com metabolismo hormonal, up e down-regulation em genes específicos que modulam, dentre outras modificações, em nível celular e molecular até o fenótipo das plantas, são intrínsecos dessa fonte de energia, fundamental para os processos bioquímicos e fisiológicos vegetais. Diante do breve exposto, demonstramos aqui, em nossa linha de pesquisa, as contribuições da luz na cascata de sinalização das plantas e interação do espectro eletromagnético. Os trabalhos aqui apresentados, demonstram parte das pesquisas desenvolvidas com ênfase nos efeitos da luz na regulação do crescimento e desenvolvimento das plantas e sobre as alterações das propriedades ópticas foliares. Integrando diferentes métodos de biologia celular e molecular, técnicas de microscopia de luz, fluorescência e eletrônica de varredura e transmissão, dentre outras abordagens multi-disciplinares, essa tese foi subdividida em três capítulos, em formato de artigos científicos publicados em revistas *peer-review*.

O Capítulo I “*Increased Gibberellins and Light Levels Promotes Cell Wall Thickness and Enhance Lignin Deposition in Xylem Fibers*” publicado na *Frontiers in Plant Science*, fator de impacto 4.106 (JCR-2019) e Qualis-Capes A1, demonstramos como a sinalização decorrentes da variação da intensidade luminosa e disponibilidade de ácido giberélico (GA₃), em promover alterações na espessura e deposição de lignina nas paredes das fibras do xilema em plantas de tabaco. Além disso, detectada a existência de um mecanismo de resposta exclusivo à luz, que as GAs não conseguem substituir.

O Capítulo II “*Cell wall structure and composition is affected by light quality in tomato seedlings*” publicado na *Journal of Photochemistry and Photobiology: B-Biology*, fator de impacto 4.067 (JCR-2019) e Qualis-Capes A1, evidenciamos alterações promovidas na estrutura e composição da parede celular, em hipocótilos de tomate crescidos em diferentes qualidades de luz. Alterações substanciais da reorganização da parede celular primária, das microfibrilas de celulose e na cascata de sinalização hormonal regulados pela qualidade da luz. Demonstramos uma profusa rede regulatória, envolvendo qualidade de luz e hormônios, sobre as microfibrilas de celulose.

O Capítulo III “High resolution leaf spectral signature as a tool for foliar pigment estimation displaying potential for species differentiation” publicado na *Journal of Plant Physiology*, fator de impacto 2.825 (JCR-2019) e Qualis-Capes A1, analisamos, propomos e discutimos como variações de classes e conteúdo de diferentes pigmentos foliares, bem como componentes estruturais e ultraestruturais, promovem alterações substanciais da interação da luz no perfil óptico foliar. Concluimos que a interação de luz com os pigmentos e estruturas foliares, se mostram um recurso valioso no estudos das plantas.

PALAVRAS-CHAVE: Crescimento e desenvolvimento, microfibrilas, qualidade da luz, propriedades ópticas foliares

ABSTRACT

Among environmental factors, light plays a vital role in plant growth and development. Cell growth and development signaling pathways, crosstalk with hormonal metabolism and up and down-regulation in specific genes that modulate, among other changes, from the cellular and molecular level to the plant phenotype, are intrinsic to this energy source, essential for biochemistry and physiology plant processes. In this context, we demonstrate light contributions to plant cascade signaling and interaction with the electromagnetic light spectrum in our line of research. The investigation presented herein demonstrates part of the research developed with emphasis on the effects of light on plant growth and development regulation and on leaf optical property alterations. Integrating different cellular and molecular biology methods and light microscopy, fluorescence and scanning and transmission electron microscopy techniques, among other multi-disciplinary approaches, this thesis was subdivided into three chapters, in the form of scientific articles published in peer-review journals.

In Chapter I “Increased Gibberellins and Light Levels Promotes Cell Wall Thickness and Enhance Lignin Deposition in Xylem Fibers”, published in *Frontiers in Plant Science*, impact factor 4.106 (JCR-2019) and Qualis-Capes A1, we demonstrate how the signaling arising from luminous intensity variation and gibberellic acid (GA₃) availability promotes changes in lignin thickness and deposition in the xylem fiber walls of tobacco plants.

In Chapter II “Cell wall structure and composition is affected by light quality in tomato Seedlings”, published in the *Journal of Photochemistry and Photobiology: B-Biology*, impact factor 4.067 (JCR-2019) and Qualis-Capes A1, we highlight changes promoted in cell wall structure and composition in tomato hypocotyls grown under different light qualities. Substantial alterations in primary cell wall reorganization, the cellulose microfibrils and in the light-regulated hormonal signaling cascade were observed.

In Chapter III “High resolution leaf spectral signature as a tool for foliar pigment estimation displaying potential for species differentiation, published in the *Journal of Plant Physiology*, impact factor 2.825 (JCR-2019) and Qualis-Capes A1, we analyse,

propose and discuss how variations in different leaf pigment classes and content, as well as structural and ultrastructural components, promote substantial changes between light interactions and leaf optical profiles.

KEYWORDS: Growth and development, light quality, leaf optical properties, microfibril

CHAPTER 1

**Increased Gibberellins and Light Levels Promotes Cell Wall Thickness
and Enhance Lignin Deposition in Xylem Fibers**



Increased Gibberellins and Light Levels Promotes Cell Wall Thickness and Enhance Lignin Deposition in Xylem Fibers

Renan Falcioni^{1,2*}, Thaise Moriwaki¹, Dyoni Matias de Oliveira², Giovana Castelani Andreotti¹, Luiz Antônio de Souza³, Wanderley Dantas dos Santos², Carlos Moacir Bonato¹ and Werner Camargos Antunes^{1,2*}

¹ Laboratório de Ecofisiologia Vegetal, Departamento de Biologia, Universidade Estadual de Maringá, Maringá, Brazil,

² Laboratório de Bioquímica de Plantas, Departamento de Bioquímica, Universidade Estadual de Maringá, Maringá, Brazil,

³ Laboratório de Histotécnica e Anatomia Vegetal, Universidade Estadual de Maringá, Maringá, Brazil

OPEN ACCESS

Edited by:

Peter Ulvskov,
University of Copenhagen, Denmark

Reviewed by:

Nobutaka Mitsuda,
National Institute of Advanced
Industrial Science and Technology
(AIST), Japan
Shinjiro Ogita,
Prefectural University of Hiroshima,
Japan

*Correspondence:

Renan Falcioni
renanfalcioni@gmail.com
Werner Camargos Antunes
wcantunes@uem.br;
wcantunes@yahoo.com

Specialty section:

This article was submitted to
Plant Physiology,
a section of the journal
Frontiers in Plant Science

Received: 30 May 2018

Accepted: 03 September 2018

Published: 20 September 2018

Citation:

Falcioni R, Moriwaki T, Oliveira DM, Andreotti GC, Souza LA, Santos WD, Bonato CM and Antunes WC (2018) Increased Gibberellins and Light Levels Promotes Cell Wall Thickness and Enhance Lignin Deposition in Xylem Fibers. *Front. Plant Sci.* 9:1391. doi: 10.3389/fpls.2018.01391

Light intensity and hormones (gibberellins; GAs) alter plant growth and development. A fine regulation triggered by light and GAs induces changes in stem cell walls (CW). Cross-talk between light-stimulated and GAs-induced processes as well as the phenolic compounds metabolism leads to modifications in lignin formation and deposition on cell walls. How these factors (light and GAs) promote changes in lignin content and composition. In addition, structural changes were evaluated in the stem anatomy of tobacco plants. GA₃ was sprayed onto the leaves and paclobutrazol (PAC), a GA biosynthesis inhibitor, via soil, at different irradiance levels. Fluorescence microscopy techniques were applied to detect lignin, and electron microscopy (SEM and TEM) was used to obtain details on cell wall structure. Furthermore, determination of total lignin and monomer contents were analyzed. Both light and GAs induces increased lignin content and CW thickening as well as greater number of fiber-like cells but not tracheary elements. The assays demonstrate that light exerts a role in lignification under GA₃ supplementation. In addition, the existence of an exclusive response mechanism to light was detected, that GAs are not able to replace.

Keywords: lignin monomers, stem, hormones, cambial activity, cell wall

INTRODUCTION

Changes in plant habitat luminosity are associated to high phenotypic plasticity (Valladares et al., 2000; Percy, 2007; Pugnaire and Valladares, 2007; Sarlikioti et al., 2011; Niinemets et al., 2015), especially in relation to stem development (Percy, 2007; Kurepin and Pharis, 2014) and either endogenous gibberellin (GAs) levels or the signaling cascade triggered by this hormone (Alabadi et al., 2008; Lau and Deng, 2010).

Plants grown in high irradiance environments present reduced stem length and shorter internodes compared to shade-grown plants (Pugnaire and Valladares, 2007; Lau and Deng, 2010; Ribeiro et al., 2012; Wang and Benning, 2012; Kurepin and Pharis, 2014; de Wit et al., 2016). They also present higher chlorophyll and carotenoid concentrations per unit of leaf area (Percy, 2007; Pugnaire and Valladares, 2007; Lambers et al., 2008), thicker leaves, more elongated

palisade parenchyma cells (Lambers and Poorter, 2004; Poorter et al., 2009) and increased tissue lignification (Onoda et al., 2017), among other biochemical and anatomical alterations that provide acclimatization to high irradiance conditions (Givnish, 1988; Kurepin et al., 2007; Pugnaire and Valladares, 2007). On the other hand, plants grown in low irradiance environment display shade avoidance syndrome with etiolated phenotype and lower lignin concentrations per biomass unit (Hoffmann and Poorter, 2002; Kurepin et al., 2007; Pugnaire and Valladares, 2007; Lau and Deng, 2010; Kurepin and Pharis, 2014; Hedden and Sponsel, 2015).

Among the various plant hormones synthesized by plants, GAs belong to a group of tetracyclic diterpenoids that promote biochemical, physiological and anatomical plant changes (Biemelt et al., 2004; Yamaguchi, 2008; Dayan et al., 2012; Hedden and Thomas, 2016). Three major enzymes that regulate GAs homeostasis and biosynthesis are known, namely GA 20-oxidase (GA20ox) and GA 3-oxidase (GA3ox), which catalyze the early phases of bioactive GA biosynthesis, and GA 2-oxidase (GA2ox), involved in the deactivation of bioactive GAs (Yamaguchi, 2008; Martins, 2013; Hedden and Thomas, 2016). A fine metabolic regulation in response to light causes GA homeostasis to be controlled by induction of GA2ox genes, with negative feedback, as well as the GA20ox and GA3ox genes. GAs, in addition to several well-known responses (Ueguchi-Tanaka et al., 2007; Yamaguchi, 2008; Dayan et al., 2010; Aloni, 2013; Bai et al., 2014) also play a regulatory role concerning terpenes and phenolic compounds, particularly lignin (Hedden and Phillips, 2000; Olszewski et al., 2002; Biemelt et al., 2004; Davies, 2010; Ribeiro et al., 2012; Kurepin and Pharis, 2014; Ye et al., 2015; Hedden and Thomas, 2016). Together, light availability and GAs influence plant cell development and cell wall composition.

The changes observed at structural and ultrastructural stem levels is an end point of sequence of events that initiate with plant perception of surrounding environment, signaling amplifying, changes in gene expression and downstream proteomic/metabolic profiling modifications and concluding with cell developmental alterations. Changes in cell wall formation, structure, and composition (e.g., lignin deposition) are associated with intense cross-talk between light perception pathways (Onoda et al., 2017) triggered by photoreceptors, such as cryptochromes (Ahmad and Wani, 2014) and phytochromes (Casal, 2012). Furthermore, responses associated to hormonal signaling (Kurepin et al., 2007; Kurepin and Pharis, 2014), regulation of gene expression patterns, and cellular changes that result in metabolic changes (Yamaguchi, 2008; Ye et al., 2015; Hedden and Thomas, 2016; Zhang et al., 2018a), cytoskeleton structure (Bashline et al., 2014; Liu et al., 2016) and cell wall architecture (Zheng et al., 2017) are intertwined, creating a complex scenario of factors that regulate cell wall structure and composition.

Gibberellins also induce cellulose synthesis by promoting the release of secondary cell wall protein regulators (NAC SECONDARY WALL THICKENING PROMOTING FACTOR) (NST1–3) via DELLA repression cascade, which, in principle, could possibly boost and correlate with lignin deposition and increased lignin content (Zhao, 2016). Thus, it is suggested that

a “normal” cellulose deposition pattern may be necessary for correct assembly and lignin deposition in primary, secondary and tertiary cell walls (Burk and Ye, 2002; Bai et al., 2014; Ye et al., 2015; Liu et al., 2016; Zhao, 2016; Zhang et al., 2018a).

Increases in GA contents stimulate lignin deposition under high irradiance conditions (Wada et al., 2005; Kurepin et al., 2006; Moura et al., 2010; Bai et al., 2014; Yang et al., 2015; Hedden and Thomas, 2016; Li et al., 2017; Zhang et al., 2018a). On the other hand, GA levels are higher under shaded conditions (Kurepin et al., 2006; Kurepin and Pharis, 2014), which in turn triggers cell stretching and etiolation, with lower lignin deposition over all secondary xylem (SX) fiber-like cells. Thus, lignification tends to be proportional to the amount of incident light, i.e., at lower luminous intensity, higher GA levels (Kurepin et al., 2006; Kurepin and Pharis, 2014) and lower lignin contents (and vice versa) are observed. This phenomenon indicates several knowledge gaps regarding individual light availability and GA responses to lignin deposition in plants, suggesting a cross-talk between light effects and GA effects on lignin metabolism. Above all, little is known on the interaction between GA levels and light on xylem fiber differentiation and lignin deposition on the cell wall (Dayan et al., 2012) or on the composition of lignin monomers (Wuddineh et al., 2015; Zheng et al., 2017) in response to light.

In this study, the hypothesis that light and GAs act independently in promoting tobacco plant structural xylem and cell wall modifications, lignin accumulation and stem monomer composition was tested. To do so, GA₃ was supplemented via foliar spraying, and a GA biosynthesis inhibitor, paclobutrazol (PAC), an ent-kauren oxidase enzyme (KO; EC 1.14.13.78) was applied via soil (Ribeiro et al., 2012; Guo et al., 2015) in order to investigate cell wall, lignin and anatomical changes in tobacco plants under the influence of different GA levels in high and low irradiance environments.

MATERIALS AND METHODS

Growth Conditions and Experimental Design

Nicotiana tabacum L. (cv. HAV 425) plants were cultivated in greenhouse conditions under full (100% sunlight) and low (low light – 8.5% of sunlight) irradiance levels. After initial growth in 5 L pots, one group was transferred to lower irradiance conditions inside the greenhouse, maintained by using two overlapping neutral nylon nets (80 and 50% shading) covering all plants until ground level reached 91.5% shading. No spectral quality differences were observed in this case, only decreased light intensity (data not shown). Gibberellic acid (GA₃) at different concentrations was sprayed for 5 times every 2 days on leaves, while paclobutrazol (PAC) was applied to the soil. All plants grew for 20 days under these conditions. Reverse osmosis water was sprayed onto the controls (Cont), 10 μM GA₃ (GA10), 100 μM GA₃ (GA100) and PAC 50 mg L⁻¹ (PAC), following the protocol reported by Falcioni et al. (2017), as well as in combined GA₃ 10 μM + PAC (GA10P) and GA₃ 100 μM + PAC (GA100P) treatments, totaling 12

treatments with 6 repetitions each. Representative plants are displayed in **Supplementary Figure S1**. The complete growth profile of these plants was evaluated following (Falcioni et al., 2018). Chloroplastidic pigments were quantified as reported by Lichtenthaler (1987).

Epifluorescence Microscopy Analysis

Stem segments ($\sim 2 \text{ cm}^3$) were fixed in a modified Karnovsky solution containing 2.5% glutaraldehyde and 2% paraformaldehyde in 0.05 M phosphate buffer, pH 7.2 (Karnovsky, 1965) and stored at 4°C until processing. The stem samples were then washed in distilled water for 5 min, rehydrated and placed in glass containers. Subsequently, a 25% (w/v) aqueous polyethylene glycol 6000 (PEG 6000) solution was added to the samples and the material placed in an oven at 60°C. When half of the initial solution volume was reached, 75% (w/v), the PEG 6000 solution was again added. When the solution reached half the total volume again, the fragments were incorporated to a 90% PEG 6000 and gum arabic solution (Ferreira et al., 2017). The stem fragments were placed in cassettes mounted on a wood base with adhesive tape and immediately frozen at -16°C . Samples were then unformed, cut using a hand-rotated microtome (thickness 25–35 μm) and plated with water between 35 and 50°C (Souza et al., 2016; Ferreira et al., 2017). Staining was performed using astra blue and safranin/basic fuchsin 1% (w/v) (Kraus et al., 1998) and slides were then mounted between the slide and a cover slip with 50% glycerin. Digital images were obtained on an EKB-2F epifluorescence microscope (Eikonal Ind., São Paulo, Brazil) at the violet excitation wavelength (400 nm) (Ferreira et al., 2017). The images were processed with the Bel Eurisko software (Bel Photonics, Piracicaba, Brazil) and analyzed qualitatively and quantitatively for changes in vascular cylinder morphology with the Image-Pro-Plus® v.4.5 software. All analyses were performed using cross sections of stem focusing on vascular cylinder in which composed by tracheary elements (tracheids and vessel elements), fibers (fiber-tracheids and libriform fibers) and parenchyma cells. In addition, some cell of primary xylem (ex. Protoxylem) were observed in slides. The term fiber-like cells refer to the all types of fiber cells on the axial system, with exception of the high differentiated vessel elements (Evert and Eichhorn, 2006).

Fiber Microscopy Analysis

The acid maceration technique was employed for the quantitative fiber analysis, according to Johansen (1940) and Kraus and Arduin (1996). Briefly, the stem fragments fixed in Karnovsky's solution (Karnovsky, 1965) were placed in 20 mL glass vials containing a 1:1 acidic solution containing 10% (v/v) chromic acid and 10% (v/v) nitric acid (Jeffrey's solution) for 30 min and then washed in water (Johansen, 1940). An aliquot of the cell contents stained with safranin 1% (v/v) was arranged between the slide and the cover slip (Souza et al., 2016). The digital images were obtained on a microscope (Leica)® coupled to a computer running the Leica Application Suite® software. Measurements were performed using the Image-Pro-Plus® v.4.5 software.

Stem Scanning Electron Microscopy

For the vascular system basal region ultrastructure analysis of tobacco plant stems, approximately 1 cm^3 stem segments obtained on the 20th treatment day were fixed in the previously mentioned modified Karnovsky's solution (Karnovsky, 1965; Kiernan, 2000). The samples were subsequently infiltrated at different concentrations with a cryoprotectant (glycerol 10, 20, and 30%) until sinking. The fragments were then immersed in liquid nitrogen and fractured with a scalpel blade, the fragments were placed in a container with distilled water and dehydrated using an increasing series of acetone (30, 50, 70, and 90%) for 1 h and finally 3x (100%) for 10 min. Critical drying was carried out on a CPD-030 Bal-Tec critical point dryer (Bal-Tec AG, Balzers, Liechtenstein). The samples were assembled into stubs and metallized with gold on a MED010 Balzers evaporator (Bal-Tec AG, Balzers, Liechtenstein). Finally, the samples were observed on a SS-550 Shimadzu scanning electron microscope (Shimadzu, Tokyo, Japan) and the digital images were obtained with the SS-550 software® coupled to the microscope and analyzed qualitatively.

Transmission Electron Microscopy

For the transmission electron microscopy analysis, similar stem samples were fixed in modified Karnovsky's solution (Karnovsky, 1965) with 2.5% glutaraldehyde and 2% paraformaldehyde in 0.05 M cacodylate buffer (pH 7.2) and post-fixed for 1 h with 1% osmium tetroxide in 0.05 M cacodylate buffer. The samples were then contrasted in bloc with 0.5% uranyl acetate overnight, dehydrated in an increasing acetone concentration series [30, 50, 70, 80, 90, and 100% (three times)], infiltrated and then polymerized into Spurr low viscosity epoxy resin. Sections (70 nm thick, Diamond Knife) were obtained using an ultramicrotome (MTX Powertome X, Boeckeler Instruments RMC Products) and contrasted with 3% uranyl acetate and lead citrate. Analyses were performed using a transmission electron microscope (JEOL JEM-1400, Leica Microsystems Inc., Buffalo Grove, IL, United States) equipped with a digital camera at 80 kV. All reagents were of high standard electron microscopy grade and purchased from Sigma (St. Louis, MO, United States) or EMS (Electron Microscopy Sciences, 1560 Industry Road Hatfield, PA, United States).

Lignin Quantification and Monomer Composition

Tobacco dry stem powder (150 mg) was washed sequentially as follows: four times with 7 mL of 0.05 M potassium phosphate buffer pH 7.0, four times with 1% (v/v) Triton X-100 in 0.05 M potassium phosphate, three times with 1 M NaCl in phosphate buffer, twice with deionized water, and twice with acetone. After each washing step, the suspensions were centrifuged for 5 min at $1,400 \times g$. Finally, the pellets were dried at 60°C for 24 h and cooled in a vacuum desiccator. The obtained dry matter was defined as the protein-free cell wall (PFCW) fraction (Moreira-Vilar et al., 2014).

Total lignin content was determined using the acetyl bromide (AcBr) method (Moreira-Vilar et al., 2014). The PFCW fraction (20 mg) was placed in a screwcap centrifuge tube containing

0.5 mL of a freshly prepared acetyl bromide solution (25% v/v acetyl bromide/glacial acetic acid) and incubated at 70°C for 30 min. After complete digestion, the samples were quickly ice-cooled and mixed with 0.9 mL of 2 M NaOH, 0.1 mL 5 M hydroxylamine-HCl and 6 mL glacial acetic acid for complete solubilization of the lignin extracts. After centrifugation (1,400 × g, 5 min), the supernatant absorbance were measured at 280 nm. A standard curve was generated with alkali lignin (Aldrich 37, 095-9) and the results were expressed as mg lignin g⁻¹ PFCW.

Lignin monomer composition was determined by alkaline nitrobenzene oxidation (Moreira-Vilar et al., 2014). This technique causes lignin degradation, forming *p*-hydroxybenzaldehyde from the H unit, vanillin from the G unit, and syringaldehyde from the S unit. PFCW aliquots (50 mg) was sealed in a Pyrex ampoule containing 1 mL of 2 M NaOH and 0.1 mL of nitrobenzene and heated to 170°C for 150 min, with occasional stirring. The samples were then cooled to room temperature, washed twice with chloroform, acidified to pH 3-4 with 5 M HCl and extracted twice with chloroform. The chloroform extracts were combined, dried, resuspended in 1 mL methanol and diluted in methanol/acetic acid 4% in water (20:80, v/v). Finally, the samples were filtered through a 0.45-μm disposable syringe filter and analyzed on a Shimadzu® Liquid Chromatograph equipped with a LC-10AD pump, a CBM-101 Communications Bus Module, a Rheodyne® injector and a SPD-10A UV-VIS detector. The compounds were separated on C18 column (150 mm × 4.6 mm, 5 μm; Supelco Discovery® HS) with an equivalent pre-column (10 × 4.6 mm). The mobile phase comprised methanol/acetic acid 4% (20:80, v/v) at a flow rate of 1.2 mL min⁻¹ in isocratic mode. Quantification of the monomer aldehyde products (*p*-hydroxybenzaldehyde, vanillin, and syringaldehyde) released by the nitrobenzene oxidation was performed at 290 nm using the corresponding standards. The results were expressed as mg monomer g⁻¹ PFCW.

Statistical Analyses

The quantitative data means were submitted to a One-Way ANOVA test for comparisons. Statistical significance was considered when $P < 0.05$ (Zar, 2010). Duncan's test was applied to compare GAs levels in a particular light level (high or low light) and Student's *t*-test was used to compare light levels in plants displaying similar GAs levels. In addition, Pearson's correlation test was also performed when applicable. All statistical analyses were carried out using the STATISTICA 10® software package (Statsoft, Tulsa, CA, United States). All graphs were prepared using the Sigma Plot 10.0® (Systat, San Jose, CA, United States) software package.

A principal component analysis (PCA) (Jolliffe, 2002) was performed in order to reduce data dimensionality and to provide more statistically stable tests than other forms of regression for the set of autocorrelated variables. The PCA sought to evaluate the individual variable contributions in order to explain lignin contents under different light and GA regimes. The primary growth analysis data collected 20th days after treatment, as well as the data derived from the primary growth analysis and subsequent mathematical relationships were used to process

the multivariate analysis. No vector rotation was performed. Only the first two main components were used for the other PCA-derived characterizations. Applying eigenvectors (linear correlation between a variable with a main component) and eigenvalues (square of the eigenvectors) allowed for statistical derivations concerning the magnitude of explanations of a particular variable (individually or groups) for accumulated lignin content and individual variable contribution. The score data estimated by the Principal Component 1 (PC1) and Principal Component 2 (PC2) were submitted to a bifactorial MANOVA and, if significant by the *F*-test ($P < 0.05$), were then submitted to a means comparison by Duncan's test or the Student *t*-test, considered significant at an error probability of less than 5%.

RESULTS

In general, morphological changes were observed in the vascular cylinder, particularly in xylem fibers-like cells, with lignin content variations under the influence of direct GA₃ and PAC applications, as well as in response to irradiance levels. Mitotic activity stimulation, with a greater number of xylem fibers-like cells in the cambial zone were found for both light and GA₃ stimulation. As expected, GA₃ supplementation induced increased internode length with similar number of leaves, except for PAC.

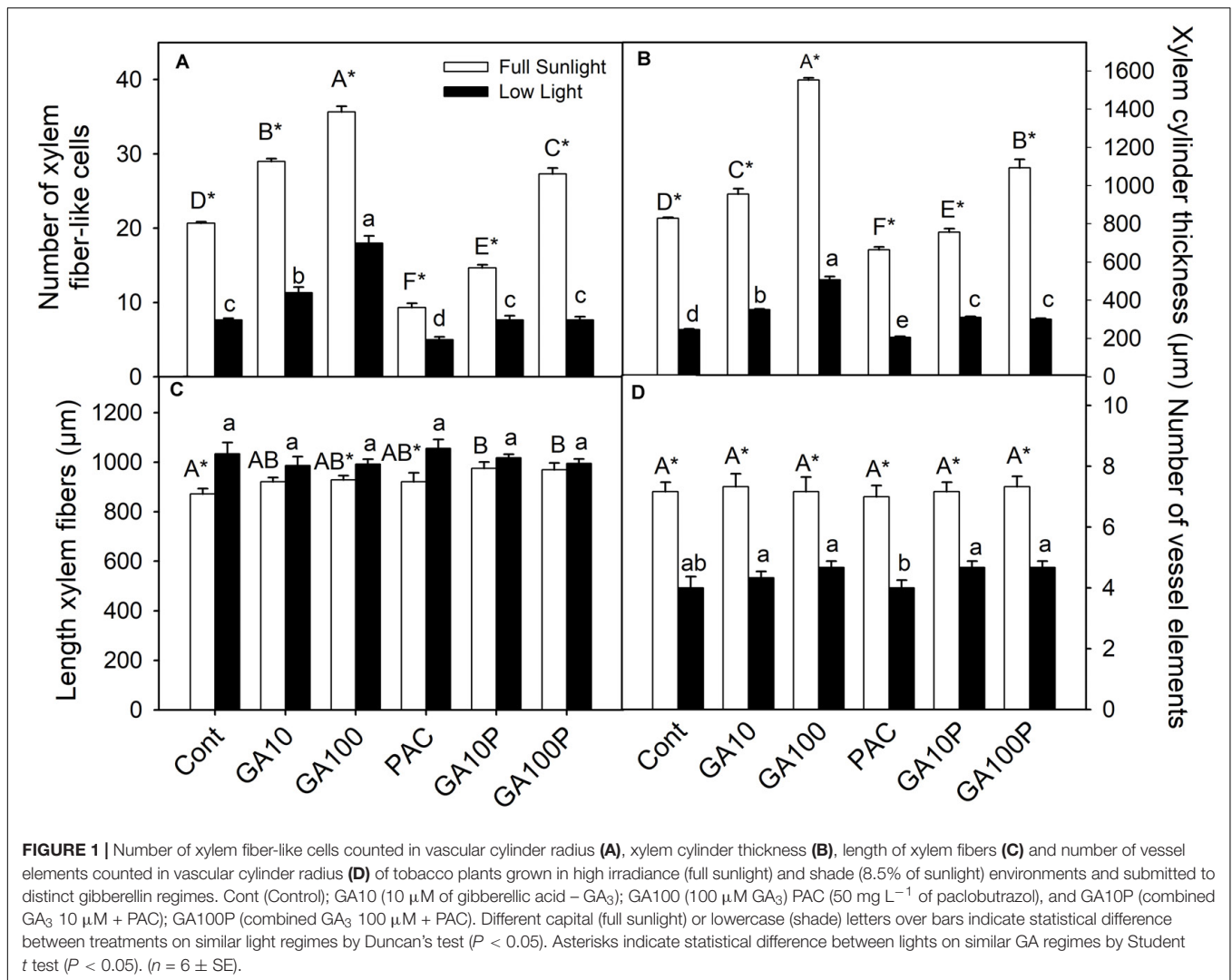
Xylem Epifluorescence and Light Microscopy

The application of GA₃, irrespectively of light levels, promoted an increase in the number of xylem fiber-like cells (>52%) (Figures 1A,B, 2), higher cambial activity and the development of secondary wall structures (e.g., secondary xylem), whereas isolated PAC application promoted a strong repression (>37.5%) of their development, both in relation to the respective controls (Figures 1A,B, 2). The number of vessel elements and fibers length were not altered ($P > 0.05$) between GA₃ and/or PAC treatments (Figures 1C,D and Supplementary Figure S3).

GA₃ application stimulated vascular cylinder thickening both in plants grown in full sunlight (>87%) (Figures 1B, 2C) and in the shaded environment (>105%) (Figures 1B, 2I), whereas plants treated with PAC only displayed decreased vascular cylinder thickness of 20.1% in the high irradiance environment (Figures 1B, 2D) and 16.6% in the shade (Figures 1B, 2J), both in relation to their respective controls (Figures 2A,G). In addition, plants treated with PAC and supplemented with GA₃ (GA100P) presented phenotype recovering, with a vascular cylinder diameter increase of 31.9% in the sunlight-irradiated plants and 22.3% in the shaded plants (Figures 1B, 2F,L), compared to their controls, whose increase was greater when compared to PAC.

Scanning Electron Microscopy and Transmission Electron Microscopy

An increase in cell wall thickness of xylem fiber-like cells in plants treated with GA₃ (10 and 100 μM) independent of light conditions (Figure 3) was qualitatively verified. In



addition, cell walls were well delimited when submitted to cryofracturing. In contrast, decreases in endogenous GAs levels through PAC application led to thinner and more fragile fiber walls in plants grown in both the full sunlight and the shade (Figures 3D,J) besides disuniformity electrodensity by TEM of cell walls. This phenotype was restored in the GA100P treatment (Figures 3E,L, inset). Regarding GA-treated plants supplemented with PAC, the cell wall of GA10P xylem fiber-like cells was partially restored (Figure 3E), while GA100P led to a complete restoration of fiber wall thickness (Figure 3F) in relation to the controls, in high irradiance conditions (Figure 3A). The ability of GA₃ to reverse plant phenotype caused by PAC applications (Figures 3K,L) in shaded plants was observed in GA10P and GA100P treated plants, who presented thicker-walled fiber-like cells compared to plants treated with PAC only (Figure 3J), but thinner when compared to the GA10 and GA100 treatments (Figures 3H,I) in shade-grown plants. No evidence of changes in vessel elements wall thickness was detected in relation to GA₃ and/or PAC treatments

in any of the evaluated combinations herein in this work (Figure 3).

Lignin Content and Monomer Composition

The application of GA₃ induced increased lignin contents in stems, of 12.4% for GA10 and 28.1% for GA100 plants in full sunlight conditions, whereas the PAC treatment led to a 32.6% decrease (Figure 4A) ($P < 0.05$). Similarly, in the shaded environment, lignin contents increased 23.1% in GA10 and 28.2% in GA100 plants, while PAC application decreased lignin contents in 5% (Figure 4A). GA₃ application induced increased stem lignin contents in PAC-treated plants in both irradiance conditions (Figure 4A). Higher *p*-hydroxyphenyl (H) deposition was observed in shade plants (Figure 4B), although to a lesser extent compared to the syringyl (S) and guaiacyl (G) monomers, which decreased in response to GA₃ (Figure 4B). In addition, PAC-treated plants exhibited higher levels of the H monomer in both irradiance conditions

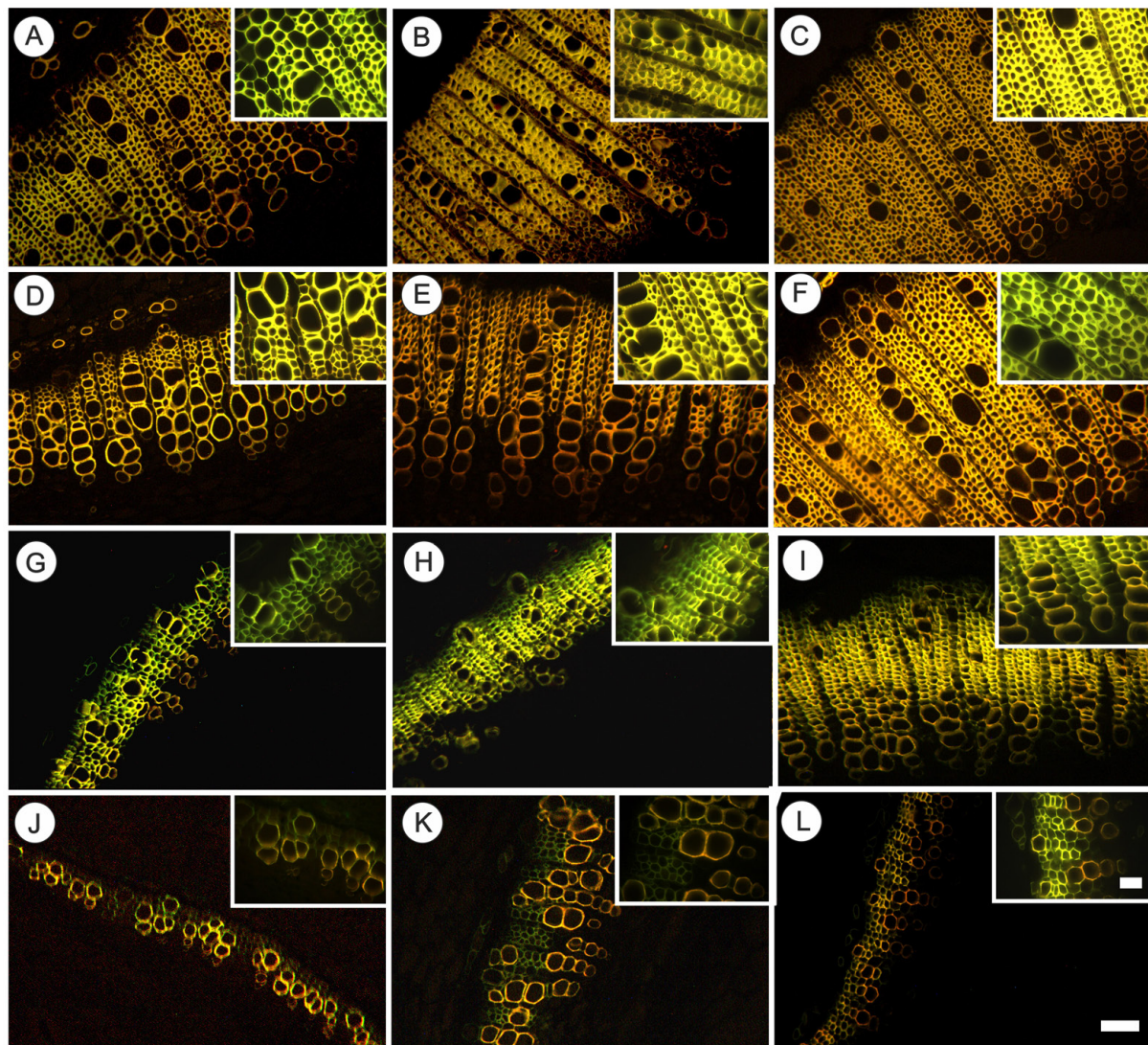


FIGURE 2 | Fluorescence microscopy of cross section of basal region of representative stem of tobacco plants grown in high irradiance (A–F; full sunlight) and shade (G–L; 8.5% of sunlight) environments and submitted to distinct gibberellin regimes. Scale bar = 100 μ m. Control (A,G), GA10 (B,H), GA100 (C,I), PAC (D,J), GA10P (E,K), and GA100P (F,L). Box sections for representative image in details fibers (Scale bar = 50 μ m). For abbreviations of treatments, see **Figure 1**. Stained by safranin and astra blue in fluorescence microscopy under excitation violet light (400 nm).

(**Figure 4B**). No changes were detected ($P > 0.05$) in the amount of G or S monomers in response to light or GA₃ (**Figures 4C,D**).

Multivariate Analysis

A PCA was carried out in order to estimate the individual contribution (or correlated groups) of the variables evaluated herein (raw data are not shown) regarding lignin accumulation in plant stems. The first component (PC1 – highest variance, 52.45%) was able to separate the applied treatments into two large groups (**Figure 5**). High participation of light levels was attributed to PC1 that, in isolation, allowed all for separation between high irradiance and low irradiance level conditions (**Figures 5A–C**).

The eigenvector analysis indicated that PC1 was strongly correlated with primary growth (root, stem, leaf and total plants dry matter and stem length) components, such as total DM (–0.9748), stem DM (–0.9326), stem diameter (–0.9178), energy cost (–0.9517), and total stem calorific energy (–0.9343) (**Supplementary Table S1**). In parallel, concerning PC2, the largest eigenvectors (in modulus) belonged to primary components and those derived from the growth analysis, such as internode length (–0.8449) and stem length (–0.6760), stem mass ratio (–0.8817) and number of fibers (–0.4514), identified as the individual variables most strongly associated to this component (**Supplementary Table S1**).

In order to further investigate the influence of the analyzed variables on lignin deposition, an empirical grouping of

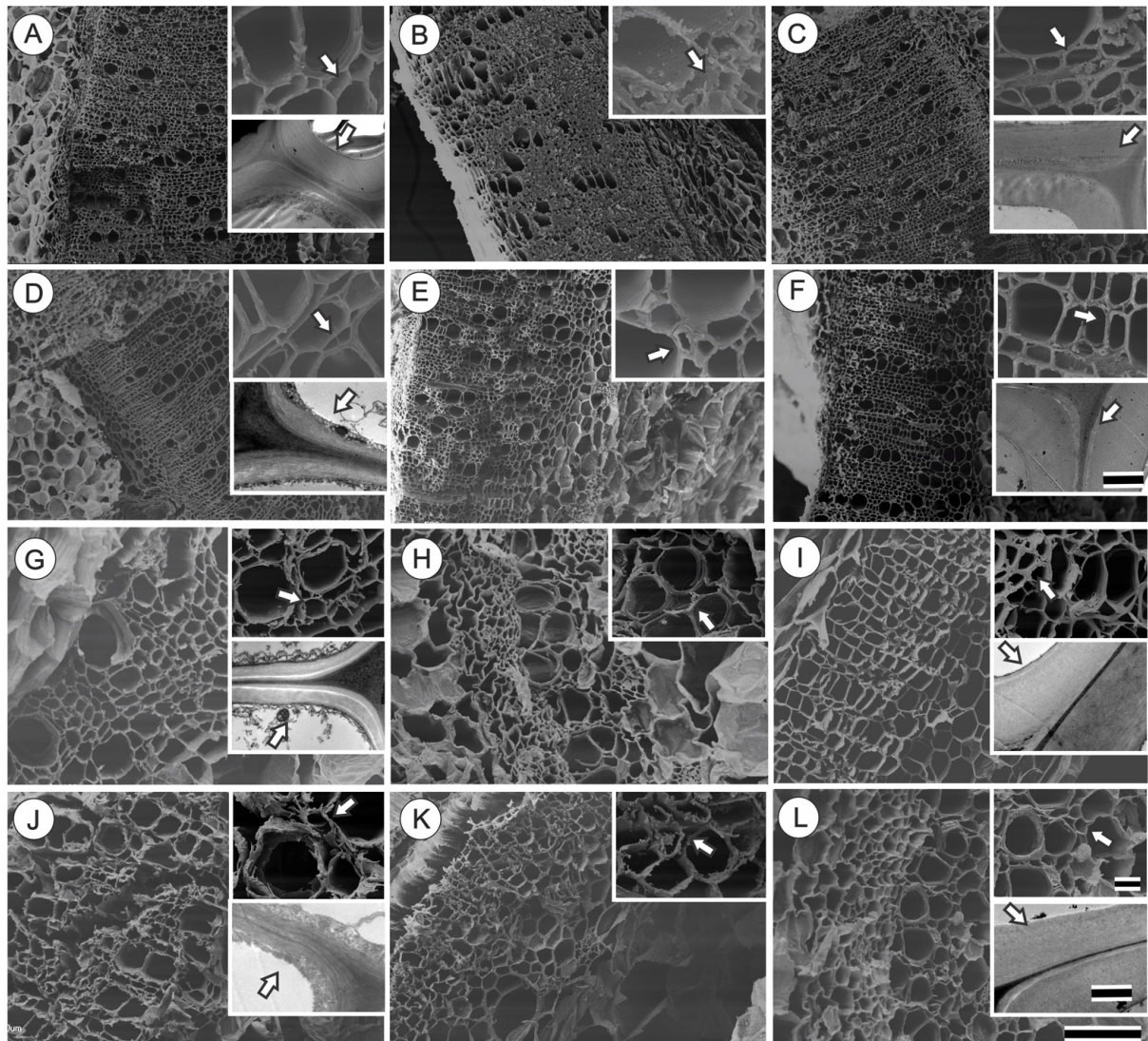


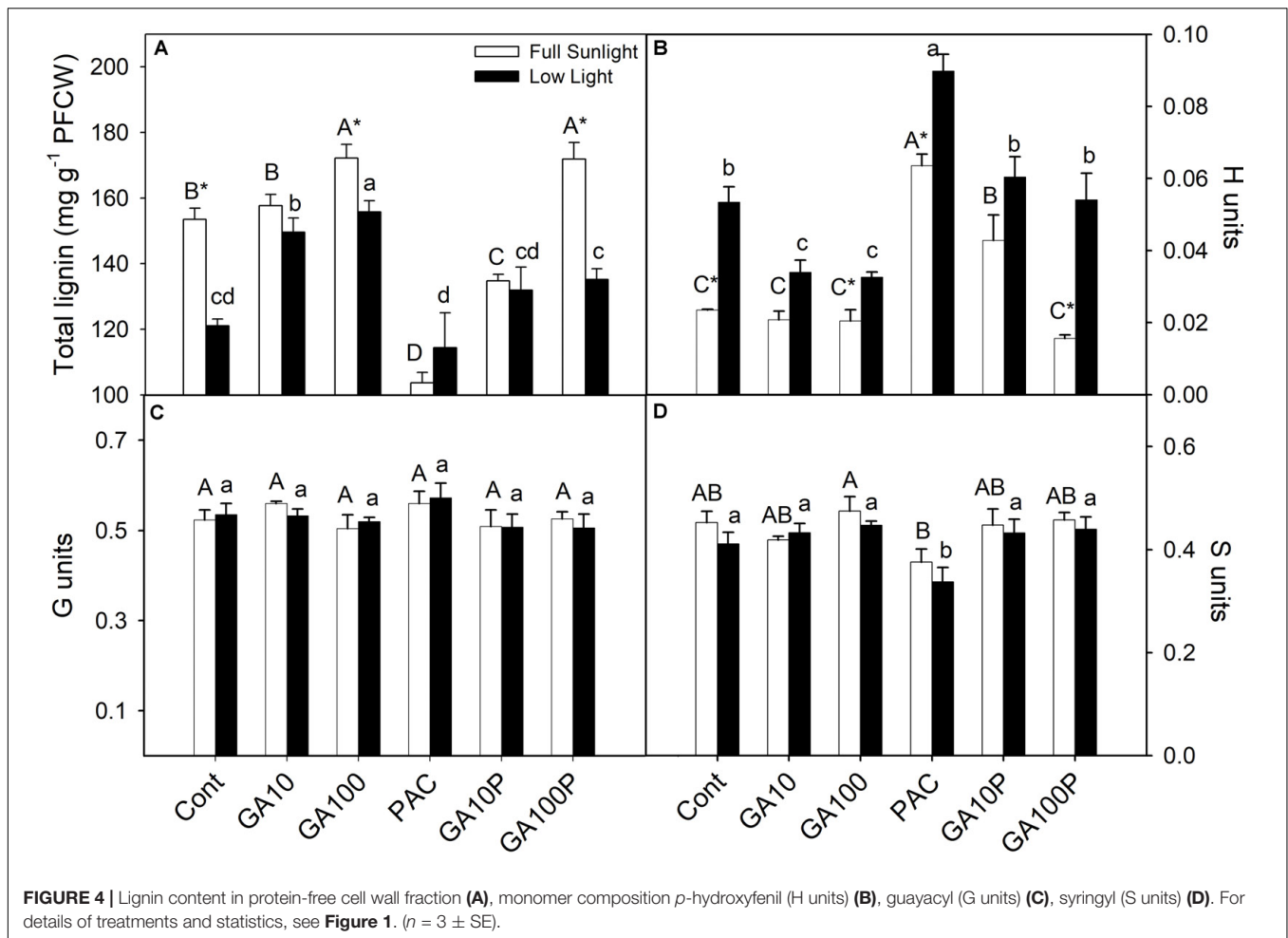
FIGURE 3 | Scanning electron microscopy (SEM) and transmission electron microscopy (TEM) of transversal section of representative basal region of stem of tobacco plants grown in high irradiance (A–F; full sunlight; Scale bar = 500 μm) and shade (G–L; 8.5% of sunlight; Scale bar = 100 μm) environments and submitted to distinct gibberellin regimes Control (A,G), GA10 (B,H), GA100 (C,I), PAC (D,J), GA10P (E,K) and GA100P (F,L). Box sections for representative image in details these cell wall thickness (Scale bar for SEM = 20 μm) and (Scale bar for TEM = 2 μm for full sunlight and 1 μm for low light). For abbreviations of treatments, see **Figure 1**. Arrows indicate details of cell wall of fiber-like cells.

the different variables analyzed in six groups according to the “natural” experimental association of each group, namely primary growth, photosynthetic pigments, derived growth, calorific energy, biochemical and anatomical data, was performed. A high degree of correlation or autocorrelated variables (residuals are not independent) among the variables of each group was observed, making simple regression analyses inappropriate (Chatterjee and Hadi, 2012). For PC1, strongly associated to light, the highest explanation percentages were linked to the calorific group (25.8%), followed by the primary growth (19.8%) and anatomical (19.2%) groups, and, to a lesser extent, the biochemistry group (4.5%), concerning total data variability (**Supplementary Table S2**). However, for PC2, which

was more strongly linked to GA levels, the highest percentage of explanation was related to the biochemistry group (32.8%), followed by the primary growth, pigments and derived growths groups (between 18.2 and 18.9%, respectively) concerning total data variability (**Supplementary Table S2**).

DISCUSSION

This study revealed an association between GA and light regarding the stimulation of lignin deposition in tobacco plant stems. GA₃ partially (but not completely) replaced the effect of light on the stimulation of lignin deposition, particularly in xylem

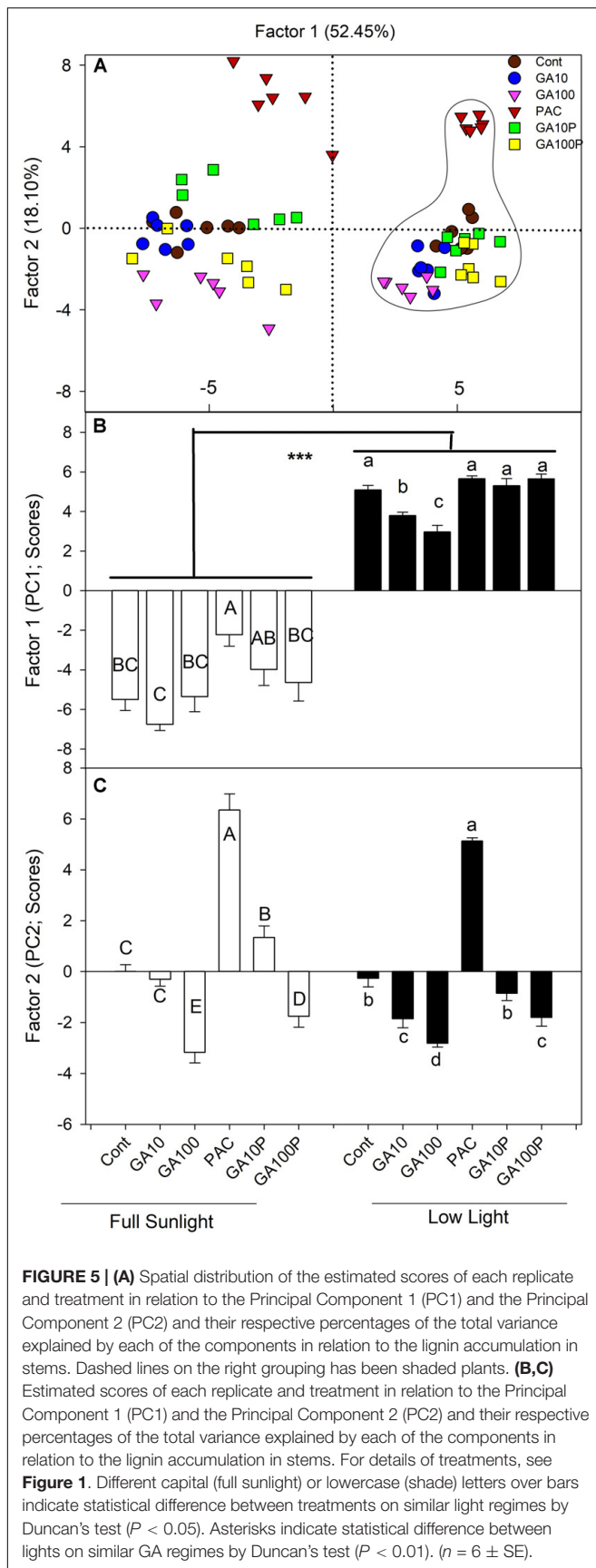


fibers. Our data indicate the existence of an exclusive response mechanism to light that GAs are not able to replace.

Lignin biosynthesis is affected in response to variations in light availability (Schopfer et al., 2001; Chen et al., 2002; Kimura et al., 2003; Syros et al., 2005; Andersson-Gunnerås et al., 2006; Yang et al., 2018). Unlike other reports, the experiments carried out herein demonstrate that light exerts a strong role in plant lignification under GA₃ supplementation. In contrast, GAs are important in the stimulation of fibers lignification and differentiation, reducing the need for light during these processes. On the other hand, for treatments such as GA10P and GA100P in shaded conditions, supplementation with GAs was not enough to stimulate lignin deposition and fibers differentiation at levels similar to the respective counterparts grown in full sunlight (Figures 2, 3, 4A), indicating that light may be a necessary stimulatory component leading to high tissue lignification rates, when repressor mechanisms are acting or modulating lignin deposition. According to Kimura et al. (2003) and Roberts et al. (2008), many genes are expressed exclusively in high irradiance environments, so different mechanisms occur at high and low irradiance levels. Thus, light is a possible environmental components that stimulates the phenylpropanoid pathway (Roberts et al., 2008; Zhang et al., 2018a), as well as the

expression of genes encoding important enzymes, such as PAL, CAD and PODs (Zhang et al., 2018b) which GAs alone are not able to replace.

Lignin biosynthesis does not only depend on the amount of the precursor components, but also on enzymatic activities, that are dependent on many other factors (e.g., gene expression, enzymatic regulation, interaction with phytochromes) (Zhao and Dixon, 2011; de Wit et al., 2016). Little is known so far at the transcription level (Wang et al., 2015b) and even less at the post-transcriptional level, such as how, and at what point (protein/metabolite), would the lignin biosynthesis pathway be affected primarily or mostly by GAs (Zhang et al., 2018a,b). In addition, it is not known whether some genes (and proteins) stimulated by GAs (Guo et al., 2015; Wang et al., 2015a; Li et al., 2017) suffer some kind of activity interaction and/or modulation by PIF proteins (Li et al., 2016). However, this study presents anatomical evidence triggered by this interaction. In *Arabidopsis thaliana*, genes correlated with lignin biosynthesis and associated to GAs variations are stimulated at high irradiance levels (Kimura et al., 2003; Moura et al., 2010). However, in general, wild plants grown in low irradiance exhibit higher GAs (Kurepin et al., 2006, 2007; Kurepin and Pharis, 2014) and lower lignin levels, according to the results reported herein (Figure 4A). That is,



the less light, the lower the lignin content (and vice versa). By this direct analogy it would be possible to infer that the GAs act in an inhibitory (and not stimulatory) way in the lignin biosynthetic pathway, whereas light would play a fundamental role in the induction of this process. This study confirmed that both conditions stimulate the biosynthetic pathway linked to lignification, that lignin contents are not the direct reflection of the number of cells, and that GAs (GA_3) promote fiber wall thickening and greater lignin content per cell, even in shaded environments, as evidenced by transmission electron microscopy (**Figure 3**, inset).

In the lignin biosynthetic pathway, a profuse metabolic flexibility and refined gene regulation is observed, as well as a complex interaction between these processes and the environment (Zhong and Ye, 2009; Zhao and Dixon, 2011). Linking data from other reports (Kurepin et al., 2007; Dayan et al., 2010; Kurepin and Pharis, 2014; Fukuda et al., 2016) with the present study, it is possible to speculate that, DELLA levels should be low at increased levels of GAs, as in plants grown in low-irradiance environments, since they are subject to degradation promoted by GAs (Ueguchi-Tanaka et al., 2007; Yamaguchi, 2008; Dixit, 2013; Racca et al., 2018), allowing PIF3 and PIF4 to be free to bind to their target genes. Shaded environments, although they lead to increased levels of endogenous GAs (Kurepin et al., 2006), appear to show poor interaction with PIFs, providing greater accumulation of DELLA proteins and inhibition of important enzymes, like PAL (Roberts et al., 2008; Locascio et al., 2013). GAs interact with the PIF (light dependent) complex, leading to the degradation of DELLA proteins and triggering the signaling required for growth induction (Li et al., 2016). In accordance to these results, in plants under the influence of PAC, which are expected to present lower endogenous GAs levels, light exerted a stimulatory role in the formation of fibers-like cells and lignin fiber wall deposition (**Figures 1B, 2, 3**). This combination is suggested to explain the decreased lignin contents observed in the stem over PAC under shade. Thus, while light controls PIF3 and PIF4 at the protein level (Soy et al., 2012; Zhong et al., 2012), GAs regulate their transcriptional activity (de Lucas et al., 2008; Li et al., 2016, 2017; Zhang et al., 2018a). This dual PIF3 and PIF4 regulation represents a point of integration (cross-talk) for the coordination of plant photomorphogenesis in response to light and GAs (Lau and Deng, 2010; Zhu et al., 2016). We emphasize that further enzymatic and gene expression studies in plants grown under controlled conditions undergoing light level manipulation should be performed to effectively confirm the data obtained by anatomical observations and direct quantification of lignin contents in stems (Guo et al., 2015; Zhu et al., 2016).

At the ultrastructural level, xylem fiber-like cells walls became thicker and more lignified as a result of increased GAs exposure, whereas decreased GAs through PAC applications lead to lower lignin contents in sun environments, but, especially, in shaded environments, making them fragile and less resistant (**Figure 3**), but not necessarily affecting stem diameter (Eriksson et al., 2000; Biemelt et al., 2004). It should be noted no evidence of changes in the number or thickening of vessel elements

walls in response to GA levels was detected. In this sense, transcriptional factors of the MYB type, particularly MYB58, are stimulated, but not MYB63 (or *Arabidopsis thaliana* analogs) in triggering cell wall thickening via lignin deposition in the fibers but not in lignin increase in vessel elements (Zhou et al., 2009; Zhang et al., 2018b). However, there is no direct evidence to date that these transcriptional factors are stimulated by GAs or by light, only that they stimulate fiber-like cell wall and vessel elements thickening, specifically (Zhou et al., 2009).

Multivariate Influence of Lignin Deposition

GA₃ supplementation is able to stimulate lignification in shade-grown plants, but always at lower levels compared to plants in full sunlight (**Figure 4A**), indicating the existence of an exclusive response mechanism to light that GAs are not able to replace.

The multivariate analysis (PCA), that incorporated the effects of all the data collected, indicated that light was associated to the first component (PC1), which discriminated all high light treatments compared to low irradiance regards lignin content in stems. For the second component (PC2), cluster formation was observed. From the first to the last treatment (PAC, Control, GA10P, GA10 and GA100) supposedly with increasing GAs levels (**Supplementary Figure S1**). A growing response to increased GAs levels is observed, where the interaction between GAs and light appears to be additive in inducing cell lignification (**Figures 1–3**).

In full sunlight the percentage of explanation of lignin deposition were shared in many variables (**Supplementary Tables S1, S2**). In the shade, with limited C supply GA₃ supplementation correlates strongly to plant height and internode length. GAs was capable of promoting phenotypic changes that trigger responses involved with biomass accumulation by maximizing light capture performance (leaf area density, **Supplementary Table S1**) in response to internode length (**Supplementary Figure S2A**) and greater efficiency of light interception by leaf area unit and number of leaves (**Supplementary Figure S2B**; Falcioni et al., 2018). In fact the increase in light interception also increases the photosynthetic rates, which would allow plants to accumulate greater DW, lignin and other components.

GAs Effects on the Cell Wall Structure

Two experimental indications on the microfibrillar arrangement pattern were observed herein. First, more uniform uniformity of cell wall electrodensity (TEM) under GA₃ action and the opposite under PAC applications (**Figure 3**, inset). This suggests a lack of uniformity in microfibril orientation under PAC applications and a reorientation with GA₃ supplementation in PAC treated plants [as reported by Inada and Shimmen (2000) and Dixit (2013)]. Second, SEM analyses indicated that the fracture pattern was relatively smooth and uniform in full sunlight plants (except PAC-grown plants), while in the shade, particularly for PAC plants, a very irregular fragmentation pattern was observed (**Figure 3**).

A developed model concerning microtubule roles (Dixit, 2013) indicates that increased GAs availability may provide a larger microtubule organization and guide cellulose microfibrils in a transversal alignment, thus allowing for space filling with lignin (Inada and Shimmen, 2000; Dixit, 2013). Conversely, lower GAs concentrations direct cortical microtubule matrices to a greater cellular disorganization and a less dense network (Dixit, 2013), reducing the spaces to be filled by lignin. Appropriate organization provides spaces between microfibrils for lignin deposition (Li et al., 2016). The proposed model suggests that higher wall thickenings (and lignin deposition) would be the primary consequence of a simultaneous action promoted by light and GAs on microtubule accumulation and organization.

CONCLUSION

The data presented herein reinforce the idea that light and GAs act exclusively in lignin promotion and deposition in tobacco plant stems, although a certain cross-talk between the routes is suggested. In high light availability environments, it is proposed that light and GAs must act in an additive way in promoting xylem fiber-like cellular differentiation. However, at low irradiance levels, even under high GA levels, lignin deposition is lower than the respective counterpart grown in high light availability, although a lignification stimulus also occurs, indicating a unique role played by light in these processes.

AUTHOR CONTRIBUTIONS

RF and WA designed the experiments, performed analysis, and wrote the manuscript. GA, CB, TM, DO, LS, and WS performed analyses and review the manuscript.

FUNDING

This study was partially funded by National Council of Technological and Scientific Development - CNPq, Brazil (Universal - 443102/2014-7). Scholarships granted by the Brazilian Government (RF, TM, and DO - CNPq and CAPES) and are gratefully acknowledged.

ACKNOWLEDGMENTS

The authors thanks to COMCAP (CMI) - UEM and LMEM - UEL for the facilities in microscopy fluorescence and electronic for the use and reviews for significantly contributions to the manuscript.

SUPPLEMENTARY MATERIAL

The Supplementary Material for this article can be found online at: <https://www.frontiersin.org/articles/10.3389/fpls.2018.01391/full#supplementary-material>

REFERENCES

- Ahmad, P., and Wani, M. R. (2014). *Physiological Mechanisms and Adaptation Strategies in Plants Under Changing Environment*, 1st Edn, eds P. Ahmad and M. R. Wani (New York, NY: Springer).
- Alabadi, D., Gallego-Bartolomé, J., Orlando, L., García-Cárcel, L., Rubio, V., Martínez, C., et al. (2008). Gibberellins modulate light signaling pathways to prevent *Arabidopsis* seedling de-etiolation in darkness. *Plant J.* 53, 324–335. doi: 10.1111/j.1365-313X.2007.03346.x
- Aloni, R. (2013). Role of hormones in controlling vascular differentiation and the mechanism of lateral root initiation. *Planta* 238, 819–830. doi: 10.1007/s00425-013-1927-8
- Andersson-Gunnerås, S., Mellerowicz, E. J., Love, J., Segerman, B., Ohmiya, Y., Coutinho, P. M., et al. (2006). Biosynthesis of cellulose-enriched tension wood in *Populus*: global analysis of transcripts and metabolites identifies biochemical and developmental regulators in secondary wall biosynthesis. *Plant J.* 45, 144–165. doi: 10.1111/j.1365-313X.2005.02584.x
- Bai, W., Xiao, Y., Zhao, J., Song, S., Hu, L., Zeng, J., et al. (2014). Gibberellin overproduction promotes sucrose synthase expression and secondary cell wall deposition in cotton fibers. *PLoS One* 9:e96537. doi: 10.1371/journal.pone.0096537
- Bashline, L., Lei, L., Li, S., and Gu, Y. (2014). Cell wall, cytoskeleton, and cell expansion in higher plants. *Mol. Plant* 7, 586–600. doi: 10.1093/mp/ssu018
- Biemelt, S., Tschiersch, H., and Sonnwald, U. (2004). Impact of altered gibberellin metabolism on biomass accumulation, lignin biosynthesis, and photosynthesis in transgenic tobacco plants. *Plant Physiol.* 135, 254–265. doi: 10.1104/pp.103.036988
- Burk, D. H., and Ye, Z.-H. (2002). Alteration of oriented deposition of cellulose microfibrils by mutation of a katanin-like microtubule-severing protein. *Plant Cell* 14, 2145–2160. doi: 10.1105/tpc.003947
- Casal, J. J. (2012). Shade avoidance. *Arabidopsis Book* 10:e0157. doi: 10.1199/tab.0157
- Chatterjee, S., and Hadi, A. (2012). *Regression Analysis by Example*, 5th Edn. New York, NY: John Wiley & Sons.
- Chen, E.-L., Chen, Y.-A., Chen, L.-M., and Liu, Z.-H. (2002). Effect of copper on peroxidase activity and lignin content in *Raphanus sativus*. *Plant Physiol. Biochem.* 40, 439–444. doi: 10.1016/S0981-9428(02)01392-X
- Davies, P. J. (2010). *Gibberellin Biosynthesis and Inactivation*, 3rd Edn. New York, NY: Springer.
- Dayan, J., Schwarzkopf, M., Avni, A., and Aloni, R. (2010). Enhancing plant growth and fiber production by silencing GA2-oxidase. *Plant Biotechnol. J.* 8, 425–435. doi: 10.1111/j.1467-7652.2009.00480.x
- Dayan, J., Voronin, N., Gong, F., Sun, T., Hedden, P., Fromm, H., et al. (2012). Leaf-induced gibberellin signaling is essential for internode elongation, cambial activity, and fiber differentiation in tobacco stems. *Plant Cell* 24, 66–79. doi: 10.1105/tpc.111.093096
- de Lucas, M., Davière, J. M., Rodríguez-Falcón, M., Pontin, M., Iglesias-Pedraz, J. M., Lorrain, S., et al. (2008). A molecular framework for light and gibberellin control of cell elongation. *Nature* 451, 480–484. doi: 10.1038/nature06520
- de Wit, M., Galvão, V. C., and Fankhauser, C. (2016). Light-mediated hormonal regulation of plant growth and development. *Annu. Rev. Plant Biol.* 67, 513–537. doi: 10.1146/annurev-arplant-043015-112252
- Dixit, R. (2013). Plant cytoskeleton?: DELLA connects gibberellins to microtubules. *Curr. Biol.* 23, 479–481. doi: 10.1016/j.cub.2013.04.037
- Eriksson, M. E., Israelsson, M., Olsson, O., and Moritz, T. (2000). Increased gibberellin biosynthesis in transgenic trees promotes growth, biomass production and xylem fiber length. *Nat. Biotechnol.* 18, 784–788. doi: 10.1038/77355
- Evert, R. F., and Eichhorn, S. E. (2006). “Xylem: cell types and developmental aspects,” in *Esau's Plant Anatomy: Meristems, Cells, and Tissues of the Plant Body: Their Structure, Function, and Development*, ed. R. F. Evert (Hoboken, NJ: Wiley-Interscience), 255–290.
- Falcioni, R., Moriwaki, T., Benedito, E., Bonato, C. M., Souza, L. A., and Antunes, W. C. (2018). Increased gibberellin levels enhance the performance of light capture efficiency in tobacco plants and promote dry matter accumulation. *Theor. Exp. Plant Physiol.* 30, 01–16. doi: 10.1007/s40626-018-0118-1
- Falcioni, R., Moriwaki, T., Bonato, C. M., de Souza, L. A., Nanni, M. R., and Antunes, W. C. (2017). Distinct growth light and gibberellin regimes alter leaf anatomy and reveal their influence on leaf optical properties. *Environ. Exp. Bot.* 140, 86–95. doi: 10.1016/j.envexpbot.2017.06.001
- Ferreira, B. G., Falcioni, R., Guedes, L. M., Avritzer, S. C., Antunes, W. C., Souza, L. A., et al. (2017). Preventing false negatives for histochemical detection of phenolics and lignins in PEG-embedded plant tissues. *J. Histochem. Cytochem.* 65, 105–116. doi: 10.1369/0022155416677035
- Fukuda, N., Ajima, C., Yukawa, T., and Olsen, J. E. (2016). Antagonistic action of blue and red light on shoot elongation in petunia depends on gibberellin, but the effects on flowering are not generally linked to gibberellin. *Environ. Exp. Bot.* 121, 102–111. doi: 10.1016/j.envexpbot.2015.06.014
- Givnish, T. J. (1988). Adaptation to sun and shade?: a whole-plant perspective. *Aust. J. Plant Physiol.* 15, 63–92. doi: 10.1071/PP9880063
- Guo, H., Wang, Y., Liu, H., Hu, P., Jia, Y., Zhang, C., et al. (2015). Exogenous GA3 application enhances xylem development and induces the expression of secondary wall biosynthesis related genes in *Betula platyphylla*. *Int. J. Mol. Sci.* 16, 22960–22975. doi: 10.3390/ijms160922960
- Hedden, P., and Phillips, A. L. (2000). Gibberellin metabolism: new insights revealed by the genes. *Trends Plant Sci.* 5, 523–530. doi: 10.1016/S1360-1385(00)01790-8
- Hedden, P., and Sponsel, V. (2015). A century of gibberellin research. *J. Plant Growth Regul.* 34, 740–760. doi: 10.1007/s00344-015-9546-1
- Hedden, P., and Thomas, S. G. (2016). *Annual Plant Review: The Gibberellins*, 1st Edn, Vol. 49. New York, NY: Wiley Blackwell. doi: 10.1002/9781119210436
- Hoffmann, W. A., and Poorter, H. (2002). Avoiding bias in calculations of relative growth rate. *Ann. Bot.* 90, 37–42. doi: 10.1093/aob/mcf140
- Inada, S., and Shimmen, T. (2000). Regulation of elongation growth by gibberellin in root segments of *Lemna minor*. *Plant Cell Physiol.* 41, 932–939. doi: 10.1093/pcp/pcd018
- Johansen, D. A. (1940). *Plant Microtechnique*. New York, NY: McGraw-Hill Book Co.
- Jolliffe, I. T. (2002). *Principal Component Analysis*, 2nd Edn, ed. I. T. Jolliffe (New York, NY: Springer).
- Karnovsky, M. J. (1965). A formaldehyde-glutaraldehyde fixative of high osmolarity for use in electron microscopy. *J. Cell Biol.* 27, 137A–138A.
- Kiernan, J. A. (2000). Formaldehyde, formalin, paraformaldehyde and glutaraldehyde: what they are and what they do. *Microsc. Today* 12, 8–12. doi: 10.1017/S1551929500057060
- Kimura, M., Yamamoto, Y. Y., Seki, M., Sakurai, T., Sato, M., Abe, T., et al. (2003). Identification of *Arabidopsis* genes regulated by high light-stress using cDNA microarray. *Photochem. Photobiol.* 77, 226–233.
- Kraus, J. E., and Arduin, M. (1996). *Manual Básico de Métodos em Morfologia Vegetal*, 2nd Edn. São Paulo: Cultrix.
- Kraus, J. E., de Sousa, H. C., Rezende, M. H., Castro, N. M., Vecchi, C., and Luque, R. (1998). Astra blue and basic fuchsin double staining of plant materials. *Biotech. Histochem.* 73, 235–243. doi: 10.3109/10520299809141117
- Kurepin, L. V., Emery, R. J. N., Pharis, R. P., and Reid, D. M. (2007). The interaction of light quality and irradiance with gibberellins, cytokinins and auxin in regulating growth of *Helianthus annuus* hypocotyls. *Plant Cell Environ.* 30, 147–155. doi: 10.1111/j.1365-3040.2006.01612.x
- Kurepin, L. V., and Pharis, R. P. (2014). Light signaling and the phytohormonal regulation of shoot growth. *Plant Sci.* 229, 280–289. doi: 10.1016/j.plantsci.2014.10.006
- Kurepin, L. V., Pharis, R. P., Reid, D. M., and Chinnappa, C. C. (2006). Involvement of gibberellins in the stem elongation of sun and shade ecotypes of *Stellaria longipes* that is induced by low light irradiance. *Plant Cell Environ.* 29, 1319–1328. doi: 10.1111/j.1365-3040.2006.01512.x
- Lambers, H., Chapin, F. S. III, and Pons, T. L. (2008). *Plant Physiology Ecology*, 2nd Edn. New York, NY: Springer. doi: 10.1007/978-0-387-78341-3
- Lambers, H., and Poorter, H. (2004). Inherent variation in growth rate between higher plants: a search for physiological causes and ecology consequences. *Adv. Ecol. Res.* 34, 283–362. doi: 10.1016/S0065-2504(03)34004-8
- Lau, O. S., and Deng, X. W. (2010). Plant hormone signaling lightens up: integrators of light and hormones. *Curr. Opin. Plant Biol.* 13, 571–577. doi: 10.1016/j.pbi.2010.07.001
- Li, K., Yu, R., Fan, L.-M., Wei, N., Chen, H., and Deng, X. W. (2016). DELLA-mediated PIF degradation contributes to coordination of light and gibberellin signalling in *Arabidopsis*. *Nat. Commun.* 7:11868. doi: 10.1038/ncomms11868

- Li, W., Katin-Grazzini, L., Gu, X., Wang, X., El-Tanbouly, R., Yer, H., et al. (2017). Transcriptome analysis reveals differential gene expression and a possible role of gibberellins in a shade-tolerant mutant of perennial ryegrass. *Front. Plant Sci.* 8:868. doi: 10.3389/fpls.2017.00868
- Lichtenthaler, H. K. (1987). Chlorophylls and carotenoids: pigments of photosynthetic biomembranes. *Methods Enzymol.* 148, 350–382. doi: 10.1016/0076-6879(87)48036-1
- Liu, J., Kim, J. I., Cusumano, J. C., Chapple, C., Venugopalan, N., Fischetti, R. F., et al. (2016). The impact of alterations in lignin deposition on cellulose organization of the plant cell wall. *Biotechnol. Biofuels* 9:126. doi: 10.1186/s13068-016-0540-z
- Locascio, A., Blázquez, M. A., and Alabadi, D. (2013). Dynamic regulation of cortical microtubule organization through prefoldin-DELLA interaction. *Curr. Biol.* 23, 804–809. doi: 10.1016/j.cub.2013.03.053
- Martins, A. O. (2013). *Impactos Ecofisiológicos e Metabólicos da Alteração nos Níveis de Giberelina em Tomate*. Available at: <http://locus.ufv.br/handle/123456789/4347>
- Moreira-Vilar, F. C., Siqueira-Soares, R. D. C., Finger-Teixeira, A., de Oliveira, D. M., Ferro, A. P., Da Rocha, G. J., et al. (2014). The acetyl bromide method is faster, simpler and presents best recovery of lignin in different herbaceous tissues than klason and thioglycolic acid methods. *PLoS One* 9:e110000. doi: 10.1371/journal.pone.0110000
- Moura, J. C. M. S., Bonine, C. A. V., de Oliveira Fernandes Viana, J., Dornelas, M. C., and Mazzafera, P. (2010). Abiotic and biotic stresses and changes in the lignin content and composition in plants. *J. Integr. Plant Biol.* 52, 360–376. doi: 10.1111/j.1744-7909.2010.00892.x
- Niinemets, Ü., Keenan, T. F., and Hallik, L. (2015). A worldwide analysis of within-canopy variations in leaf structural, chemical and physiological traits across plant functional types. *New Phytol.* 205, 973–993. doi: 10.1111/nph.13096
- Olszewski, N., Sun, T. P., and Gubler, F. (2002). Gibberellin signaling: biosynthesis, catabolism, and response pathways. *Plant Cell* 14, 61–80. doi: 10.1105/tpc.010476
- Onoda, Y., Wright, I. J., Evans, J. R., Hikosaka, K., Kitajima, K., Niinemets, Ü., et al. (2017). Physiological and structural tradeoffs underlying the leaf economics spectrum. *New Phytol.* 214, 1447–1463. doi: 10.1111/nph.14496
- Pearcy, R. W. (2007). “Responses of plants to heterogeneous light environments,” in *Functional Plant Ecology*, eds F. Pugnaire and F. Valladares (New York, NY: CRC Press), 213–258.
- Poorter, H., Niinemets, Ü., Poorter, L., Wright, I. J., Villar, R., Niinemets, U., et al. (2009). Causes and consequences of variation in leaf mass per area (LMA): a meta-analysis. *New Phytol.* 182, 565–588. doi: 10.1111/j.1469-8137.2009.02830.x
- Pugnaire, F., and Valladares, F. (2007). *Functional Plant Ecology*, 2nd Edn. New York, NY: CRC Press.
- Racca, S., Welchen, E., Gras, D. E., Tarkowská, D., Turečková, V., Maurino, V. G., et al. (2018). Interplay between cytochrome c and gibberellins during *Arabidopsis* vegetative development. *Plant J.* 94, 105–121. doi: 10.1111/tpj.13845
- Ribeiro, D. M., Araujo, W. L., Fernie, A. R., Schippers, J. H. M., and Mueller-Roeber, B. (2012). Action of gibberellins on growth and metabolism of *Arabidopsis thaliana* plants associated with high concentration of carbon dioxide. *Plant Physiol.* 160, 1781–1794. doi: 10.1104/pp.112.204842
- Roberts, L. W., Gahan, P., and Aloni, R. (2008). *Vascular Differentiation and Plant Growth Regulators*, 2nd Edn, eds L. W. Roberts, P. Gahan, and R. Aloni (Berlin: Springer).
- Sarlikioti, V., De Visser, P. H. B., Buck-Sorlin, G. H., and Marcelis, L. F. M. (2011). How plant architecture affects light absorption and photosynthesis in tomato: towards an ideotype for plant architecture using a functional structural plant model. *Ann. Bot.* 108, 1065–1073. doi: 10.1093/aob/mcr221
- Schopfer, P., Lapiere, C., and Nolte, T. (2001). Light-controlled growth of the maize seedling mesocotyl: mechanical cell-wall changes in the elongation zone and related changes in lignification. *Physiol. Plant.* 111, 83–92. doi: 10.1034/j.1399-3054.2001.1110111.x
- Souza, L. A., Rosa, S. M., Moscheta, I. S., Mourão, K. S. M., Rodella, R. A., Rocha, D. C., et al. (2016). *Morfologia e Anatomia Vegetal: Técnicas e Práticas*, 3rd Edn. Ponta Grossa: Editora UEPG.
- Soy, J., Leivar, P., González-Schain, N., Sentandreu, M., Prat, S., Quail, P. H., et al. (2012). Phytochrome-imposed oscillations in PIF3 protein abundance regulate hypocotyl growth under diurnal light/dark conditions in *Arabidopsis*. *Plant J.* 71, 390–401. doi: 10.1111/j.1365-3113.2012.04992.x
- Syros, T. D., Yupsanis, T. A., and Economou, A. S. (2005). Expression of peroxidases during seedling growth in *Ebenus cretica* L. as affected by light and temperature treatments. *Plant Growth Regul.* 46, 143–151. doi: 10.1007/s10725-005-8087-1
- Ueguchi-Tanaka, M., Nakajima, M., Motoyuki, A., and Matsuoka, M. (2007). Gibberellin receptor and its role in gibberellin signaling in plants. *Annu. Rev. Plant Biol.* 58, 183–198. doi: 10.1146/annurev.arplant.58.032806.103830
- Valladares, F., Wright, J., Lasso, E., Kitajima, K., and Pearcy, R. (2000). Plastic phenotypic response to light of 16 congenetic shrubs from panamanian rainforest. *Ecology* 81, 1925–1936. doi: 10.1890/0012-9658(2000)081[1925:PPRTL0]2.0.CO;2
- Wada, M., Shimazaki, K., and Iino, M. (2005). *Light Sensing in Plants*, 1st Edn, eds M. Wada, K. Shimazaki, and M. Iino (Zurich: Springer Japan). doi: 10.1007/b138587
- Wang, G.-L., Que, F., Xu, Z.-S., Wang, F., and Xiong, A.-S. (2015a). Exogenous gibberellin altered morphology, anatomic and transcriptional regulatory networks of hormones in carrot root and shoot. *BMC Plant Biol.* 15:290. doi: 10.1186/s12870-015-0679-y
- Wang, G.-L., Xiong, F., Que, F., Xu, Z.-S., Wang, F., and Xiong, A.-S. (2015b). Morphological characteristics, anatomical structure, and gene expression: novel insights into gibberellin biosynthesis and perception during carrot growth and development. *Hortic. Res.* 2:15028. doi: 10.1038/hortres.2015.28
- Wang, Z., and Benning, C. (2012). Chloroplast lipid synthesis and lipid trafficking through ER-plastid membrane contact sites. *Biochem. Soc. Trans.* 40, 457–463. doi: 10.1042/BST20110752
- Wuddineh, W. A., Mazarei, M., Zhang, J., Poovaiah, C. R., Mann, D. G. J., Ziebell, A., et al. (2015). Identification and overexpression of gibberellin 2-oxidase (GA2ox) in switchgrass (*Panicum virgatum* L.) for improved plant architecture and reduced biomass recalcitrance. *Plant Biotechnol. J.* 13, 636–647. doi: 10.1111/pbi.12287
- Yamaguchi, S. (2008). Gibberellin metabolism and its regulation. *Annu. Rev. Plant Biol.* 59, 225–251. doi: 10.1146/annurev.arplant.59.032607.092804
- Yang, S. L., Zhang, X. N., Lu, G. L., Wang, C. R., and Wang, R. (2015). Regulation of gibberellin on gene expressions related with the lignin biosynthesis in “Wangkumbae” pear (*Pyrus pyrifolia* Nakai) fruit. *Plant Growth Regul.* 76, 127–134. doi: 10.1007/s10725-014-9982-0
- Yang, Y., Liang, T., Zhang, L., Shao, K., Gu, X., Shang, R., et al. (2018). UVR8 interacts with WRKY36 to regulate HY5 transcription and hypocotyl elongation in *Arabidopsis*. *Nat. Plants* 4, 98–107. doi: 10.1038/s41477-017-0099-0
- Ye, Y., Liu, B., Zhao, M., Wu, K., and Cheng, W. (2015). CEF1 / OsMYB103L is involved in GA - mediated regulation of secondary wall biosynthesis in rice. *Plant Mol. Biol.* 89, 385–401. doi: 10.1007/s11103-015-0376-0
- Zar, J. H. (2010). *Biostatistical analysis*, 5th Edn. Upper Saddle River, NJ: Pearson Education.
- Zhang, H., Wang, H., Zhu, Q., Gao, Y., Wang, H., Zhao, L., et al. (2018a). Transcriptome characterization of moso bamboo (*Phyllostachys edulis*) seedlings in response to exogenous gibberellin applications. *BMC Plant Biol.* 18:125. doi: 10.1186/s12870-018-1336-z
- Zhang, H., Ying, Y. Q., Wang, J., Zhao, X. H., Zeng, W., Beahan, C., et al. (2018b). Transcriptome analysis provides insights into xylogenesis formation in Moso bamboo (*Phyllostachys edulis*) shoot. *Sci. Rep.* 8, 1–16. doi: 10.1038/s41598-018-21766-3
- Zhao, Q. (2016). Lignification: flexibility, biosynthesis and regulation. *Trends Plant Sci.* 21, 713–721. doi: 10.1016/j.tplants.2016.04.006
- Zhao, Q., and Dixon, R. A. (2011). Transcriptional networks for lignin biosynthesis: more complex than we thought? *Trends Plant Sci.* 16, 227–233. doi: 10.1016/j.tplants.2010.12.005
- Zheng, Y., Cosgrove, D. J., and Ning, G. (2017). High-resolution field emission scanning electron microscopy (FESEM) imaging of cellulose microfibril organization in plant primary cell walls. *Microsc. Microanal.* 23, 1048–1054. doi: 10.1017/S143192761701251X
- Zhong, R., and Ye, Z. H. (2009). Transcriptional regulation of lignin biosynthesis. *Plant Signal. Behav.* 4, 1028–1034. doi: 10.4161/psb.4.11.9875

- Zhong, S., Shi, H., Xue, C., Wang, L., Xi, Y., Li, J., et al. (2012). A molecular framework of light-controlled phytohormone action in *Arabidopsis*. *Curr. Biol.* 22, 1530–1535. doi: 10.1016/j.cub.2012.06.039
- Zhou, J., Lee, C., Zhong, R., and Ye, Z.-H. (2009). MYB58 and MYB63 are transcriptional activators of the lignin biosynthetic pathway during secondary cell wall formation in *Arabidopsis*. *Plant Cell* 21, 248–266. doi: 10.1105/tpc.108.063321
- Zhu, X., Chai, M., Li, Y., Sun, M., Zhang, J., Sun, G., et al. (2016). Global transcriptome profiling analysis of inhibitory effects of paclobutrazol on leaf growth in lily (*Lilium longiflorum*-Asiatic hybrid). *Front. Plant Sci.* 7:491. doi: 10.3389/fpls.2016.00491

Conflict of Interest Statement: The authors declare that the research was conducted in the absence of any commercial or financial relationships that could be construed as a potential conflict of interest.

Copyright © 2018 Falcioni, Moriwaki, Oliveira, Andreotti, Souza, Santos, Bonato and Antunes. This is an open-access article distributed under the terms of the Creative Commons Attribution License (CC BY). The use, distribution or reproduction in other forums is permitted, provided the original author(s) and the copyright owner(s) are credited and that the original publication in this journal is cited, in accordance with accepted academic practice. No use, distribution or reproduction is permitted which does not comply with these terms.

Supplementary Material

Increased gibberellins and light levels promotes cell wall thickness and enhance lignin deposition in xylem fibers

Renan Falcioni^{1,2*}, Thaise Moriwaki¹, Dyoni Matias de Oliveira², Giovana Castelani Andreotti¹, Luiz Antonio de Souza³, Wanderley Dantas dos Santos², Carlos Moacir Bonato⁴, Werner Camargos Antunes^{1,2*}

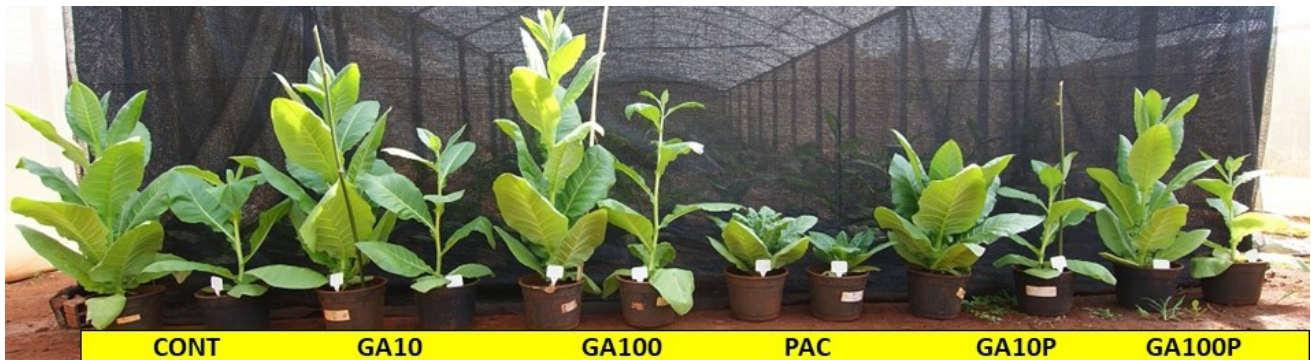
*** Correspondence:** Corresponding Author: wcantunes@yahoo.com; wcantunes@uem.br and renanfalcioni@gmail.com

1 Supplementary Figures and Tables

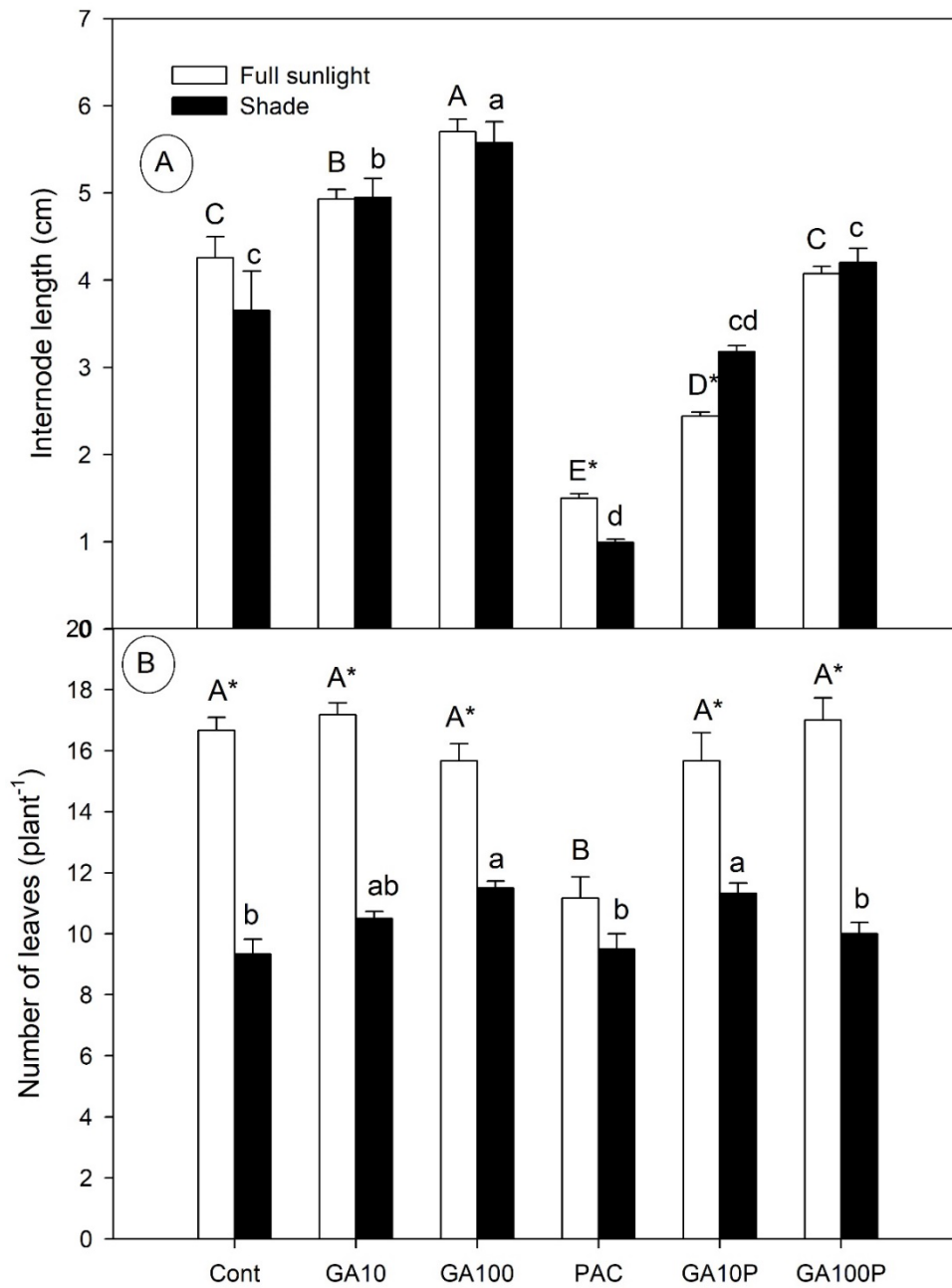
Figures: 03

Tables: 02

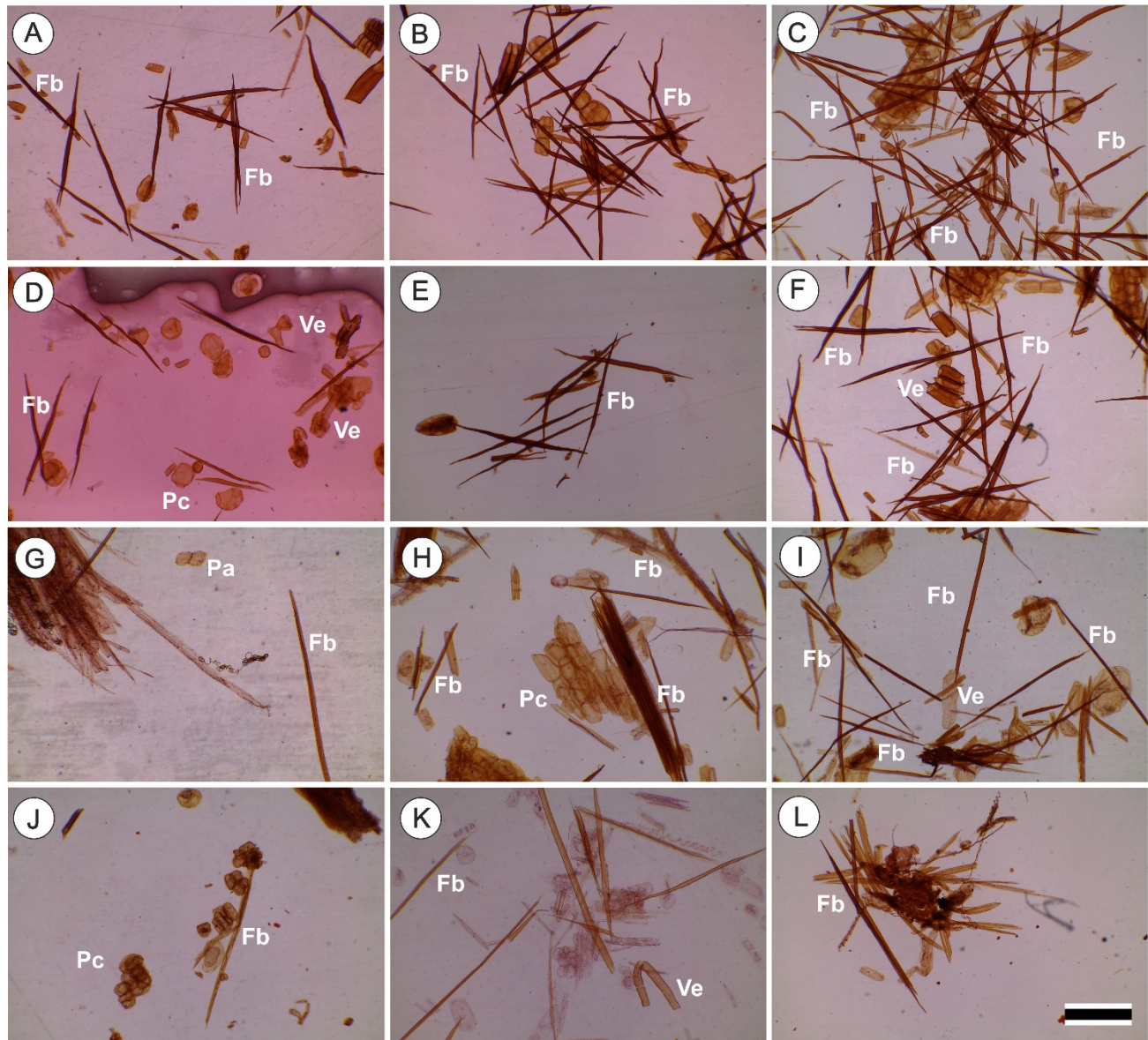
1.1 Supplementary Figures



Supplementary Figure 1. Representative image of tobacco plants. Grown in high irradiance (full sunlight, left in each pair) and shade (8.5% of sunlight, right in each pair) environments and submitted to distinct gibberellin regimes. From left to right the treatments Cont (Control); GA10 (10 μM of gibberellic acid - GA_3); GA100 (100 μM GA_3) PAC (50 mg L^{-1} of paclobutrazol), and GA10P (combined GA_3 10 μM + PAC); GA100P (combined GA_3 100 μM + PAC).



Supplementary Figure 2. (A) Mean of internode lengths and (B) number of leaves (> 5cm) of plants submitted to distinct gibberelins or light levels. Cont (Control); GA10 (10 μM of gibberellic acid - GA_3); GA100 (100 μM GA_3) PAC (50 mg L^{-1} of paclobutrazol), and GA10P (combined GA_3 10 μM + PAC); GA100P (combined GA_3 100 μM + PAC). Means followed by upper or lower case letters represent statistical differences by Duncan's test ($P < 0.05$) among different GA levels within the same irradiance level. Asterisks over the means represent statistical differences by Student's t test ($P < 0.05$) between different irradiance levels at the same GA regimen. $n = 6 \pm \text{SE}$.



Supplementary Figure 3. Light microscopy of the macerated fibers of tobacco stems cultivated in high irradiance (full sunlight; A-F) and shade (8.5% sunlight; G-L) in response to variation of the content of GA3: Cont (A and G); GA10 (B and H); GA100 (C and I); PAC (D and J); GA10P (E and K) and GA100P (F and L) at 20 days. For abbreviations of treatments, see Figure 1 in main text. Dyeing with safranin 1%. Scale bar = 500 μ m. Ve = Vessel element; Fb = Xylem fibers; Pc = Parenchyma cells.

1.2 Supplementary Table

Supplementary Table S1. Distribution of variables in relation to principal component (PC1) and the principal component 2 (PC2).

Groups	Variables	Eigenvectors		% of explication	
		PC1 (<i>light</i>)	PC2 (<i>GAs</i>)	PC1	PC2
Growth (primary)	Root length (cm)	-0.4272	0.2539	0.710%	0.727%
	Root DW (g)	-0.8520	0.2983	2.824%	1.003%
	Stem length (cm)	-0.6428	-0.6760	1.607%	5.152%
	Stem DW (g)	-0.9326	-0.1794	3.384%	0.363%
	Stem diameter (cm)	-0.9178	0.1538	3.277%	0.267%
	Internode length (cm)	-0.2363	-0.8449	0.217%	8.047%
	Leaf number	-0.8993	-0.1898	3.146%	0.406%
	Leaf area (cm ²)	-0.8960	-0.1412	3.124%	0.225%
	Leaf DW (g)	-0.9714	0.0686	3.671%	0.053%
	Plant length (cm)	-0.6864	-0.6101	1.833%	4.197%
	Plant DW (g)	-0.9748	0.0570	3.697%	0.037%
	Larger leaf (cm)	-0.7120	-0.3856	1.972%	1.676%
	Cone volume (cm ³ plant ⁻¹)	-0.7454	-0.4484	2.162%	2.267%
	Leaf area density (cm ² cm ⁻³)	0.0141	0.8665	0.001%	8.465%
Pigments	Chl <i>a</i> (mg m ⁻²)	-0.1404	0.7119	0.077%	5.714%
	Chl <i>b</i> (mg m ⁻²)	0.1704	0.6960	0.113%	5.461%
	Chl total (mg m ⁻²)	-0.0563	0.7437	0.012%	6.236%
	Carotenoids (mg m ⁻²)	-0.3202	0.7149	0.399%	5.763%
	Chl <i>a</i> /Chl <i>b</i> (mg m ⁻²)	-0.4889	0.0502	0.930%	0.028%
	Chl <i>a</i> (mg g ⁻¹)	0.8704	-0.0563	2.948%	0.036%
	Chl <i>b</i> (mg g ⁻¹)	0.9074	-0.0790	3.204%	0.070%
	Chl total (mg g ⁻¹)	0.8969	-0.0643	3.130%	0.047%
	Carotenoids (mg g ⁻¹)	0.8902	-0.1109	3.083%	0.139%

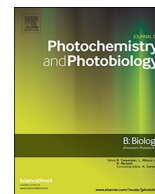
	Chl <i>a</i> /Chl <i>b</i> (mg g ⁻¹)	-0.4889	0.0502	0.930%	0.028%
Growth derivates	Root mass fraction (g g ⁻¹)	-0.5499	0.5297	1.177%	3.163%
	Stem mass fraction (g g ⁻¹)	-0.1955	-0.8817	0.149%	8.764%
	Leaf mass fraction (g g ⁻¹)	0.6926	0.2990	1.866%	1.008%
	Leaf area fraction (cm ² g ⁻¹)	0.9070	-0.2444	3.201%	0.674%
	Specific leaf area (cm ² g ⁻¹)	0.8365	-0.3664	2.723%	1.513%
	A:R (g g ⁻¹)	0.6846	-0.3913	1.823%	1.726%
	LAI (cm ² cm ⁻²)	-0.9017	0.1430	3.163%	0.231%
Calorimetry	Root (cal g ⁻¹)	-0.7028	0.2228	1.922%	0.560%
	Stem (cal g ⁻¹)	-0.9517	0.1119	3.524%	0.141%
	Leaf (cal g ⁻¹)	-0.6826	0.0532	1.813%	0.032%
	DWT (cal g ⁻¹)	-0.8994	0.1533	3.147%	0.265%
	Root cost (kcal)	-0.8493	0.3082	2.806%	1.071%
	Stem cost (kcal)	-0.9343	-0.1639	3.397%	0.303%
	Leaf cost (kcal)	-0.9738	0.0625	3.689%	0.044%
	DWT cost (kcal)	-0.9745	0.0691	3.695%	0.054%
	LA cost (cal cm ⁻²)	-0.7962	0.4036	2.467%	1.836%
Biochemistry	H - <i>p</i> -Hydroxybenzaldehyde	0.6634	0.6192	1.712%	4.323%
	G - Guayacyl	-0.0497	0.4943	0.010%	2.755%
	S - Syringyl	-0.2632	-0.7113	0.269%	5.704%
	S/G ratio	-0.1236	-0.6063	0.059%	4.145%
Anatomy	Leaf thickness (µm)	-0.6965	0.4376	1.887%	2.158%
	Secondary xylem thickness (µm)	-0.8514	-0.2657	2.820%	0.796%
	Fiber xylem thickness (µm)	0.5300	0.0228	1.093%	0.006%
	Vessel elements (number relative)	-0.8358	0.0472	2.718%	0.025%
	Fiber in vascular xylem (number relative)	-0.7882	-0.4514	2.417%	2.297%
Total		-16.345	0.774	100%	100%

Supplementary Table S2. Explications of the estimated scores of each replicate and treatment in relation to the Principal Component 1 (PC1) and the Principal Component 2 (PC2) and their respective percentages of the total variance explained by each of the components in relation to the increased lignin accumulation of plants.

Groups	Factor 1 - <i>Light</i>	Factor 2 - <i>GAs</i>
Growth (primary)	19.8%	18.2%
Pigments	13.0%	18.2%
Growth derivates	17.7%	18.9%
Calorimetry	25.8%	3.7%
Biochemistry	4.5%	32.8%
Anatomy	19.2%	8.2%
Total	100%	100%

CHAPTER 2

Cell Wall Structure And Composition is Affected By Light Quality In Tomato Seedlings



Cell wall structure and composition is affected by light quality in tomato seedlings



Renan Falcioni^{a,b}, Thaise Moriwaki^a, Marina Perez-Llorca^c, Sergi Munné-Bosch^c, Mariana Sversut Gibin^d, Francielle Sato^d, Andressa Pelozo^{a,e}, Mariana Carmona Pattaro^a, Marina Ellen Giacomelli^a, Markus Rüggeberg^f, Werner Camargos Antunes^{a,*}

^a Plant Ecophysiology Laboratory, Department of Biology, State University of Maringá, Av. Colombo, 5790, 87020-900 Maringá, Paraná, Brazil

^b Plant Biochemistry Laboratory, Department of Biochemistry, State University of Maringá, Av. Colombo, 5790, 87020-900 Maringá, Paraná, Brazil

^c Antiox Research Group, Department of Evolutionary Biology, Ecology and Environmental Sciences, Facultat de Biologia, Universitat de Barcelona, Avinguda Diagonal, 645, 08028 Barcelona, Spain

^d Optical Spectroscopy and Thermophysical Properties Research Group, Department of Physics, State University of Maringá, Av. Colombo, 5790, 87020-900 Maringá, Paraná, Brazil

^e Plant Anatomy Laboratory, Department of Biology, State University of Maringá, Av. Colombo, 5790, 87020-900 Maringá, Paraná, Brazil

^f Wood Material Science, Institute for Building Materials, Swiss Federal Institute of Technology Zurich (ETH Zurich), Schafmattstrasse 6, CH-8093 Zurich, Switzerland

ARTICLE INFO

Keywords:

Cell wall
Cellulose microfibrils angle
Hormone profile
Photomorphogenesis
Skotomorphogenesis
Small angle X-ray scattering

ABSTRACT

Light affects many aspects of cell development. Tomato seedlings growing at different light qualities (white, blue, green, red, far-red) and in the dark displayed alterations in cell wall structure and composition. A strong and negative correlation was found between cell wall thickness and hypocotyl growth. Cell walls were thicker under blue and white lights and thinner under far-red light and in the dark, while intermediate values were observed for red or green lights. Additionally, the inside layer surface of cell wall presented random deposited microfibrillae angles under far-red light and in the dark. However, longitudinal transmission electron microscopy indicates a high frequency of microfibrils close to parallels related to the elongation axis in the outer layer. This was confirmed by ultra-high resolution small angle X-ray scattering. These data suggest that cellulose microfibrils would be passively reoriented in the longitudinal direction. As the cell expands, the most recently deposited layers (inside) behave differentially oriented compared to older (outer) layers in the dark or under FR lights, agreeing with the multinet growth hypothesis. High Ca and pectin levels were found in the cell wall of seedlings growing under blue and white light, also contributing to the low extensibility of the cell wall. Low Ca and pectin contents were found in the dark and under far-red light. Auxins marginally stimulated growth in thin cell wall circumstances. Hypocotyl growth was stimulated by gibberellins under blue light.

1. Introduction

Light is an essential signal concerning plant development [1–3]. Light is perceived and processed by complex sensorial systems based on photoreceptors that affect plants at distinct regulation levels, including gene expression, protein function and metabolism, which, in turn, result in long-term anatomical and morphological alterations [4,5]. Light affects leaf expansion, pigment accumulation and promotes cell wall thickness in many species [6,7]. This has also been related to the development of shade avoidance-syndrome, promoting the opening of the apical hook, among other known responses [8–10]. Most of these responses are light quality-dependent, from the UV-A (350 nm) to the far-

red (800 nm) regions, whilst dark responses are taken as reference, as light-promoted effects are absent [2,11].

Both photomorphogenesis (light-grown) or skotomorphogenesis (dark-grown), growth occurs through a profuse regulation of the signaling transduction cascade [12,13]. Photomorphogenesis is a negative-regulated signal transduction in which transcription factors are degraded in the nucleus through the ubiquitin-mediated CONSTITUTIVE PHOTOMORPHOGENIC (COP1) [14,15]. In light, this process is inhibited, allowing for a sequence of physiological events, including the up- and down-regulation of hormones linked to biosynthesis, cell wall organization and expansion and cell division [13]. In the dark, the etiolated phenotype with an elongated hypocotyl is emphasized, while

* Corresponding author at: Plant Ecophysiology Laboratory, Department of Biology, State University of Maringá, Av. Colombo, 5790, 87020-900 Maringá, Paraná, Brazil.

E-mail address: wcantunes@uem.br (W.C. Antunes).

<https://doi.org/10.1016/j.jphotobiol.2019.111745>

Received 8 October 2019; Received in revised form 22 November 2019; Accepted 13 December 2019

Available online 15 December 2019

1011-1344/ © 2019 Elsevier B.V. All rights reserved.

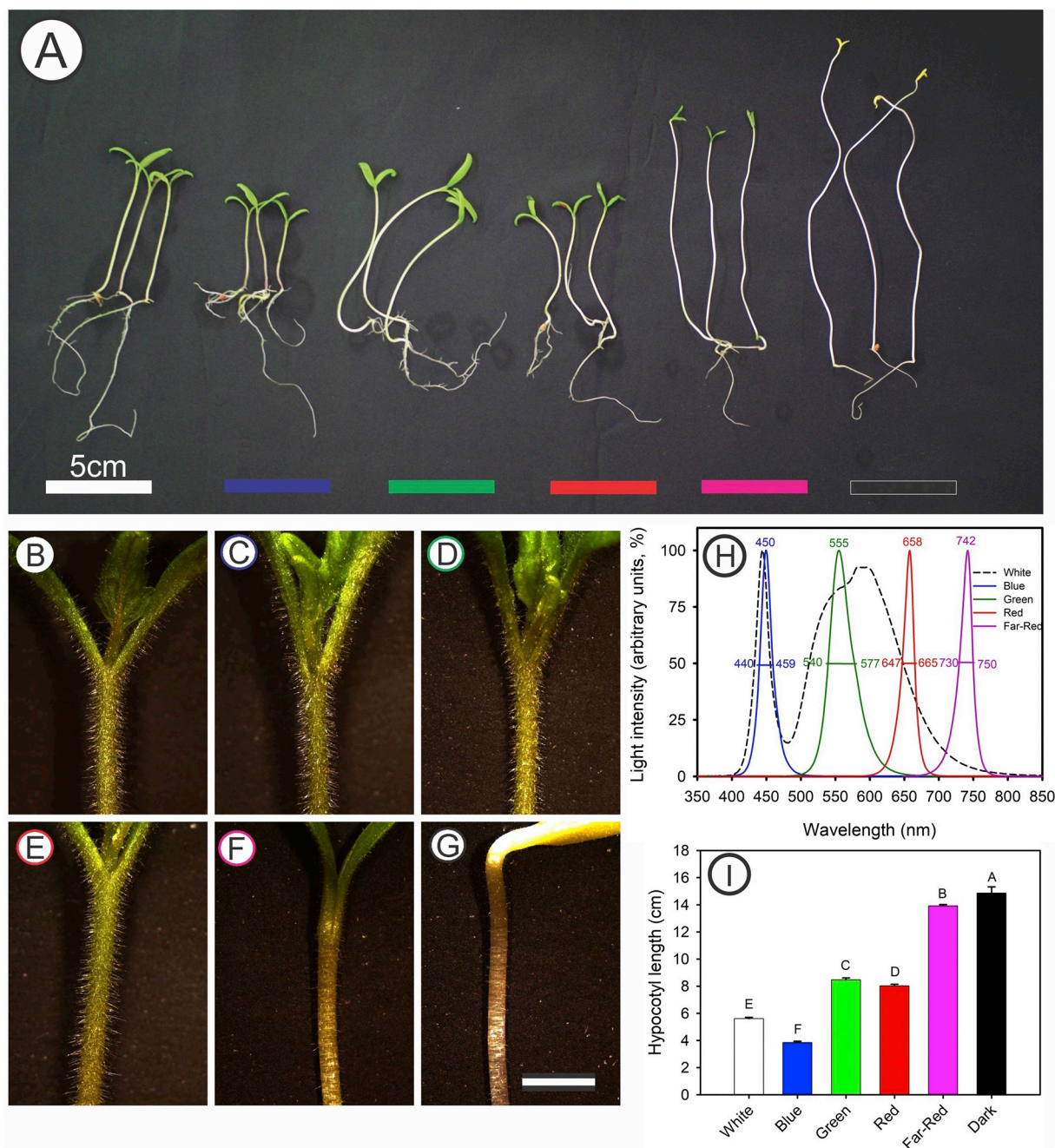


Fig. 1. Representative image of tomato seedlings grown under distinct light qualities (and dark) 10 days after the beginning of the treatment. (A) from left to right, seedlings grown under white light, blue light, green light, red light, far-red light and in the dark. Scale bar = 5 cm. (B-G) embryonic leaf close-up showing the upper hypocotyl section. Scale bar = 2 mm. (H) LED spectral emissivity indicating peak wavelength and band-width at half peak height. Data were normalized to peak = 100%. (I) hypocotyl length. Different letters over the bars indicate statistical differences between treatments by Duncan's test ($P < .05$). ($n = 80 \pm SE$). (For interpretation of the references to colour in this figure legend, the reader is referred to the web version of this article.)

short hypocotyl length is verified in the light. In addition, PHYTOCHROME INTERACTING FACTORS (PIFs), as well as, auxins (IAA), cytokinins (CKs), gibberelins (GAs), brassinosteroids (BRs), jasmonates (JAs) and abscisic acid (ABA) act as key factors to promote the (de) etiolated phenotype [13].

Among photoreceptors, phytochromes (phyA-E) are responsible for red (600–700 nm) and far-red (700–800 nm) perception [11,16], while cryptochromes (cry) and phototropins (phot) are blue-light (400–500 nm) activated [17–19]. Blue light activates CRY1 and CRY2 which are involved in de-etiolation, promoting the short length of hypocotyls and cells [18,20] and stimulating secondary cell wall thickening [7]. To date, green light (500–600 nm) is not associated to any

known photoreceptor [5,21,22] and green light responses are attributed to the interaction between CRYs [23] and PHYs. The use of LEDs with narrow bands has now contributed to the elucidation of many of these interactions and photomorphogenic responses [24–28].

Many factors affect cell growth [29–31]. Light affects cell wall development by increased cell turgor pressure through osmotically active solutes [32,33], cell wall extensibility alterations [34–36] and hormonal effects (GAs, CKs, IAA, ethylene) [37–40]. Together, these steps are associated to initial primary cell wall development stages [29,41–43]. A well-studied effect is IAA-induced wall loosening through H^+ -ATPases and expansins, resulting in acid growth, increasing cell wall extensibility and allowing for cellular expansion

[44–46]. However, it is not clear that only IAA-induced acidification is sufficient to stimulate and modify cellulose microfibrils arrangement, and it has been suggested that other hormones, such as GAs, BRs, JAs and CKs, may also play a role in this process [47,48]. In addition, the Ca^{2+} signaling cascade, particularly the conjugation of calcium with pectates (Ca-pectin) in the middle lamella and cytoskeleton organization has been associated to cellulose microfibril orientation [20,31,43,49–52].

The primary cell wall is mainly formed by a cellulose microfibril net combined with hemicellulose, pectin and structural proteins [53,54] and their alignment is determinant for cell and tissue form, organization and extensibility [55–59]. Growth direction is determined by microfibril angle, arrangement and spacing variations [55,60]. If the cellulose microfibril deposition orientation is random, cells grow isotropically, expanding equally in all directions, approaching a sphere [51,59,61,62]. However, if the microfibrils are aligned in a preferred direction (transverse, oblique or longitudinal), the result is anisotropic growth [42,51,59,63–65]. Cellulose microfibrils deposited circumferentially (transverse) at right angles to the longitudinal axis restrict circumference growth and, therefore, promote length increases [43,51,57,65,66]. However, other cellulose microfibrils angle (MFA) variations may also contribute to longitudinal growth and cell expansion [67]. The current consensus is that a random MFA pattern promotes diffuse growth (isotropic) [68], as observed during ethylene-induced growth [63,69].

To date, three hypothesis are being investigated on how primary cell wall organization affects cell growth: (1) The multinet growth hypothesis, which states that, as the cell expands longitudinally, it is expected that the microfibrils in older layers become passively reoriented, more parallel to the elongation axis; (2) microfibrils do not respond to passive (re)orientation, indicating failures in transverse angle changes and suggesting that they can be separated from one another layer in a coordinated way; (3) the older layers of the primary wall become fragmented as a result of enlargement (radial expansion), which can contribute to some extent to longitudinal growth control [31,34,35,70]. In the present study, we investigated why hypocotyls grow longer in the dark and shorter under light following the three aforementioned hypotheses. Additionally, we also investigated how different light qualities influence cell wall structure and composition. The use of ultra-high resolution small angle X-ray scattering (SAXS), longitudinal and transversal transmission electron microscopy (TEM), scanning electron microscopy (SEM) and field-emission-gun scanning electron microscopy (FEG-SEM) [52,57,59,60,68,71,72] allowed for the evaluation of microfibril angle distribution and cell growth [55,57–60,71], as well as cell wall thickness and wall texture. In addition, we also evaluated cell wall composition by attenuated-total-reflection Fourier transform infrared spectroscopy and carried out seedling hormonal profiling to identify significant alterations in dark or far-red growth in comparison to white, blue, green or red light growth.

2. Material and Methods

2.1. Growth Conditions and Experimental Design

Solanum lycopersicum (tomato, cv. Santa Clara) seeds were germinated on Germitest® paper immersed with 20 mL of Hoagland's solution (pH 5.3) in 1 L transparent pots in the dark for three days at 25 °C. Each pot was covered by a perforated PVC film to avoid ethylene accumulation. On the 3rd day, pots were transferred to white-covered wood boxes illuminated by low spectral dispersion LEDs (Fig. 1), with light irradiance fixed at $100 \mu\text{mol m}^{-2} \text{s}^{-1}$, individually adjusted by a LI-190R quantum sensor (LiCor, Nebraska, USA), under a 12 h/12 h photoperiod (light/dark). On the 10th day, the seedlings were collected and freshly analyzed, frozen in liquid N_2 , stored at $-80 \text{ }^\circ\text{C}$, and freeze-dried ($70 \text{ }^\circ\text{C}$) for the various analyses.

LED emissivity was verified using a high resolution

spectroradiometer (ADS Inc.; FieldSpec 3, Colorado, USA). White (WL – peaks at 443 and 580 nm), Blue (BL – peak at 450 nm), Green (GL – peak at 555 nm), Red (RL – peak at 658 nm) and Far-Red (FR – peak at 742 nm) (Fig. 1H).

2.2. Seedling Growth and Hypocotyl Analysis

Seedlings were scanned (HP Scanjet 300, California, USA) and the length of 80 hypocotyls were measured using the ImageJ Software (<https://imagej.nih.gov/ij>). The morphological characterization of the seedlings and epidermal modifications were monitored under a Leica ES2 stereomicroscope (Leica Company, Wetzlar, DEU).

2.3. Photosynthetic Pigments and Anthocyanin Content

Chlorophylls and carotenoids were extracted in 80% (v/v) acetone saturated with CaCO_3 for 24 h in the dark at 25 °C. Absorbances were determined at 470, 647 and 663 nm [73]. Anthocyanins were extracted with a water:methanol:acetic acid mixture (50: 45: 5) and absorbances were determined at 530 and 637 nm [74]. Chlorophyll (a, b and total), carotenoid (carotenes and xanthophylls) and anthocyanin (AnC) contents were expressed as fresh matter (FW) and by seedling unit.

2.4. Light and Epi-Fluorescence Microscopy Analysis

Hypocotyl segments (2 cm) were immersed in Karnovsky's fixative solution [75]. The fixed samples were dehydrated in an ethanol series [50, 70, 80, 90 and 100% (three times)] and infiltrated with methyl-methacrylate (Leica HistoResin®) [76]. Block sectioning (7 μm) was carried out and the sections were dyed with Toluidine Blue in acetate buffer pH 4.7 [77] and analyzed under a Leica ICC50 light microscope (Leica Company, Wetzlar, DEU). Additional slides were double stained with Calcofluor Bright White 28 (0.01%) and Auramine O (0.01%) [78] for cellulose (blue) and lignin (yellow) staining and analyzed under a Zeiss, Axiostar Plus epi-fluorescence microscope with a UV filter [37].

2.5. Hypocotyl Scanning Electron Microscopy

Scanning electron microscopy (SEM) of epidermal cells from hypocotyls (external) and ultra-high-resolution field-emission-gun SEM (FEG-SEM) of cellulose microfibrils (internal cell wall surface of cortical parenchyma cell, wall texture) were performed. Samples were fixed in modified Karnovsky's solution [75] containing 2.5% glutaraldehyde and 2% paraformaldehyde in a 0.05 M cacodylate buffer (pH 7.2).

For the SEM analyses, hypocotyl segments (2 cm) were dehydrated in an acetone series [30, 50, 70, 90 and 100% (three times)] for 1 h each. Critical point drying (CPD) was carried out on a CPD-030 equipment (Bal-Tec AG Balzers, Liechtenstein, DEU). The samples were assembled into stubs and metallized with gold (50 mA and 150 s) on a MED010 Balzer evaporator (Bal-Tec AG Balzers, Liechtenstein, DEU) and observed under a Quanta 250 Scanning Electron Microscope at 15 kV (FEI Company, Oregon, USA). Energy-dispersive X-ray spectroscopy (EDS) was carried out for elemental composition.

For the FEG-SEM analyses, similar hypocotyl segments were used for cell wall texture determinations. Fixed samples were infiltrated at different concentrations with a cryoprotectant (glycerol 10, 20 and 30%) until sinking. The fragments were then immersed into N_2 liquid and vertically fractured with a scalpel blade. A 1% (v/v) sodium hypochlorite solution was added to the treatments for 15 min, following [58]. They were then dehydrated using an increasing series of anhydrous *tert*-butanol (50, 70, 90 and 100%) following [71], *tert*-butanol and HMDS (hexamethyldisilazane) (3:1, 1:1 and 1:3) for 10 min and HMDS (100%) overnight. Samples were assembled into stubs and metallized with gold (50 mA and 20 s) on a MED010 Balzers evaporator. Cell walls were analyzed by ultra-high resolution Dual Beam Scious Field Emission Gun Electron Microscopy at 10 kV and 13 pA (FEI

Company, Oregon, USA).

2.6. Transmission Electron Microscopy

Transversal and longitudinal transmission electron microscopy (TEM) analyses of hypocotyl sections were performed. Hypocotyl samples were fixed in modified Karnovsky's solution as described previously. Samples were post-fixed for 1 h with 1% osmium tetroxide and then contrasted in bloc with 0.5% uranyl acetate overnight, dehydrated in an acetone concentration series [30, 50, 70, 80, 90 and 100% (three times)], infiltrated and polymerized onto Spurr low viscosity epoxy resin. Sections (70 nm thick, Diamond Knife) were obtained using an ultramicrotome MTX Powertome X (Boeckeler Instruments RMC Products, Egham, UK) and contrasted with 3% uranyl acetate and lead citrate. The analyses were performed using a JEOL JEM 1400 transmission electron microscope (Leica Microsystems Inc., Illinois, USA) in 80 kV.

2.7. Protein-Free Cell Wall (PFCW) Preparation

A total of 100 mg of hypocotyl powder was weighed into 2 mL microtubes. At each step, the samples were washed 5× with 50 mM of potassium phosphate buffer (pH 7.0), 5× with 0.1% Triton X-100 (pH 7.0), 4× with 1 M NaCl (pH 7.0), 4× with distilled water and 3× with acetone. A centrifugation was performed at 15,000 rpm for 2 min for each step. At the end, the pellets were oven dried (60 °C, 24 h). The obtained material was defined as protein-free cell wall fraction (PFCW) [79]. PFCW is free of water-soluble compounds (polar) and apolar compounds [6].

2.8. Lignin Content Determinations

Lignin contents were determined using 20 mg of PFCW by the acetyl bromide method [79]. Quantification was carried out by the use of a standard curve with lignin alkali (Aldrich 370959) and the obtained absorbance value (ϵ) was 22.9 g L⁻¹ cm⁻¹. The results were expressed as mg lignin g⁻¹ PFCW.

2.9. Monomeric Lignin Composition

A total of 20 mg of PFCW were used and hydrolyzed with NaOH (4 M) at 95 °C overnight on a thermoblock. The samples were then acidified with HCl (6 M) and centrifuged at 13,000 rpm for 5 min. Next, two extractions using ethyl acetate were performed, storing the supernatant in a new tube. The solvent was evaporated using the thermoblock at 50 °C and the pellets were dissolved in deionized water [80]. The samples were then filtered through a 0.22 µm PTFE membrane and injected in an HPLC (Waters Alliance e2695 Separations Module and Waters 2998 Photodiode Array Detector; Waters Comp., Massachusetts, USA), using Discovery® HS C18 HPLC (15 cm × 4.6 mm; 5 µm) column. The mobile phase consisted of 4% methanol and 4% acetic acid (20:80 v/v), at 1.2 mL min⁻¹ under an isocratic mode for 20 min. Absorbances were monitored at 290 nm. *p*-hydroxybenzaldehyde, vanillin and syringaldehyde standards were used for quantification [79].

2.10. Cellulose Quantification and Calorimetric Analysis

Cellulose quantification were performed as described in [81,82]. Three hypocotyl segments from different seedlings were used for each sample. Cellulose concentrations were expressed as equivalent to glucose concentration (µmol glucose g⁻¹ DW) against a standard curve. Additionally, seedling accumulated energy was obtained using a Parr 6100 adiabatic calorimetric bomb (Parr, Instrument Company, Illinois, USA) following [37].

2.11. Hormone Profiling

Hormone levels were quantified by ultra high-performance liquid chromatography coupled to tandem mass spectrometry (UPLC/ESI-MS/MS) as described in [83]. Briefly, freeze-dried hypocotyl seedlings (20 mg) were extracted in a 2 mL microcentrifuge tube with 500 µL of the extraction solvent (ice-cold methanol 100%) using ultra sonication (4–7 °C) for 30 min. Then, after centrifugation at 12,000 rpm for 10 min at 4 °C (centrifuge MR18–22, Jouan, Saint-Herblain, FR), the pellet was re-extracted as above and the resulting supernatants were pooled and filtered through a 0.22-µm PTFE filter (Waters, Milford, Massachusetts, USA) before UHPLC-MS/MS analyses. The endogenous contents of the hormones auxin indole-3-acetic acid (IAA), the cytokinins *trans*-zeatin (*t*-Z), its riboside (*t*-ZR), isopentenyl adenosine (IPA) and 2-isopentenyl adenine (2iP), the bioactive gibberellins GA₁, GA₃, GA₄, GA₇, abscisic acid (ABA), jasmonic acid (JA), salicylic acid (SA) and melatonin (MEL) were quantified using deuterium-labelled compounds as internal standards.

2.12. Attenuated Total Reflection Fourier Transform Infrared Spectroscopy (ATR-FTIR/) Analysis

Fourier transform infrared spectroscopy was performed on oven-dried (70 °C) hypocotyl samples on a Bruker Vertex 70v FTIR spectrometer (Bruker Optik GmbH, Ettlingen, DEU) with a platinum attenuated reflectance accessory (ATR). The spectra were obtained from 4000 to 400 cm⁻¹ with a spectral resolution of 4 cm⁻¹. Two replications were performed for each sample and each spectrum was composed of an average of 300 scans. All measurements were carried out at room temperature (25 °C). Standard cellulose and lignin were also analyzed. A multivariate principal component analysis (PCA) was run using total (or portion) spectra.

2.13. Cellulose Microfibrils Orientation by SAXS Analysis

Ultra-high resolution small angle X-ray scattering (SAXS) was performed on fresh hypocotyl samples using a Xenocs 2.0 (Xeuss, Sassenage, FR), equipped with a Dectris PILATUS 300 K detector and Cu K α source of radiation with a wavelength of 0.154 nm (50 kV, 0.6 mA and 600 s). The beam diameter was of 400 µm. Sample-detector distance was of 986 mm (~1 m). The samples were measured in an air chamber, with the long axis of the hypocotyl perpendicular to the incident X-ray microbeam. Ag-Behenate and vitreous carbon were used as calibration standards. Azimuthal intensity profiles of the diffraction patterns were obtained by radially integrating the intensity with an azimuthal step size of 1°. The detail simulation, fitting procedure and calculation of the azimuthal position cellulose microfibril angle in a cell wall model were exactly as described in Rüggeberg et al [72] and Saxe et al [57].

2.14. Statistical Analyses

A One-Way ANOVA was used for mean comparisons of quantitative data. Statistical significances were considered when $p < .05$ [84]. Duncan's post-hoc test was applied to compare treatments (white light, blue light, green light, red light, far-red light and dark). Pearson's correlation test was also applied to test for significant relationships between response variables. A principal component analysis (PCA) was performed with the spectroscopy data [85]. All statistical analyses were carried out using the Statistica 10® (Statsoft Inc., California, USA) software package. All graphs were prepared using the Sigma Plot 10.0 (Systat Inc., California, USA) software.

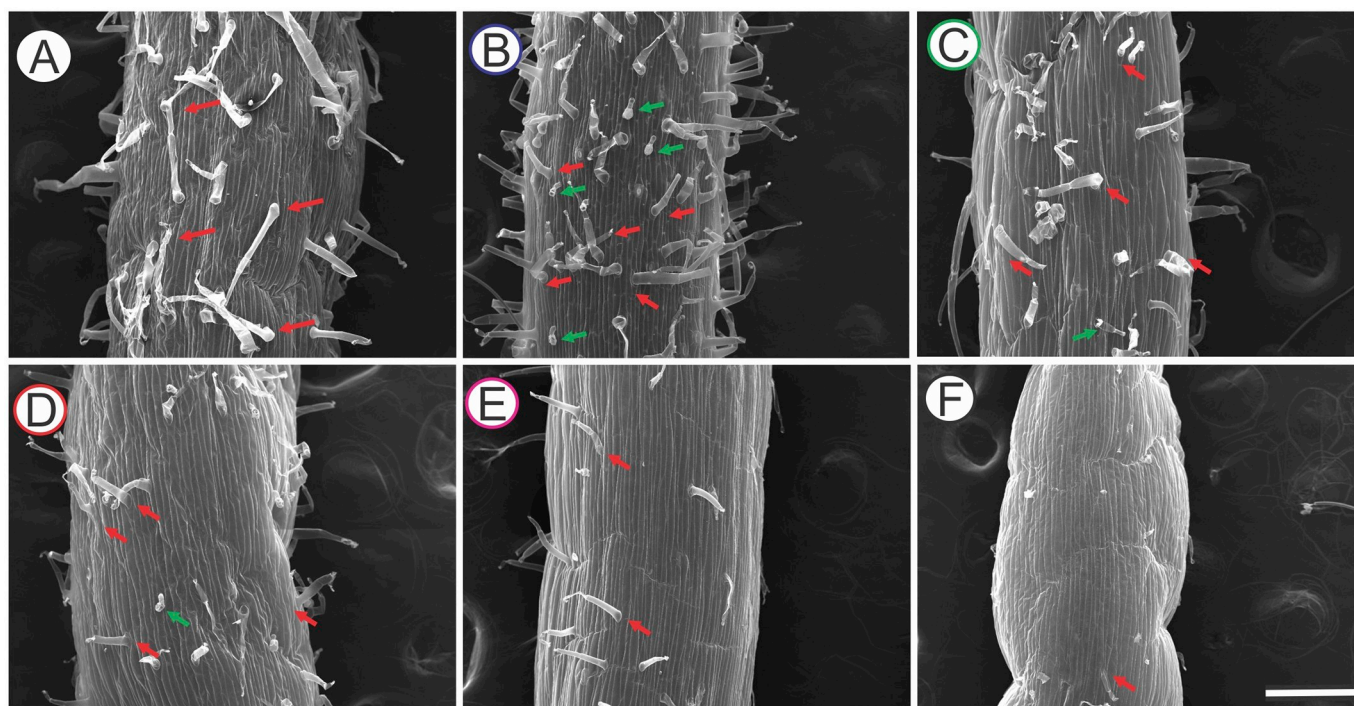


Fig. 2. Scanning electron microscopy from the medial section of tomato hypocotyls 10 days after the beginning of the treatments. Red arrows point to tector trichomes and green arrows points to glandular trichomes. (A) white light, (B) blue light, (C) green light, (D) red light, (E) far-red light, (F) dark. Scale bar = 250 μ m. (For interpretation of the references to colour in this figure legend, the reader is referred to the web version of this article.)

3. Results

3.1. Morphological Seedling Alterations

Tomato seedlings growing under distinct light qualities presented distinct hypocotyl lengths, shorter when grown under blue light (BL) and longer in the dark. Intermediate values were found under white (WL), green (GL), red (RL) or far-red (FR) lights (Fig. 1). Moreover, hypocotyl growth was highly correlated with cell length (Fig. S1). Additionally, all light-grown seedlings accumulated photosynthetic pigments and BL stimulated anthocyanin hypocotyl accumulation (Fig. S2). Higher Chl *a/b* ratios were detected under BL, lower under FR (Fig. S2, inset). FR grown seedlings maintained closed embryonic leaves, but opened the apical hook. In the dark, a typical etiolated phenotype developed (Fig. 1; Fig. S1, S2).

BL stimulated trichome development (both tector and glandular) in tomato hypocotyls, while reduced amounts of trichomes were observed under GL and RL. Sporadic trichomes were found in FR, rare in the dark (Fig. 2).

Light microscopy of a transversal section of hypocotyl displayed a single-layered protoderm in all treatments (Fig. S3). Increased hypocotyl diameter (Fig. 2, Fig. S3 and Table 1) was observed when plants were grown under RL and FR. These responses were related to increased cortical parenchyma thickness, but not to number of cells (Table 1). Fluorescence microscopy using double staining demonstrated that lignin is deposited in xylem fibers and protoxylem cells. In addition, xylem cells displayed higher differentiation under BL and WL in comparison to plants grown in the dark. Moreover, Calcofluor Bright White 28 dye demonstrated that the parenchyma and phloem cell walls are mainly formed by a cellulose polymer (Fig. S3).

3.2. Cell Wall Structure

BL stimulated cell wall thickness (256.8 nm), at three times the thickness than FR, at a thickness of 80.5 nm (Fig. 3, Table 1). Cell walls under WL were also considered thick (223.9 nm). WL encompassed

18% of blue light (430–485 nm) and stimulated cell wall thickness while under RL or GL was approximately half times thinner than under BL (160.5 nm, 131.5 nm, respectively). In addition, an increase in middle lamella thickness and cell wall electron density under BL and WL in comparison to dark was observed (Fig. 3). Energy-dispersive X-ray spectroscopy (EDS) of the elemental cell wall composition indicated 45.5% of Ca under WL, 36.1% under BL, 10.3% under FR and 16.1% in the dark (Fig. S4). Intermediate values were found for GL and RL growths. No obvious relationship were identified for the others elements (Fig. S4).

The longitudinal TEM analysis, with progressive magnifications from 40,000 \times to 200,000 \times (Fig. 4) aided in understanding the organization, arrangement and electron density variation of the cellulose microfibrils, which were lined up perpendicularly in the primary cell wall to the middle lamella (ML). Microfibrils displaying higher electron density were evidenced under WL and BL, being smaller-spaced between each other under BL (Fig. 4). Microfibrils were well organized circumferentially in short hypocotyls under WL and BL, but the degree of disorganization increased under GL and RL. These structures were highly disorganized (randomly deposited) in the inside surface (newer layer) and parallel to the elongation axis on the outside (older layer) under FR or in the dark. It is important to note that seedling hypocotyls growing under FR or in the dark were longer, with lengthy cells (Fig. 1, S1). A very high and negative correlation was found between cell wall thickness and hypocotyl length (Fig. 5). Microtubules were observed in some TEM images, following a similar orientation pattern to that of cellulose microfibrils (data not shown).

In order to adequately evaluate macro- and microfibril orientations in the primary cell wall, an ultra-high resolution field-emission-gun scanning electron microscopy (FEG-SEM) was performed on the inner cell wall surface of cortical parenchyma cells (Fig. 6). The cell wall texture indicated that the inner microfibril layer is deposited lining up and in a juxtaposed and more organized manner under BL and RL and randomly deposited in FR and in the dark. The inner surface cell wall formed under WL or GL, which display a transitional texture between BL and the dark, presented loose but organized and arranged in non-

Table 1
Anatomical measurements from transversal tomato hypocotyl sections 10 days after the beginning of the treatments (white light, blue light, green light, red light, far-red light, dark). Data were collected by light microscopy, fluorescence microscopy, transmission electron microscopy and scanning electron microscopy. Different letters following the means indicate statistical differences between treatments by Duncan's test ($p < .05$). ($n = 30 \pm SE$).

Treatments	Hypocotyl diameter (μm)	Protoderm thickness (μm)	Cortical parenchyma thickness (μm)	Radial number of parenchyma cell (units)
White	760.78 \pm 5.14	B 30.17 \pm	223.82 \pm 1.03	A 3.02 \pm 6.17
Blue	757.17 \pm 14.06	B 28.63 \pm	252.13 \pm 0.97	AB 4.50 \pm 6.07
Green	705.86 \pm 6.60	C 26.86 \pm	216.27 \pm 0.89	B 2.53 \pm 5.87
Red	811.08 \pm 8.62	A 30.58 \pm	261.52 \pm 0.70	A 2.22 \pm 6.40
Far-red	814.64 \pm 13.35	A 31.08 \pm	280.12 \pm 1.00	A 4.11 \pm 5.67
Dark	629.98 \pm 8.08	C 19.44 \pm	204.52 \pm 0.61	C 5.75 \pm 6.03

Treatments	Radial number of parenchyma cell (units)	Diameter of vascular cylinder (μm)	Number of xylem cells (units)	Cell wall thickness (nm)
White	0.12 \pm AB	102.41 \pm	12.33 \pm A	223.88 \pm B
Blue	0.08 \pm B	107.51 \pm	10.00 \pm A	256.80 \pm A
Green	0.08 \pm BC	87.10 \pm	9.00 \pm B	131.50 \pm D
Red	0.12 \pm A	87.88 \pm	10.33 \pm B	160.53 \pm C
Far-red	0.12 \pm C	92.58 \pm	10.00 \pm B	80.50 \pm F
Dark	0.13 \pm B	64.60 \pm	12.33 \pm C	90.95 \pm E

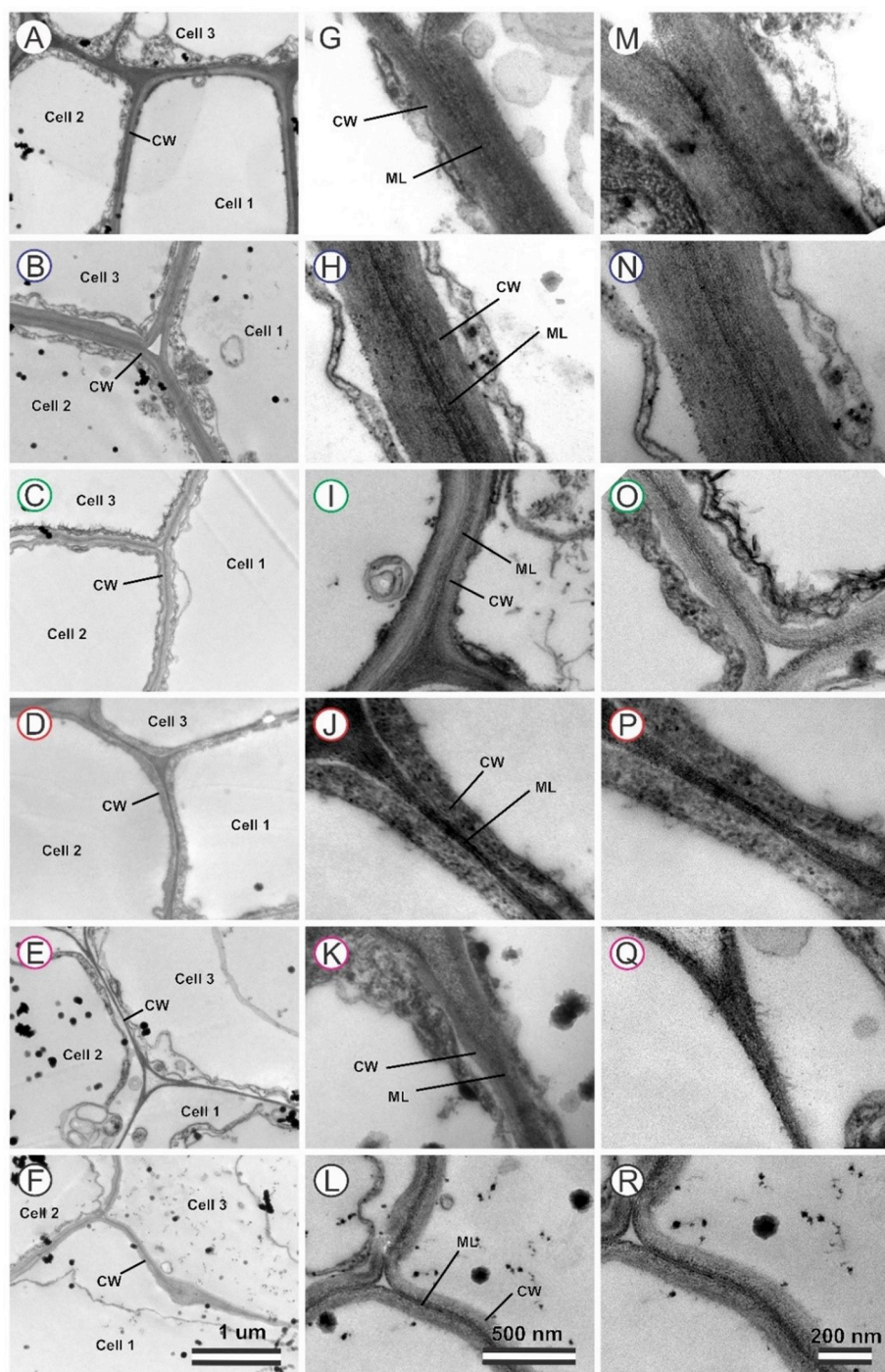


Fig. 3. Transmission electron microscopy of a transversal section of cortical parenchyma cells showing the primary cell wall of tomato hypocotyls 10 days the beginning of the treatments. (A, G, M) white light, (B, H, N) blue light, (C, I, O) green light, (D, J, P) red light, (E, K, Q) far-red light, (F, L, R) dark. Alterations in cell wall thickness and differences in cell wall (CW) and middle lamella (ML) electrondensities are highlighted. Micrographs on the same column are on the same scale. From left to right, scale bar = 1 μm , 500 nm and 200 nm. (For interpretation of the references to colour in this figure legend, the reader is referred to the web version of this article.)

random inward spaces. The responses stimulated by FR and in the dark (Fig. 6E, F) displayed an apparent disruption of cellulose macro- and microfibrils.

3.3. Microfibril Angle Distribution Measurements by SAXS

Ultra high resolution small angle X-ray scattering (SAXS) (Fig. 7) was performed to deeply evaluate MFA in the entire hypocotyl section (Fig. S3), instead of the wall texture of the inner cell wall surface of cortical parenchyma cells (Fig. 6). The SAXS analysis revealed distinct X-ray scattering patterns among different light qualities (Fig. 7A). For plants grown under WL and BL, GL and RL, FR and in the dark the pattern were similar between respective treatments. A higher scattering

intensity concerning the azimuthal angle was verified for seedlings grown in the dark for angles between 160° and 190° (Fig. 7C). Modeling X-ray scattering distribution following Rüggeberg et al [57] and Saxe et al [72] allowed for estimations of the relative contribution of MFA (Fig. 7B). MFA revealed a high frequency of angles smaller than 30° (0.001° - 30°) for all treatments, of 54.1% under WL, 51.4% under BL, 51.3% under GL, 51.5% under RL, 64.9% under FR and 65.1% in the dark. 0° indicates parallel to the elongations axis and 90° , orthogonal to the elongation axis. In the dark and under FR, peaks at 3.5° and 5.0° , respectively, were observed, while the peak appears between 10.5° and 12.0° under other lights (Fig. 7B). On average, considering the entire transversal hypocotyl section, a minor frequency of high angles (aleatory distribution) concerning cellulose microfibril distribution was

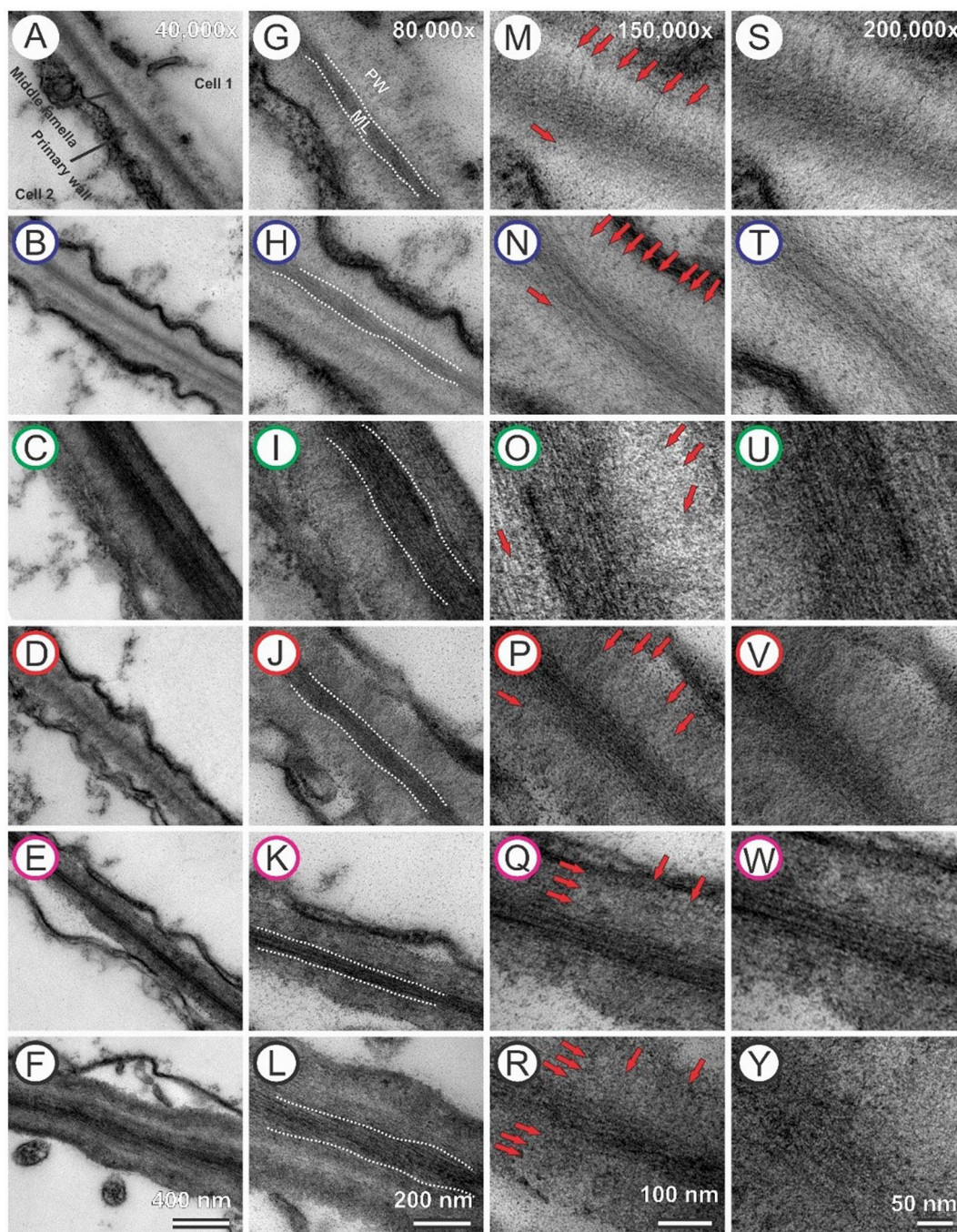


Fig. 4. Transmission electron microscopy of a longitudinal section of cortical parenchyma cells showing the primary cell wall of tomato hypocotyls 10 days after the beginning of the treatments. Red arrows highlight alterations in cellulose microfibril orientation, distribution and distance from each other. (A, G, M, S) white light, (B, H, N, T) blue light, (C, I, O, U) green light, (D, J, P, V) red light, (E, K, Q, W) far-red light, (F, L, R, Y) dark. Micrographs on the same column are on the same scale. From left to right, scale bar = 400 nm (40,000 \times), 200 nm (80,000 \times), 100 nm (150,000 \times), 50 nm (200,000 \times). Differences in electron density distinguish the primary cell wall (PW) from the middle lamella (ML) or plasma membrane. (For interpretation of the references to colour in this figure legend, the reader is referred to the web version of this article.)

observed in the dark and under FR.

3.4. Cell Wall Composition

Cellulose (Fig. 8A) and lignin contents (Fig. 8B), including monomeric lignin composition, (Fig. S5) were statistically different in seedlings grown under different light treatments ($p < .05$). Particularly, cellulose levels were higher by 163.9% and 76.3% in the dark and under FR compared to WL, whilst WL, BL, GL or RL plants were similar ($p > .05$). In contrast, lignin content was reduced ($p < .05$) by a

52.85% in the dark and by 19.47% under FR compared to WL, whilst slightly higher ($p < .05$) values were observed under GL. A strong and negative linear correlation ($r = -0.9572$; $p < .001$) was observed between cell wall cellulose and lignin contents (Fig. 8A, inset).

Monomeric lignin composition varied ($p < .05$) when comparing WL (or the other imposed lights) to the dark (Fig. S5). Under FR and in the dark, 22.9% and 35.2% decreases in *p*-hydroxybenzaldehyde (H units, Fig. S5A), were observed, respectively. In addition, 28.8% and 49.5% increases in guaiacyl (G units, Fig. S5B) and 67.3% and 90.5% in syringyl content (S units, Fig. S5C) were observed under FR and in the

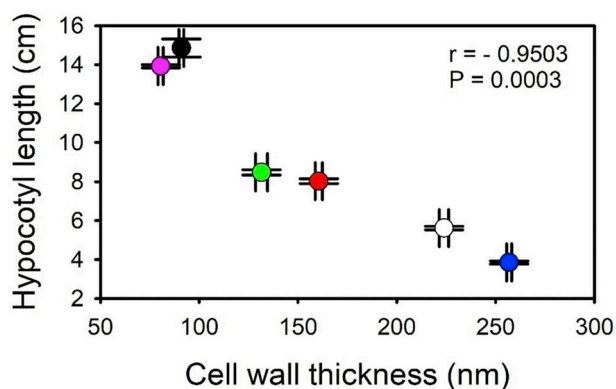


Fig. 5. Linear correlation between cell wall thickness and hypocotyl length. Different colored dots represent different light treatments (white light, blue light, green light, red light, far-red light, dark). ($n = 6 \pm SE$). (For interpretation of the references to colour in this figure legend, the reader is referred to the web version of this article.)

dark, respectively. Given that H units decreased and S units increased with increasing imposed wavelengths, the S/H ratios changed significantly ($p < .05$), 125.0% and 200.2% higher under FR and in the dark, respectively, compared to WL (Fig. S5D).

In order to broadly evaluate cell wall composition, attenuated-total-reflectance Fourier-transform-infrared spectroscopy was carried out on dried seedlings. A multivariate principal component analysis (PCA) from wavenumbers 4000 to 400 cm^{-1} (Fig. 8C) discriminated FR and the dark to the other treatments with grouped clusters (Fig. 8D), in which the principal component (PC) 1 score explained 55% of the total of data variation. The vibrational modes between the bands at 1460–1290 cm^{-1} are strongly associated to compounds such as cellulose (Fig. 8F), hemicellulose and pectin. PC1 explained 95% of total variation whose clusters are completely separated by others,

distinguishing the clusters formed from seedlings grown under FR and in the dark from those grown under WL, BL, GL and RL (Fig. 8E). In this range, the 1428 cm^{-1} vibrational wavenumber was associated to the symmetrical angular deformation of the $-\text{CH}_2$ group and the angular deformation of the C=O and C–H bonds, forming polysaccharide molecules. At 1336 cm^{-1} , the flexural vibration of the C–H and C=O stretching symmetric in polysaccharides is highlighted.

The ATR-FTIR analysis of seedlings growing under FR and in the dark also indicated alterations in vibrational wavenumbers from 3100 to 3000 cm^{-1} , associated to = C–H stretching symmetric in aromatic and phenolic compounds (Fig. 8, arrow), mainly lignin, since this region is characteristic of the reference lignin spectrum (Fig. 8F). However, other vibrational wavenumbers indicate vibrational modes for phenol compounds and aromatic groups (1750–1700 cm^{-1}), such as 1750–1735 cm^{-1} associated to saturated aliphatic esters (C=O stretching), 1740–1720 cm^{-1} , associated to saturated aliphatic aldehydes (C–C) and α , β -unsaturated esters or 1715 cm^{-1} , related to saturated aliphatic ketones (Fig. 8).

As a result of the total variation in seedling composition (mainly lignin), higher accumulated energy was detected in seedlings grown under BL and lower accumulated energy was detected under FR or in the dark. Intermediate accumulated energy values were observed for the other treatments (Fig. S6).

3.5. Hormone and Hormone-Related Molecule Profiling

Hormonal profiling evaluated by UPLC/ESI-MS/MS revealed variations in seedlings grown under distinct light qualities and in the dark (Fig. 9, Fig. S7). Abscisic acid contents were higher ($p < .05$) under BL and RL and lower ($p < .05$) under FR and in the dark. Melatonin was also higher under BL, while lower contents were found under GL or in the dark. Jasmonic acid contents were reduced under BL. Salicylic acid contents were lower under WL compared to BL, GL and FR. *trans*-Zeatin levels were higher under WL, BL and RL while the lowest contents corresponded to seedlings grown in the dark and intermediate levels

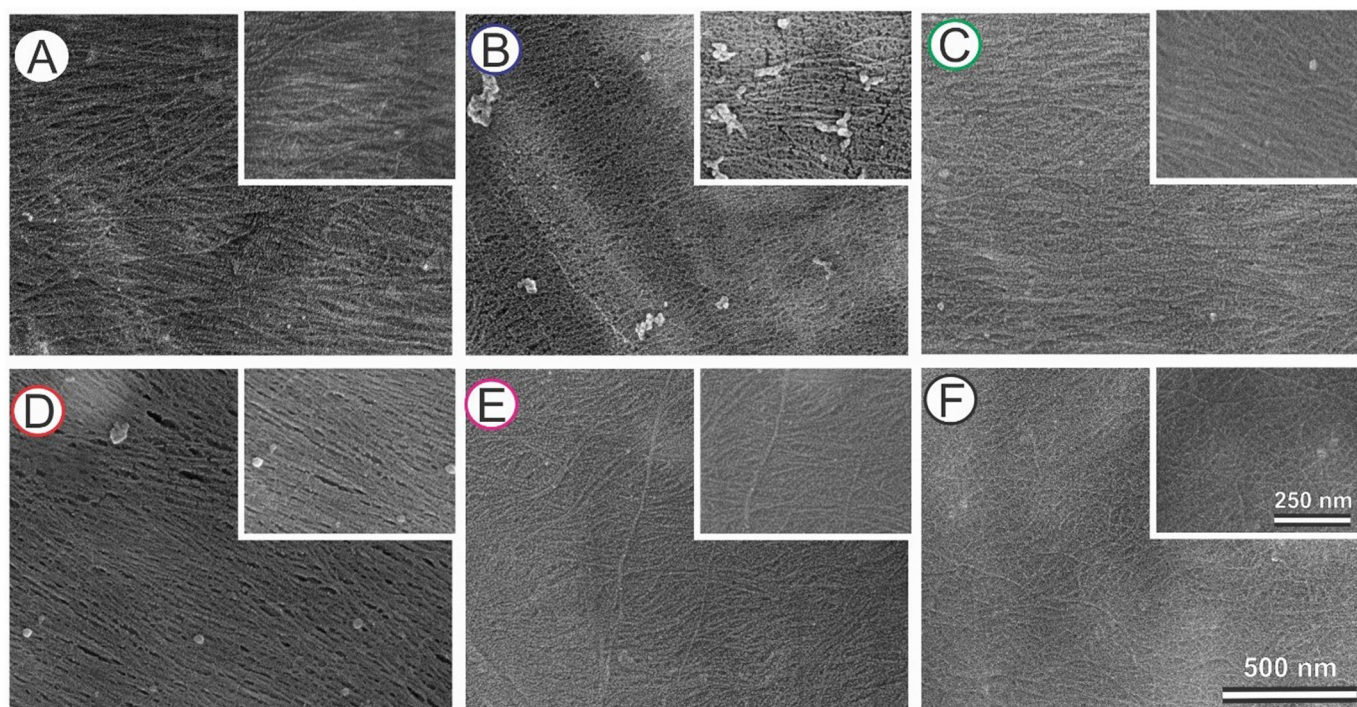


Fig. 6. Scanning electron microscopy by ultra-high resolution field emission gun (FEG-SEM) showing the inner surface of cortical parenchyma cells of tomato hypocotyls 10 days after the beginning of the treatments. Images highlight cellulose macro- and microfibrils depositions on the primary cell wall. (A) white light, (B) blue light, (C) green light, (D) red light, (E) far-red light, (F) dark. Scale bar = 500 nm and inset 250 nm. (For interpretation of the references to colour in this figure legend, the reader is referred to the web version of this article.)

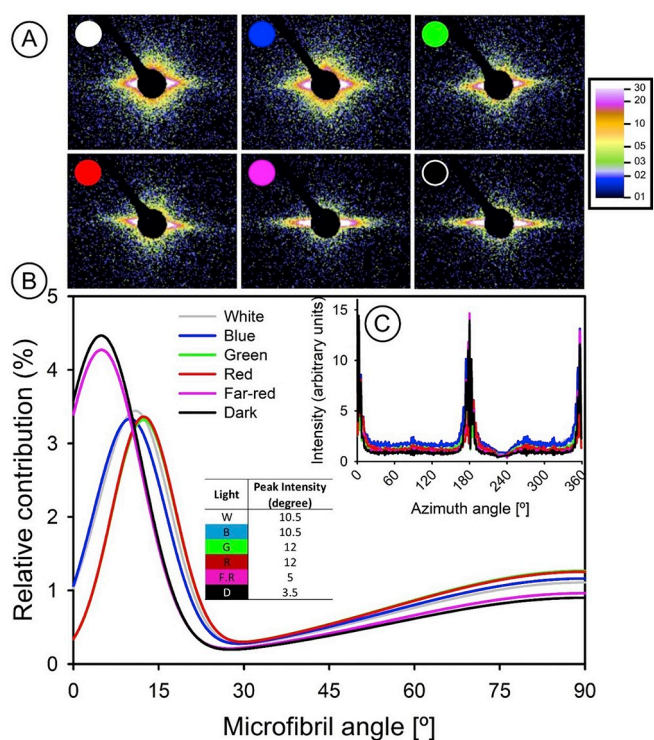


Fig. 7. Ultra-high resolution small angle X-ray scattering (SAXS) of fresh tomato hypocotyls 10 day after the beginning of the treatments (white light, blue light, green light, red light, far-red light, dark). (A) 2D scattering image: a 360° azimuthal integration was used to obtain degree and intensity relationship (1D). The scattering signal originates from the electron density contrast between cellulose microfibrils and water. The colour scale indicates the scattering signal intensity. (B) Relative contribution of each cellulose microfibril angle to the simulated scattering signal. The microfibril orientation from 0° is longitudinal towards the cell axis to 90°, transverse to the longitudinal axis of the cell. (C) Integrated scattering signal (measured data) can be fitted by microfibril angle when simulated by the model proposed by Rüggeberg et al [72] and Saxe et al [57]. The inset table indicates peak intensity angle or location of the MFA distribution maximum. (For interpretation of the references to colour in this figure legend, the reader is referred to the web version of this article.)

between both were observed under GL and FR. In contrast, *trans*-zeatin-riboside presented the lowest values under WL and higher values under GL and in the dark. GL strongly inhibited isopentenyladenosine (−53.4%) and isopentenyladenine (−78.3%) accumulations compared to seedlings grown in the dark. Indole-3-acetic acid (IAA) levels were higher under BL by 625.7% and under FR by 545%, while intermediate values were found under WL, GL and RL and, the lowest values occurred in the dark.

Active gibberellin GA₁ and GA₃ contents were reduced under GL compared to WL and in the dark. In contrast, GA₃ accumulated under RL (320.3% compared to dark) and under FR (495.1% compared to dark), while GA₄ levels were around 30-fold higher than other active gibberellins, with relatively unchanged contents among treatments, with the exception of a slight decrease observed under RL ($p < .05$). GA₇ contents were reduced under RL and in the dark.

4. Discussion

4.1. Seedling Development

Tomato seedling growth assays carried out under different light qualities and in the dark revealed many cell wall structure and composition alterations. Cryptochrome (CRY) activation by BL [18,19,86,87] strongly represses hypocotyl length and phytochrome

(PHY) B by RL [11,16,88,89] also acts in the same manner when compared to FR (Fig. 1), repressing cell enlargement. Notwithstanding, the signaling cascade promoting by CRY or PHY are different [90,91]. However, a weak action of PHYA under FR [17] does not completely repress the etiolated phenotype. Growth under FR results in seedlings that accumulate certain photosynthetic pigments, but do not stimulate embryonic leaf growth, and seedlings with elongated hypocotyls, although shorter than completely etiolated dark-grown seedlings (Fig. 1). In addition, FR represses PHYB and induces peroxidase and expansins activities [92], probably related to cell wall expansion.

Activation of CRY proteins promotes many developmental alterations, including trichome development (Fig. 2) and primary cell wall thickening (Fig. 3) as well as secondary wall thickening [7], not only under BL but also under WL (which encompass 18% of BL). GL (555 nm) activate CRY proteins in a very weak manner [16,23]. Trichome development may be associated to R2MYB proteins (cell cycle regulation) [93,94] with the influence of other hormonal effects [10,95–97]. The way in which the signaling cascade leads BL to promote trichome development is uncertain.

4.2. Cell Wall Structure

Smaller hypocotyls (Fig. 1) were associated to highly circumferentially organized cell wall cellulose microfibril arrangements, with smaller spaces between each other when under BL (Fig. 4). As the cell elongates, the spaces become larger, as observed for WL. Strikingly, randomly deposited cellulose microfibrils in the inner cell wall surface were found under FR and in dark-grown seedlings (Fig. 6). These responses raise a question of whether the inside layer of cellulose microfibril in the cell wall is associated to (an)isotropic growth or cell enlargement. In general, the inner layer (most recent) of cellulose microfibril organization in the cell wall was unrelated to cell length. In contrast, the outer layers of microfibrils were parallel to the elongation axis under FR and in the dark. The longitudinal TEM images and SAXS data indicate that microfibrils passively realign as the cell axis grows. Cell wall deposition continues as the cell expands. If the newer layers are randomly deposited and older layers are parallel to the elongation axis, this suggests that cellulose microfibrils reorganize during cell elongation, agreeing with the multinet growth hypothesis (hypothesis #1).

Hypothesis #2, which states that microfibrils do not passively reorientate, indicating failure in microfibril angle changes, and do not control longitudinal growth, seems improbable. This would make sense if only the inner layer (wall texture) were analyzed (Fig. 6). Inner surface show random pattern of microfibrils deposition on lengthy cells, then new layer seems to be disconnected from older layers. When including high magnification longitudinal TEM and accurately evaluating relative MFA contribution in the whole cell wall, hypothesis #1 (multinet growth), which states that older layers become reoriented, seems plausible. Herein, we have demonstrated microfibrils parallel to each other and parallel to the elongation axis in the outer layers. The ultra-high resolution small angle X-ray scattering (SAXS) analysis of the entire hypocotyl section revealed that, on average, a high frequency of signals around 0° and around 180°, modeled following Rüggeberg et al [72] and Saxe et al [57], indicate a high frequency of small angles (close to the parallel to elongation axis) between cellulose microfibrils and the longitudinal cell wall. The low relative contribution of high angles (randomly orientated) in seedlings growing under FR and in the dark (Fig. 7) would be associated to newer layers deposited after cell elongation. Intermediate (between blue and dark) 2D X-ray scattering signals (Fig. 7) and reorientation degrees of cellulose microfibrils (Fig. 4) were observed under GL and RL.

Physically, cell growth required a flexible cell wall and turgor pressure [36,98–100]. Thus, how does light affect cell wall flexibility? There is not a simple answer [36]. IAA supplementation presumably stimulates acid growth through the stimulation of H⁺ATPases and

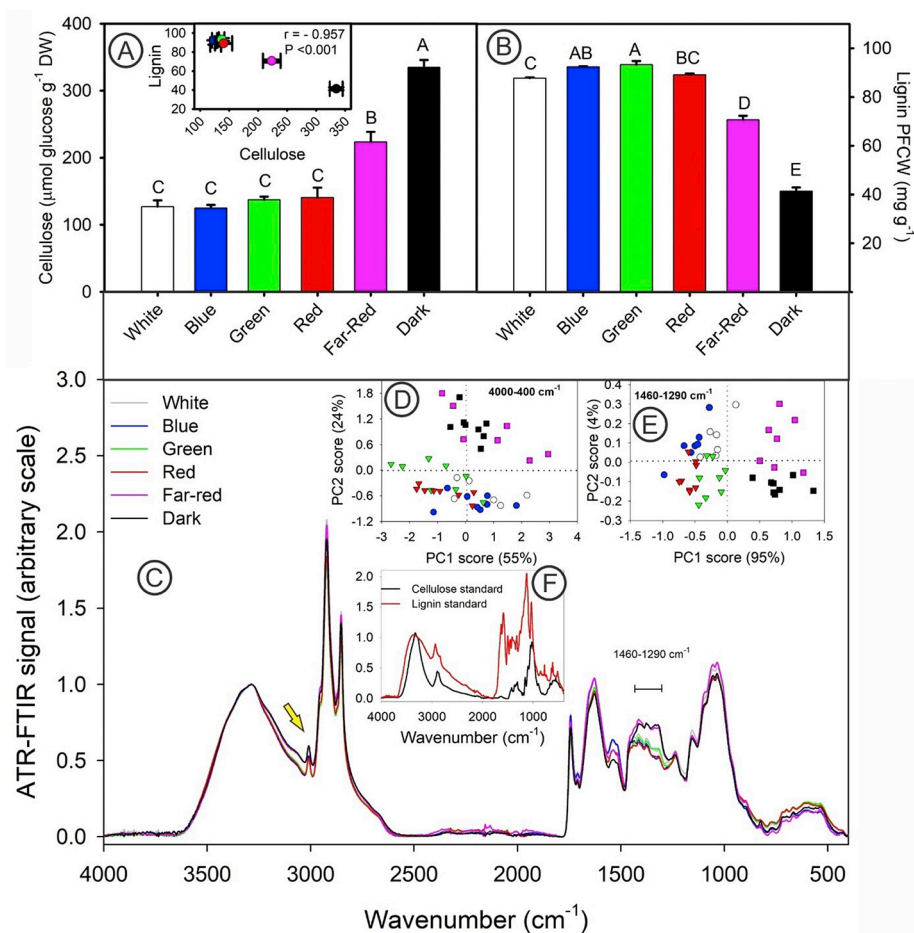


Fig. 8. (A) Cellulose content in tomato hypocotyls. (B) lignin content in protein-free cell wall (PFCW). The inset indicates the linear correlation between cellulose and lignin contents. (C) normalized ATR-FTIR spectra ($4000\text{--}400\text{ cm}^{-1}$) from dried tomato hypocotyls 10 days after the beginning of the treatments (white light, blue light, green light, red light, far-red light, dark). (D) Principal component analysis from entire spectra ($4000\text{--}400\text{ cm}^{-1}$) and (E) from $1460\text{ to }1290\text{ cm}^{-1}$ (mainly cellulose, hemicellulose and pectin associations). (F) Standard cellulose and lignin reference spectra ($4000\text{--}400\text{ cm}^{-1}$). Each spectrum is an average of two measurements for four different samples. The standard error was omitted for clarity. The yellow arrow at the $3100\text{--}3000\text{ cm}^{-1}$ band is lignin-associated. Reference value $3300\text{ cm}^{-1} = 1.0$. (For interpretation of the references to colour in this figure legend, the reader is referred to the web version of this article.)

expansins [101], resulting in a loose cell wall, but IAA stimulated hypocotyl elongation under FR and in the dark only marginally, or in circumstances where the cell wall was thin. These data indicate that endogenous IAA levels under BL and FR were similar (Fig. 9), but parenchyma cells displayed different cell wall thickness (Fig. 3) and lengths (Fig. 1, Fig. S1). Gibberellic acid supplementation stimulated growth under BL, not IAA (Fig. S8). Taken together, these results point to a concerted action of many factors regarding cell wall structure and composition, which, in turn, influence cell growth, not only a simple hypothesis of acid growth induced by IAA [101]. A strong and negative correlation ($r = -0.95$) was observed between cell wall thickness and hypocotyl growth. Thus smaller hypocotyl lengths would result in thicker walls as noted under BL and WL growth. IAA expansin-induced action [102] was not sufficient to stimulate growth in thick cell wall conditions. A high cytoskeleton organization associated to cellulose microfibril orientation induced by GAs [20,31,43,49–52] may possibly explain growth under BL.

A degree of cellulose fragmentation becomes significant in thin cell walls, as observed under FR or in the dark. Theoretically, a randomly deposited layers of cellulose microfibril should repress longitudinal growth promoting isotropic instead of anisotropic growth [31,34]. Evidence of cellulose loosening was found when IAA induced growth only under specific treatments, not in general (Fig. S8), particularly at under FR and in the dark. Similarly orientated cellulose microfibrils when deposited by cellulose synthases allow for the formation of larger diameter macrofibrils [103]. It is predicted that significant conformational changes take place when microfibril aggregation occurs [104]. The formation of aggregates and macrofibrils indicates rigidity and compaction [52,104,105]. These aggregates hamper glucanase and expansins activities and the hydrolysis of oriented and randomly

deposited microfibrils is easier than macrofibril hydrolysis [106]. Thus, it is plausible that cellulose fragmentation (and loosening) under BL becomes insignificant and explains why IAA supplementation does not stimulate cell growth. Taken together, this evidence indicates that cellulose microfibrils do not fragment during cell expansion in thicker cell walls.

4.3. Cell Wall Composition

The EDS analysis indicated high Ca cell wall levels under WL and BL and low levels under FR and in the dark (Fig. S4). Ca and pectin complex and form Ca-pectate. Divalent ions form cross-links between non-esterified negative charged carboxyl (COO⁻) groups. Calcium cross-links play a structural role in cell walls [107,108]. A pectin gel-like matrix is important for cell adhesion by the middle lamella and makes the primary cell wall less extensible, which, in turn, may influence cell wall ion concentrations and electronegativity. Hydrophilic pectins gels and hemicellulose can bind to microfibrils. Decreased primary wall thickness was related to high cellulose (Fig. 8) and lower middle lamella pectin contents, and is associated with flexible, looser and fragile walls, which would, in turn, allow for greater expansion [109]. Around three-fold higher Ca was found in thicker cell walls (WL and BL) compared to thinner counterparts (FR and dark), which may be related to extra crosslinks that significantly reduce cell wall flexibility [109].

A negative correlation between cellulose and lignin contents was observed (Fig. 8). Likewise, cellulose deficient mutant plants typically show increased lignification [30,110,111]. Not only was a lignin content reduction observed under FR and in the dark, but also decreased H monomer and increased G and S contents, where PHY action is suggested. Indeed, S/H ratio variations along treatments (Fig. S5) point to

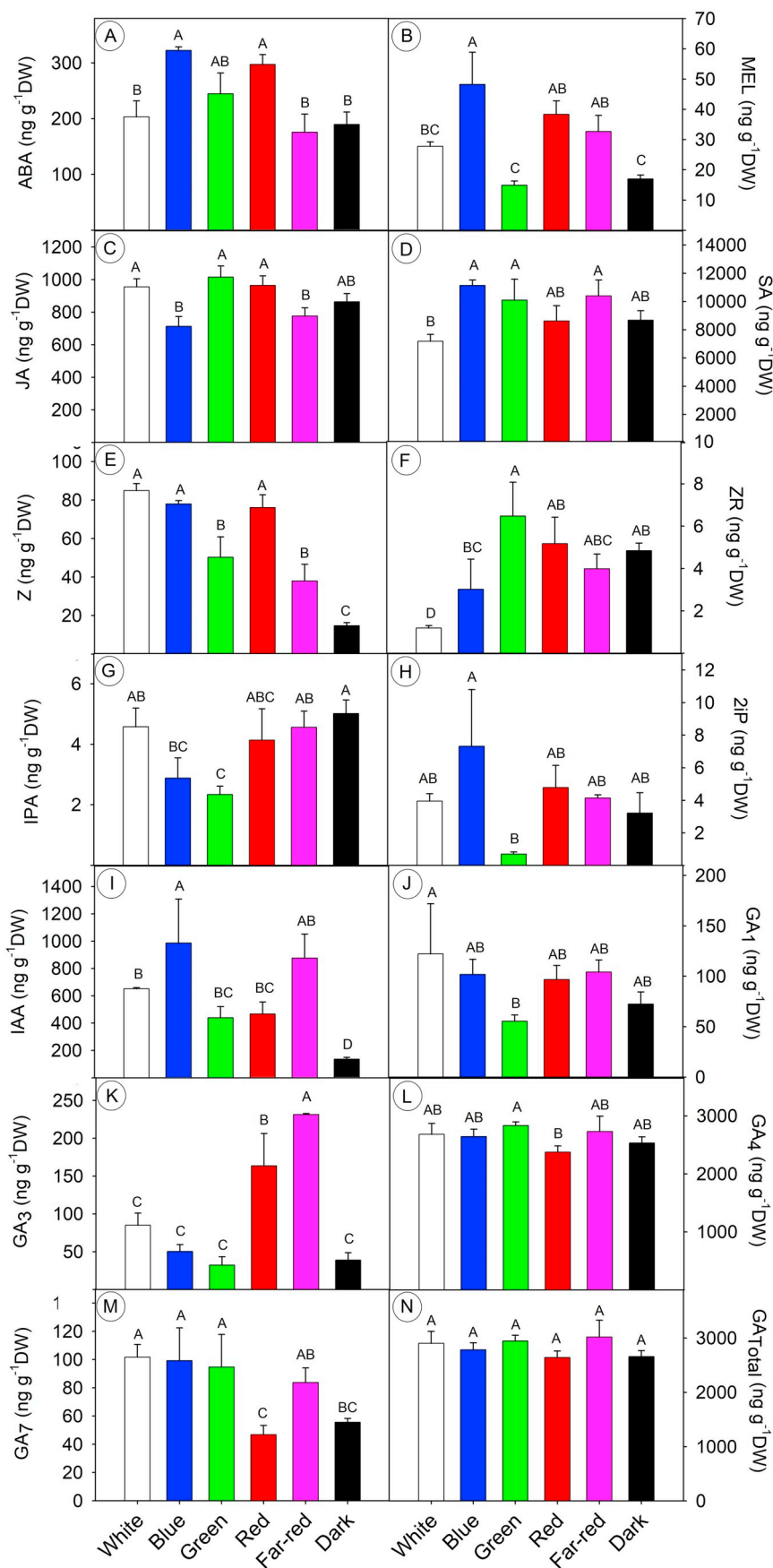


Fig. 9. Hormone profile of tomato seedlings 10 days after the beginning of the treatments (white light, blue light, green light, red light, far-red light, dark). (A) ABA: abscisic acid; (B) MEL: melatonin; (C) JA: jasmonic acid; (D) SA: salicylic acid; (E) t-Z: trans-zeatin; (F) t-ZR: trans-zeatin-riboside; (G) IPA: isopentenyladenosine; (H) 2iP: isopentenyladenine; (I) IAA: indole-3-acetic acid and (J-M) GAs (GA₁, GA₃, GA₄, GA₇ and GATotal): gibberellins. Bars represent the means of $n = 4 \pm SE$. Different letters above the bars indicate statistical differences between treatments by Duncan's test ($p < .05$). (For interpretation of the references to colour in this figure legend, the reader is referred to the web version of this article.)

the important role of PHYB in inducing H and repressing S biosyntheses. In contrast, PHYA induces S and represses H monomers. Some important steps in phenylpropanoids pathways [112], such as in CCR (Cinnamoyl-CoA reductase), which drives H monomer formation, in F5H (Ferulate 5-Hydroxylase) and HTC (p-Hydroxycinnamoyl-CoA:Quinate/Shikimate p-Hydroxycinnamoyltransferase), which drives S and G monomer formation, respectively should be candidates to be modulated by light quality, not only by light intensity [6]. Additionally, alterations in functional groups and cell wall composition (mainly cellulose/pectin and lignin) contributed significantly to accumulated energy alterations [113], which increased under BL and decreased under FR or in the dark.

4.4. Hormonal Effects

Hormonal contents varied widely among tomato seedlings grown under different light qualities. Some variations may be unrelated to cell wall biosynthesis, such as increased active cytokinin forms (and reduced conjugated *t*-Z; *t*-ZR), which have been reported as playing a role in chloroplast development and photosynthetic pigment accumulation [114]. Melatonin levels were closely related to anthocyanin accumulation under BL. Recently, [115] reported an upregulating effect of melatonin on anthocyanins, improving the stress resistance of cabbage during growth, especially in the presence of light. Thus, given that cryptochromes exposed to light tend to synthesize a higher amount of reactive oxygen species (ROS) [116], seedlings exposed to BL could stimulate melatonin synthesis and, in turn, anthocyanin synthesis, contributing to the total antioxidant capacity and, ultimately, to ROS scavenging. Increased isopentenyladenine (2iP) levels are observed during de-etiolation to photomorphogenesis [117]. Similarly results have been reported for tomato seedlings grown under BL whose de-etiolated phenotype is evident.

Total active gibberellins ($GA_1 + GA_3 + GA_4 + GA_7$) were unrelated to light treatment. It is also important to note the high amounts of GA_4 observed under all light regimes. Nonetheless, a negative response of a specific GA_3 was associated to cell wall thickness, where high levels were observed under FR and reduced content was found under WL and BL, except for the dark whose levels were low (Fig. 9, Fig. S7). No relationship was found for other active GA content concerning MFA and cell wall thickness. PHY activation under RL was related to reduced GA_3 , GA_7 , and also marginally to GA_4 , as well as to IAA compared to FR whose PHY is inactivated.

5. Conclusions

Many alterations were observed in primary tomato hypocotyl cell walls grown under different light qualities and in the dark. The most striking was random microfibril angle distribution in newer cell wall layers (inner surface) of seedlings grown in the dark or under FR light, whose cell walls are thin and presented low Ca content. However, parallel microfibril alignment was observed in older (outer) layers, indicating that cellulose microfibril realignment occurs during cell elongation, agreeing with the multinet growth hypothesis. In addition, a negative correlation was found between cell wall thickness, hypocotyl length and Ca content, indicating a certain degree of thickness and middle lamella interference concerning cell wall extensibility and cellulose microfibril reorganization.

Declaration of Competing Interests

The authors declare that they have no known competing financial interests or personal relationships that could have appeared to influence the work reported in this paper.

Author Contributions

RF, WCA, designed the experiment, performed analyses, and wrote the manuscript. TM, MPL, SMB, MSG, FS, AP, MCP, MEG, MR performed analyses and reviewed the manuscript.

Author Statement

Renan Falcioni: Conceptualization, Methodology, Investigation, Formal analysis, Writing, Funding acquisition, Review and Editing.

Thaise Moriwaki: Conceptualization, Methodology, Investigation, Formal analysis, Writing, Review and Editing.

Marina Perez-Llorca: Formal analysis, Review.

Sergi Munné-Bosch: Formal analysis, Review.

Mariana Sversut Gibin: Formal analysis, Review.

Francielle Sato: Formal analysis, Review.

Andressa Pelozo: Formal analysis, Review.

Mariana Carmona Pattaro: Formal analysis, Review.

Marina Ellen Giacomelli: Formal analysis, Review.

Markus Rüggeberg: Formal analysis, Methodology, Software, Review.

Werner Camargos Antunes: Conceptualization, Methodology, Investigation, Formal analysis, Writing, Funding acquisition, Review and Editing.

Funding

Scholarships granted by the Brazilian Government to RF (CNPq-GD 142218/2017-0) are gratefully acknowledged.

Acknowledgments

The authors would like to thank Prof. Dr. Cristiano LP Oliveira (University of São Paulo) for the SAXS analysis and Prof. Guinther Kellermann (Federal University of Paraná) for theoretical support concerning the SAXS measurements. Thanks are also due to professors from the State University of Maringá, namely Prof. Luiz F Cótica for the SEM, FEG-SEM, TEM laboratory facilities, Prof. Wanderley D Santos and Prof. Rogério Marchiosi for the lignin monomer analysis, Prof. Evanilde Benedito for the calorimetric analysis and Prof. Luiz A Souza for the anatomical review. This study was partially supported by Brazilian government finance research CNPq, CAPES, FINEP and Fundação Araucária. Scholarships granted by the Brazilian Government (R.F – CNPq–GD 142218/2017-0) are gratefully acknowledged.

Appendix A. Supplementary data

Supplementary data to this article can be found online at <https://doi.org/10.1016/j.jphotobiol.2019.111745>.

References

- [1] H. Smith, Light quality, photoperception, and plant strategy, *Annu. Rev. Plant Physiol.* 33 (1982) 481–518.
- [2] L. Huché-Théliet, L. Crespel, J. Le Gourrierec, P. Morel, S. Sakr, N. Leduc, Light signaling and plant responses to blue and UV radiations-perspectives for applications in horticulture, *Environ. Exp. Bot.* 121 (2016) 22–38.
- [3] M. Wada, K. Shimazaki, M. Iino, *Light Sensing in Plants*, 1st ed., Springer Japan, Japan, 2005.
- [4] Q. Wang, Q. Liu, X. Wang, Z. Zuo, Y. Oka, C. Lin, New insights into the mechanisms of phytochrome–cryptochrome coaction, *New Phytol.* 217 (2018) 547–551.
- [5] K.M. Folta, S.A. Maruhnich, Green light: a signal to slow down or stop, *J. Exp. Bot.* 58 (2007) 3099–3111.
- [6] R. Falcioni, T. Moriwaki, D.M. de Oliveira, G.C. Andreotti, L.A. de Souza, W.D. dos Santos, C.M. Bonato, W.C. Antunes, Increased gibberellins and light levels promotes cell wall thickness and enhance lignin deposition in xylem fibers, *Front. Plant Sci.* 9 (2018) 1–13.
- [7] Q. Zhang, Z. Xie, R. Zhang, P. Xu, H. Liu, H. Yang, M.S. Doblin, A. Bacic, L. Li, Blue light regulates secondary cell wall thickening via MYC2/MYC4 activation of the

- NST1 -directed transcriptional network in Arabidopsis, *Plant Cell* 30 (2018) 2512–2528.
- [8] S. Enriquez, K. Sand-Jensen, Variation in light absorption properties of *Mentha aquatica* L. as a function of leaf form: implications for plant growth, *Int. J. Plant Sci.* 164 (2003) 125–136.
- [9] G.-L. Wang, F. Xiong, F. Que, Z.-S. Xu, F. Wang, A.-S. Xiong, Morphological characteristics, anatomical structure, and gene expression: novel insights into gibberellin biosynthesis and perception during carrot growth and development, *Hortic. Res.* 2 (2015) 15028.
- [10] A.F. Macedo, M.V. Leal-Costa, E.S. Tavares, C.L.S. Lage, M.A. Esquibel, The effect of light quality on leaf production and development of in vitro-cultured plants of *Alternanthera brasiliana* Kuntze, *Environ. Exp. Bot.* 70 (2011) 43–50.
- [11] M. de Wit, V.C. Galvão, C. Fankhauser, Light-mediated hormonal regulation of plant growth and development, *Annu. Rev. Plant Biol.* 67 (2016) 513–537.
- [12] D. Alabadi, J. Gallego-Bartolomé, L. Orlando, L. García-Cárcel, V. Rubio, C. Martínez, M. Frigerio, J.M. Iglesias-Pedraz, A. Espinosa, X.W. Deng, M.A. Blázquez, Gibberellins modulate light signaling pathways to prevent Arabidopsis seedling de-etiolation in darkness, *Plant J.* 53 (2008) 324–335.
- [13] E.M. Josse, K.J. Halliday, Skotomorphogenesis: the dark side of light signaling, *Curr. Biol.* 18 (2008) R1144–R1146.
- [14] S. Chen, N. Lory, J. Stauber, U. Hoecker, Photoreceptor specificity in the light-induced and COP1-mediated rapid degradation of the repressor of photomorphogenesis SPA2 in Arabidopsis, *PLoS Genet.* 11 (2015) e1005516.
- [15] D. Xu, Y. Jiang, J. Li, F. Lin, M. Holm, X.W. Deng, BBX21, an Arabidopsis B-box protein, directly activates HY5 and is targeted by COP1 for 26S proteasome-mediated degradation, *Proc. Natl. Acad. Sci. U. S. A.* 113 (2016) 7655–7660.
- [16] V.C. Galvão, C. Fankhauser, Sensing the light environment in plants: photoreceptors and early signaling steps, *Curr. Opin. Neurobiol.* 34 (2015) 46–53.
- [17] J.J. Casal, Photoreceptor signaling networks in plant responses to shade, *Annu. Rev. Plant Biol.* 64 (2013) 403–427, <https://doi.org/10.1146/annurev-arplant-050312-120221>.
- [18] M. Ahmad, J.A. Jarillo, O. Smirnova, A.R. Cashmore, The CRY1 blue light photoreceptor of Arabidopsis interacts with phytochrome a in vitro, *Mol. Cell* 1 (1998) 939–948.
- [19] P. Ahmad, M.R. Wani, *Physiological Mechanisms and Adaptation Strategies in Plants under Changing Environment*, 1st ed., Springer, New York, 2014.
- [20] D.H. Keuskamp, R. Sasidharan, I. Vos, A.J.M. Peeters, L.A.C.J. Voeseenek, R. Pierik, Blue-light-mediated shade avoidance requires combined auxin and brassinosteroid action in Arabidopsis seedlings, *Plant J.* 67 (2011) 208–217.
- [21] Y. Wang, K.M. Folta, Contributions of green light to plant growth and development, *Am. J. Bot.* 100 (2013) 70–78.
- [22] C. Kami, S. Lorrain, P. Hornitschek, C. Fankhauser, Light-regulated plant growth and development, *Curr. Top. Dev. Biol.* 91 (2010) 29–66.
- [23] M. Battle, M. Jones, Cryptochromes integrate green light signals into the circadian system, *Plant Cell Environ.* (2019), <https://doi.org/10.1111/pce.13643>.
- [24] C. Arena, T. Tsonev, D. Doneva, V. DeMicco, M. Michelozzi, C. Brunetti, M. Centritto, S. Fineschi, V. Velikova, F. Loreto, The effect of light quality on growth, photosynthesis, leaf anatomy and volatile isoprenoids of a monoterpene-emitting herbaceous species (*Solanum lycopersicum* L.) and an isoprene-emitting tree (*Platanus orientalis* L.), *Environ. Exp. Bot.* 130 (2016) 122–132.
- [25] M. Johkan, K. Shoji, F. Goto, S. Hahida, T. Yoshihara, Effect of green light wavelength and intensity on photomorphogenesis and photosynthesis in *Lactuca sativa*, *Environ. Exp. Bot.* 75 (2012) 128–133.
- [26] S. Muneer, E.J. Kim, J.S. Park, J.H. Lee, Influence of green, red and blue light emitting diodes on multiprotein complex proteins and photosynthetic activity under different light intensities in lettuce leaves (*Lactuca sativa* L.), *Int. J. Mol. Sci.* 15 (2014) 4657–4670.
- [27] K. Kitazaki, A. Fukushima, R. Nakabayashi, Y. Okazaki, M. Kobayashi, T. Mori, T. Nishizawa, S. Reyes-Chin-Wo, R.W. Michelmore, K. Saito, K. Shoji, M. Kusano, Metabolic reprogramming in leaf lettuce grown under different light quality and intensity conditions using narrow-band LEDs, *Sci. Rep.* 8 (2018) 1–12.
- [28] H.L. Smith, L. Mcausland, E.H. Murchie, Don't ignore the green light: exploring diverse roles in plant processes, *J. Exp. Bot.* 68 (2017) 2099–2110.
- [29] L. Bashline, L. Lei, S. Li, Y. Gu, Cell wall, cytoskeleton, and cell expansion in higher plants, *Mol. Plant* 7 (2014) 586–600.
- [30] A. Caño-Delgado, S. Penfield, C. Smith, M. Catley, M. Bevan, Reduced cellulose synthesis invokes lignification and defense responses in *Arabidopsis thaliana*, *Plant J.* 34 (2003) 351–362.
- [31] D.J. Cosgrove, Growth of the plant cell wall, *Nat. Rev. Mol. Cell Biol.* 6 (2005) 850–861.
- [32] A. Sampathkumar, A. Peaucelle, M. Fujita, C. Schuster, S. Persson, G.O. Wasteneys, E.M. Meyerowitz, Primary wall cellulose synthase regulates shoot apical meristem mechanics and growth, *Development* 146 (2019) dev179036.
- [33] S.N. Shabala, R.R. Lew, Turgor regulation in osmotically stressed Arabidopsis epidermal root cells. Direct support for the role of cell turgor measurement, *Plant Physiol* 129 (2002) 290–299 <http://www.pubmedcentral.nih.gov/articlerender.fcgi?artid=155892&tool=pmcentrez&rendertype=abstract>.
- [34] D.S. Thompson, How do cell walls regulate plant growth? *J. Exp. Bot.* 56 (2005) 2275–2285.
- [35] S.A. Braybrook, H. Jönsson, Shifting foundations: the mechanical cell wall and development, *Curr. Opin. Plant Biol.* 29 (2016) 115–120.
- [36] D.J. Cosgrove, Plant cell wall extensibility: connecting plant cell growth with cell wall structure, mechanics, and the action of wall-modifying enzymes, *J. Exp. Bot.* 67 (2016) 463–476, <https://doi.org/10.1093/jxb/erv511>.
- [37] R. Falcioni, T. Moriwaki, E. Benedito, C.M. Bonato, L.A. de Souza, W.C. Antunes, Increased gibberellin levels enhance the performance of light capture efficiency in tobacco plants and promote dry matter accumulation, *Theor. Exp. Plant Physiol.* 30 (2018) 235–250.
- [38] D.M. Ribeiro, W.L. Araujo, A.R. Fernie, J.H.M. Schippers, B. Mueller-Roeber, Action of gibberellins on growth and metabolism of *Arabidopsis thaliana* plants associated with high concentration of carbon dioxide, *Plant Physiol.* 160 (2012) 1781–1794.
- [39] Y. Yu, R. Huang, Integration of ethylene and light signaling affects hypocotyl growth in Arabidopsis, *Front. Plant Sci.* 8 (2017) 57.
- [40] R. Falcioni, T. Moriwaki, C.M. Bonato, L.A. de Souza, M.R. Nanni, W.C. Antunes, Distinct growth light and gibberellin regimes alter leaf anatomy and reveal their influence on leaf optical properties, *Environ. Exp. Bot.* 140 (2017) 86–95.
- [41] P. Sarkar, E. Bosneaga, M. Auer, Plant cell walls throughout evolution: towards a molecular understanding of their design principles, *J. Exp. Bot.* 60 (2009) 3615–3635.
- [42] A.J. Bidhendi, A. Geitmann, Relating the mechanics of the primary plant cell wall to morphogenesis, *J. Exp. Bot.* 67 (2016) 449–461.
- [43] V. Mirabet, P. Krupinski, O. Hamant, E.M. Meyerowitz, H. Jönsson, A. Boudaoud, The self-organization of plant microtubules inside the cell volume yields their cortical localization, stable alignment, and sensitivity to external cues, *PLoS Comput. Biol.* 14 (2018) 1–23.
- [44] M. Majda, S. Robert, The role of auxin in cell wall expansion, *Int. J. Mol. Sci.* 19 (2018) 1–21.
- [45] U. Kutschera, P. Schopfer, Effect of auxin and abscisic acid on cell wall extensibility in maize coleoptiles, *Planta.* 167 (1986) 527–535.
- [46] D.B. Baker, P.M. Ray, Relation between effects of auxin on cell wall synthesis and cell elongation, *Plant Physiol.* 40 (1965) 360–368.
- [47] M. Yu, K. Liu, S. Liu, H. Chen, L. Zhou, Y. Liu, Effect of exogenous IAA on tension wood formation by facilitating polar auxin transport and cellulose biosynthesis in hybrid poplar (*Populus deltoids* × *Populus nigra*) wood, *Holzforschung.* 71 (2017) 179–188.
- [48] T.A. Napoleão, G. Soares, C.E. Vital, C. Bastos, R. Castro, M.E. Loureiro, A. Giordano, Methyl jasmonate and salicylic acid are able to modify cell wall but only salicylic acid alters biomass digestibility in the model grass *Brachypodium distachyon*, *Plant Sci.* 263 (2017) 46–54, <https://doi.org/10.1016/j.plantsci.2017.06.014>.
- [49] S. Inada, T. Shimmen, Regulation of elongation growth by gibberellin in root segments of *Lemna minor*, *Plant Cell Physiol.* 41 (2000) 932–939.
- [50] R. Dixit, Plant cytoskeleton: DELLA connects gibberellins to microtubules, *Curr. Biol.* 23 (2013) 479–481.
- [51] J. Chan, E. Crowell, M. Eder, G. Calder, S. Bunnewell, K. Findlay, S. Vernhettes, H. Hofte, C. Lloyd, The rotation of cellulose synthase trajectories is microtubule dependent and influences the texture of epidermal cell walls in Arabidopsis hypocotyls, *J. Cell Sci.* 123 (2010) 3490–3495, <https://doi.org/10.1242/jcs.074641>.
- [52] J.D. Kubicki, H. Yang, D. Sawada, H. O'Neill, D. Oehme, D. Cosgrove, The shape of native plant cellulose microfibrils, *Sci. Rep.* 8 (2018) 4–11, <https://doi.org/10.1038/s41598-018-32211-w>.
- [53] L.H. Thomas, V.T. Forsyth, A. Sturcova, C.J. Kennedy, R.P. May, C.M. Altaner, D.C. Apperley, T.J. Wess, M.C. Jarvis, Structure of cellulose microfibrils in primary cell walls from collenchyma, *Plant Physiol.* 161 (2013) 465–476.
- [54] S.-Y. Ding, M.E. Himmel, The maize primary cell wall microfibril: a new model derived from direct visualization, *J. Agric. Food Chem.* 54 (2006) 597–606.
- [55] J. Liu, J.I. Kim, J.C. Cusumano, C. Chapple, N. Venugopalan, R.F. Fischetti, L. Makowski, The impact of alterations in lignin deposition on cellulose organization of the plant cell wall, *Biotechnol. Biofuels.* 9 (2016) 126.
- [56] G. Musel, T. Schindler, R. Bergfeld, K. Ruel, G. Jacquet, C. Lapierre, V. Speth, P. Schopfer, Structure and distribution of lignin in primary and secondary cell walls of maize coleoptiles analyzed by chemical and immunological probes, *Planta.* 201 (1997) 146–159.
- [57] F. Saxe, M. Eder, G. Benecke, B. Aichmayer, P. Fratzl, I. Burgert, M. Rüggeberg, Measuring the distribution of cellulose microfibril angles in primary cell walls by small angle X-ray scattering, *Plant Methods* 10 (2014) 1–8.
- [58] K. Sugimoto, R.E. Williamson, G.O. Wasteneys, New techniques enable comparative analysis of microtubule orientation, wall texture, and growth rate in intact roots of Arabidopsis, *Plant Physiol.* 124 (2000) 1493–1506.
- [59] D.H. Burk, Z.-H. Ye, Alteration of oriented deposition of cellulose microfibrils by mutation of a katanin-like microtubule-severing protein, *Plant Cell* 14 (2002) 2145–2160.
- [60] C. Driemeier, W.D. Santos, M.S. Buckeridge, Cellulose crystals in fibrovascular bundles of sugarcane culms: orientation, size, distortion, and variability, *Cellulose.* 19 (2012) 1507–1515, <https://doi.org/10.1007/s10570-012-9743-z>.
- [61] D.H. Burk, B. Liu, R. Zhong, W.H. Morrison, Z.-H. Ye, A katanin-like protein regulates normal cell wall biosynthesis and cell elongation, *Plant Cell* 13 (2001) 807–828.
- [62] R. Zhong, D. Burk, W. Morrison III, Z.-H. Ye, A kinesin-like protein is essential for oriented deposition of cellulose microfibrils and cell wall strength, *Plant Cell* 14 (2002) 3101–3117.
- [63] K. Soga, A. Yamaguchi, T. Kotake, K. Wakabayashi, T. Hoson, 1-Aminocyclopropane-1-carboxylic acid (ACC)-induced reorientation of cortical microtubules is accompanied by a transient increase in the transcript levels of B-tubulin complex and katanin genes in azuki bean epicotyls, *J. Plant Physiol.* 167 (2010) 1165–1171, <https://doi.org/10.1016/j.jplph.2010.04.001>.
- [64] N. Gierlinger, T. Keplinger, M. Harrington, Imaging of plant cell walls by confocal Raman microscopy, *Nat. Protoc.* 7 (2012) 1694–1708.
- [65] T.I. Baskin, Anisotropic expansion of the plant cell wall, *Annu. Rev. Cell Dev. Biol.* 21 (2005) 203–222.
- [66] G. Setterfield, S. Bayley, Arrangement of cellulose microfibrils in walls of

- elongating parenchyma cells, *J. Cell Biol.* 4 (1958) 377–382.
- [67] M. Baskin, S. Liang, Regulation of growth anisotropy in well-watered and water-stressed maize roots. II. Role Of cortical microtubules and cellulose microfibrils, *Plant Physiol* 119 (1999) 681–692.
- [68] D.J. Cosgrove, Diffuse growth of plant cell walls, *Plant Physiol.* 176 (2018) 16–27.
- [69] Q. Ma, J. Sun, T. Mao, Microtubule bundling plays a role in ethylene-mediated cortical microtubule reorientation in etiolated *Arabidopsis* hypocotyls, *J. Cell Sci.* 129 (2016) 2043–2051.
- [70] G. Costa, I. Plazanet, Plant cell wall, a challenge for its characterisation, *Adv. Biol. Chem.* 06 (2016) 70–105.
- [71] Y. Zheng, D.J. Cosgrove, G. Ning, High-resolution field emission scanning electron microscopy (FESEM) imaging of cellulose microfibril organization in plant primary cell walls, *Microsc. Microanal.* (2017) 1–7.
- [72] M. Rüggeberg, F. Saxe, T.H. Metzger, B. Sundberg, P. Fratzl, I. Burgert, Enhanced cellulose orientation analysis in complex model plant tissues, *J. Struct. Biol.* 183 (2013) 419–428, <https://doi.org/10.1016/j.jsb.2013.07.001>.
- [73] H.K. Lichtenthaler, Chlorophylls and carotenoids: pigments of photosynthetic biomembranes, *Methods Enzymol.* 148 (1987) 350–382.
- [74] M. Nakata, N. Mitsuda, M. Herde, A.J.K. Koo, J.E. Moreno, K. Suzuki, G.A. Howe, M. Ohme-Takagi, A bHLH-Type transcription factor, ABA-INDUCIBLE BHLH-TYPE TRANSCRIPTION FACTOR/JA-ASSOCIATED MYC2-LIKE1, acts as a repressor to negatively regulate jasmonate signaling in *Arabidopsis*, *Plant Cell* 25 (2013) 1641–1656.
- [75] M.J. Karnovsky, A formaldehyde-glutaraldehyde fixative of high osmolarity for use in electron microscopy, *J. Cell Biol.* 27 (1965) 137A.
- [76] L.A. Souza, S.M. Rosa, I.S. Moscheta, K.S.M. Mourão, R.A. Rodella, D.C. Rocha, M.I.G.A. Lolis, *Morfologia e anatomia vegetal: técnicas e práticas*, 3rd ed., Editora UEPG, Ponta Grossa, 2016.
- [77] T.P. O'Brien, N. Feder, M.E. McCully, Polychromatic staining of plant cell walls by toluidine blue O, *Protoplasma.* 59 (1964) 368–373.
- [78] L. Ibrahim, An investigation of wound healing in sugar beet roots using light and fluorescence microscopy, *Ann. Bot.* 88 (2001) 313–320.
- [79] F.C. Moreira-Vilar, R.D.C. Siqueira-Soares, A. Finger-Teixeira, D.M. de Oliveira, A.P. Ferro, G.J. Da Rocha, M.D.L.L. Ferrarese, W.D. Dos Santos, O. Ferrarese-Filho, The acetyl bromide method is faster, simpler and presents best recovery of lignin in different herbaceous tissues than klason and thioglycolic acid methods, *PLoS One* 9 (2014) e110000.
- [80] J.B. Mokochnski, G.A. Bataglion, E. Kiyota, L.M. De Souza, P. Mazzafera, A.C.H.F. Sawaya, A simple protocol to determine lignin S/G ratio in plants by UHPLC-MS, *Anal. Bioanal. Chem.* 407 (2015) 7221–7227.
- [81] D.M. Updegraff, Semimicro determination of cellulose in biological materials, *Anal. Biochem.* 32 (1969) 420–424.
- [82] S. Gillmor, P. Poindexter, J. Lorieau, M.M. Palcic, C. Somerville, α -glucosidase I is required for cellulose biosynthesis and morphogenesis in *Arabidopsis*, *J. Cell Biol* 156 (2002) 1003–1013.
- [83] M. Müller, S. Munné-Bosch, Rapid and sensitive hormonal profiling of complex plant samples by liquid chromatography coupled to electrospray ionization tandem mass spectrometry, *Plant Methods* 7 (2011) 1–11.
- [84] J.H. Zar, *Biostatistical Analysis*, 5th ed., Pearson Education, Upper Saddle River - New Jersey, 2010.
- [85] I.T. Jolliffe, *Principal Component Analysis*, 2nd ed., Springer USA, New York, 2002.
- [86] M. Ahmad, N. Grancher, M. Heil, R. Black, B. Giovani, P. Galland, D. Lardemer, Action spectrum for cryptochrome-dependent hypocotyl growth inhibition in *Arabidopsis*, *Plant Physiol.* 129 (2002) 774–785.
- [87] M. Procopio, J. Link, D. Engle, J. Witzczak, T. Ritz, M. Ahmad, Kinetic modeling of the *Arabidopsis* cryptochrome photocycle: FADH₀ accumulation correlates with biological activity, *Front. Plant Sci.* 7 (2016) 1–16.
- [88] O.I.L. Mawphlang, E.V. Kharshiing, Photoreceptor mediated plant growth responses: implications for photoreceptor engineering toward improved performance in crops, *Front. Plant Sci.* 8 (2017) 1–14.
- [89] D.P. Fraser, S. Hayes, K.A. Franklin, Photoreceptor crosstalk in shade avoidance, *Curr. Opin. Plant Biol.* 33 (2016) 1–7.
- [90] C. Fankhauser, R. Ulm, A photoreceptor's on-off-switch, *Science* 354 (80) (2016) 282–283.
- [91] C. Fankhauser, J. Chory, Light control of plant development, *Annu. Rev. Cell Dev. Biol.* 13 (1997) 203–229.
- [92] J.J. Casal, R.A. Mella, C.L. Ballaré, S. Maldonado, Phytochrome-mediated effects on extracellular peroxidase activity, lignin content and bending resistance in etiolated *Vicia faba* epicotyls, *Physiol. Plant.* 92 (1994) 555–562.
- [93] R. Stracke, M. Werber, B. Weisshaar, The R2R3-MYB gene family in *Arabidopsis thaliana*, *Curr. Opin. Plant Biol.* 4 (2001) 447–456.
- [94] Y. Jiao, Trichome formation: Gibberellins on the move, 170 (2016), pp. 1174–1175.
- [95] S.D. Novak, G.A. Whitehouse, Auxin regulates first leaf development and promotes the formation of protocorm trichomes and rhizome-like structures in developing seedlings of *Spathoglottis plicata* (Orchidaceae), *AoB Plants.* 5 (2013) 1–12.
- [96] P. Hedden, S.G. Thomas, *Annual plant review: The gibberellins*, 1st ed, Vol. 49 Wiley Blackwell, New York, 2016.
- [97] C.L. Ballaré, R. Pierik, The shade-avoidance syndrome: multiple signals and ecological consequences, *Plant Cell Environ.* (2017) 2530–2543.
- [98] P.M. Ray, P.B. Green, R. Cleland, Role of turgor in plant cell growth, *Nature.* 239 (1972) 163–164.
- [99] D. Cosgrove, Biophysical control of plant cell growth, *Annu. Rev. Plant Physiol.* 37 (1986) 377–405.
- [100] L. Taiz, Plant cell expansion: regulation of cell wall mechanical properties, *Annu. Rev. Plant Physiol.* 35 (1984) 585–657.
- [101] R. Sasidharan, R. Pierik, Cell wall modification involving XTHs controls phytochrome-mediated petiole elongation in *Arabidopsis thaliana*, *Plant Signal. Behav.* 5 (2010) 1491–1492.
- [102] D.J. Cosgrove, Loosening of plant cell walls by expansins, *Nature.* 407 (2000) 321–326.
- [103] S.H. Cho, P. Purushotham, C. Fang, C. Maranas, S.M. Díaz-Moreno, V. Bulone, J. Zimmer, M. Kumar, B.T. Nixon, Synthesis and self-assembly of cellulose microfibrils from reconstituted cellulose synthase, *Plant Physiol.* 175 (2017) 146–156.
- [104] D.P. Oehme, M.S. Doblin, J. Wagner, A. Bacic, M.T. Downton, M.J. Gidley, Gaining insight into cell wall cellulose macrofibril organisation by simulating microfibril adsorption, *Cellulose.* 22 (2015) 3501–3520.
- [105] G. Chinga-Carrasco, Cellulose fibres, nanofibrils and microfibrils: the morphological sequence of MFC components from a plant physiology and fibre technology point of view, *Nanoscale Res. Lett.* 6 (2011) 1–7.
- [106] K. Karimi, *Lignocellulose-Based Bioproducts*, 1st ed., Springer International Publishing, Switzerland, 2015.
- [107] S. Glazowska, L. Baldwin, J. Mravec, C. Bukh, T.H. Hansen, M.M. Jensen, J.U. Fangel, W.G.T. Willats, M. Glasius, C. Felby, J.K. Schjoerring, The impact of silicon on cell wall composition and enzymatic saccharification of *Brachypodium distachyon*, *Biotechnol. Biofuels.* 11 (2018) 171.
- [108] P.K. Hepler, Calcium: a central regulator of plant growth and development, *Plant Cell Online.* 17 (2005) 2142–2155, <https://doi.org/10.1105/tpc.105.032508>.
- [109] A. Peaucelle, S.A. Braybrook, L. Le Guillou, E. Bron, C. Kuhlemeier, H. Höfte, Pectin-induced changes in cell wall mechanics underlie organ initiation in *Arabidopsis*, *Curr. Biol.* 21 (2011) 1720–1726.
- [110] T. Hamann, Plant cell wall integrity maintenance as an essential component of biotic stress response mechanisms, *Front. Plant Sci.* 3 (2012) 1–5.
- [111] F.G. Malinovsky, J.U. Fangel, W.G.T. Willats, The role of the cell wall in plant immunity, *Front. Plant Sci.* 5 (2014) 1–12.
- [112] R. Vanholme, B. Demedts, K. Morreel, J. Ralph, W. Boerjan, Lignin biosynthesis and structure, *Plant Physiol.* 153 (2010) 895–905.
- [113] Q. Liu, L. Luo, L. Zheng, Lignins: biosynthesis and biological functions in plants, *Int. J. Mol. Sci.* 19 (2018) 2–16.
- [114] M. Zdarska, T. Dobisová, Z. Gelová, M. Pernisová, S. Dabravolski, J. Hejrátko, Illuminating light, cytokinin, and ethylene signalling crosstalk in plant development, *J. Exp. Bot.* 66 (2015) 4913–4931.
- [115] N. Zhang, Q. Sun, H. Li, X. Li, Y. Cao, H. Zhang, S. Li, L. Zhang, Y. Qi, S. Ren, B. Zhao, Y.-D. Guo, Melatonin improved anthocyanin accumulation by regulating gene expressions and resulted in high reactive oxygen species scavenging capacity in cabbage, *Front. Plant Sci.* 7 (2016) 197, <https://doi.org/10.3389/fpls.2016.00197>.
- [116] L. Consentino, S. Lambert, C. Martino, N. Jourdan, P.E. Bouchet, J. Witzczak, P. Castello, M. El-Esawi, F. Corbineau, A. D'Harlingue, M. Ahmad, Blue-light dependent reactive oxygen species formation by *Arabidopsis* cryptochrome may define a novel evolutionarily conserved signaling mechanism, *New Phytol.* 206 (2015) 1450–1462.
- [117] V. Bergougnoux, D. Zalabák, M. Jandová, O. Novák, A. Wiese-Klinkenberg, M. Fellner, Effect of blue light on endogenous isopentenyladenine and endoreduplication during photomorphogenesis and De-etiolation of tomato (*Solanum lycopersicum* L.) seedlings, *PLoS One* 7 (2012) e45255.

Supplementary Material

Title: Cell wall structure and composition is affected by light quality in tomato seedlings

Renan Falcioni^{1,2,a}, Thaise Moriwaki^{1,a}, Marina Perez-Llorca^{3,b}, Sergi Munné-Bosch^{3,b}
Mariana Sversut Gibin^{4,a}, Francielle Sato^{4,a}, Andressa Pelozo^{1,5,a}, Mariana Carmona
Pattaro^{1,a}, Marina Ellen Giacomelli^{1,a}, Markus Rüggeberg^{6,c}, Werner Camargos
Antunes^{1,a*}

¹Plant Ecophysiology Laboratory. Department of Biology.

²Plant Biochemistry Laboratory. Department of Biochemistry.

³Antiox Research Group. Department of Evolutionary Biology, Ecology and Environmental Sciences.

⁴Optical spectroscopy and thermophysical properties research group. Department of Physics.

⁵Plant Anatomy Laboratory. Department of Biology.

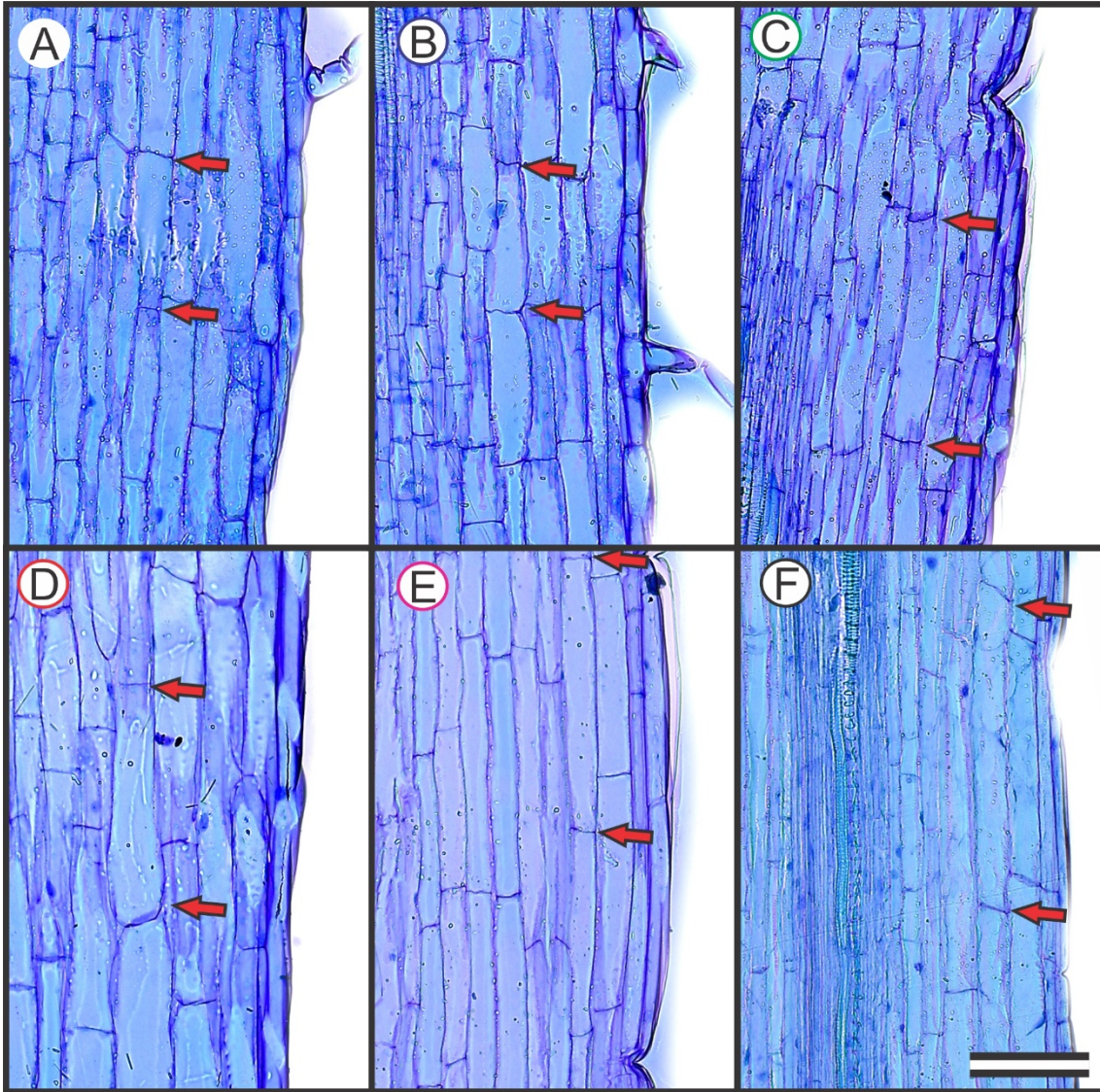
⁶Wood Material Science. Institute for Building Materials.

^aState University of Maringá, Av. Colombo, 5790, 87020-900 Maringá, Paraná, Brazil.

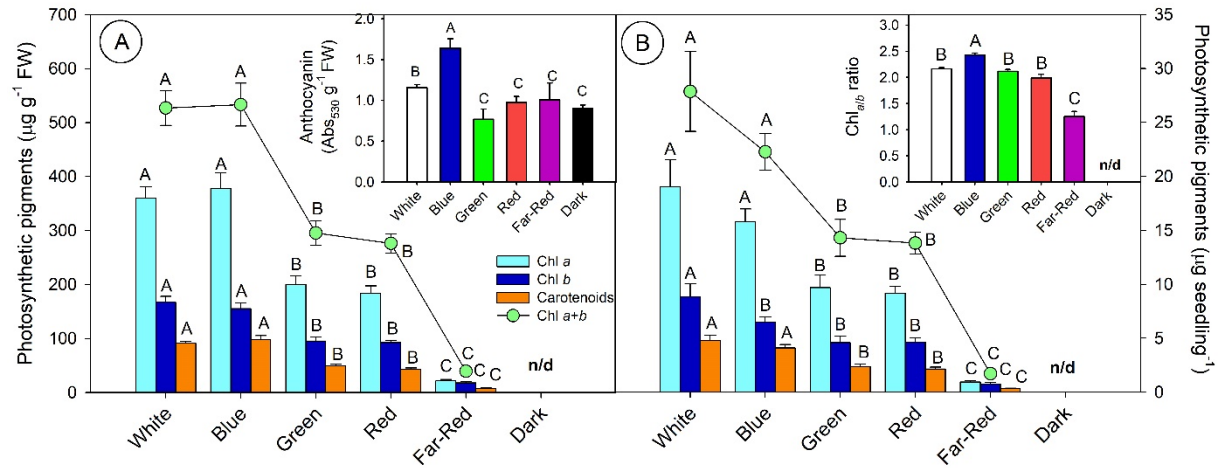
^bFacultat de Biologia. Universitat de Barcelona, Avinguda Diagonal, 645, 08028, Barcelona, Spain.

^cSwiss Federal Institute of Technology Zurich (ETH Zurich), Schafmattstrasse 6, CH-8093 Zurich, Switzerland.

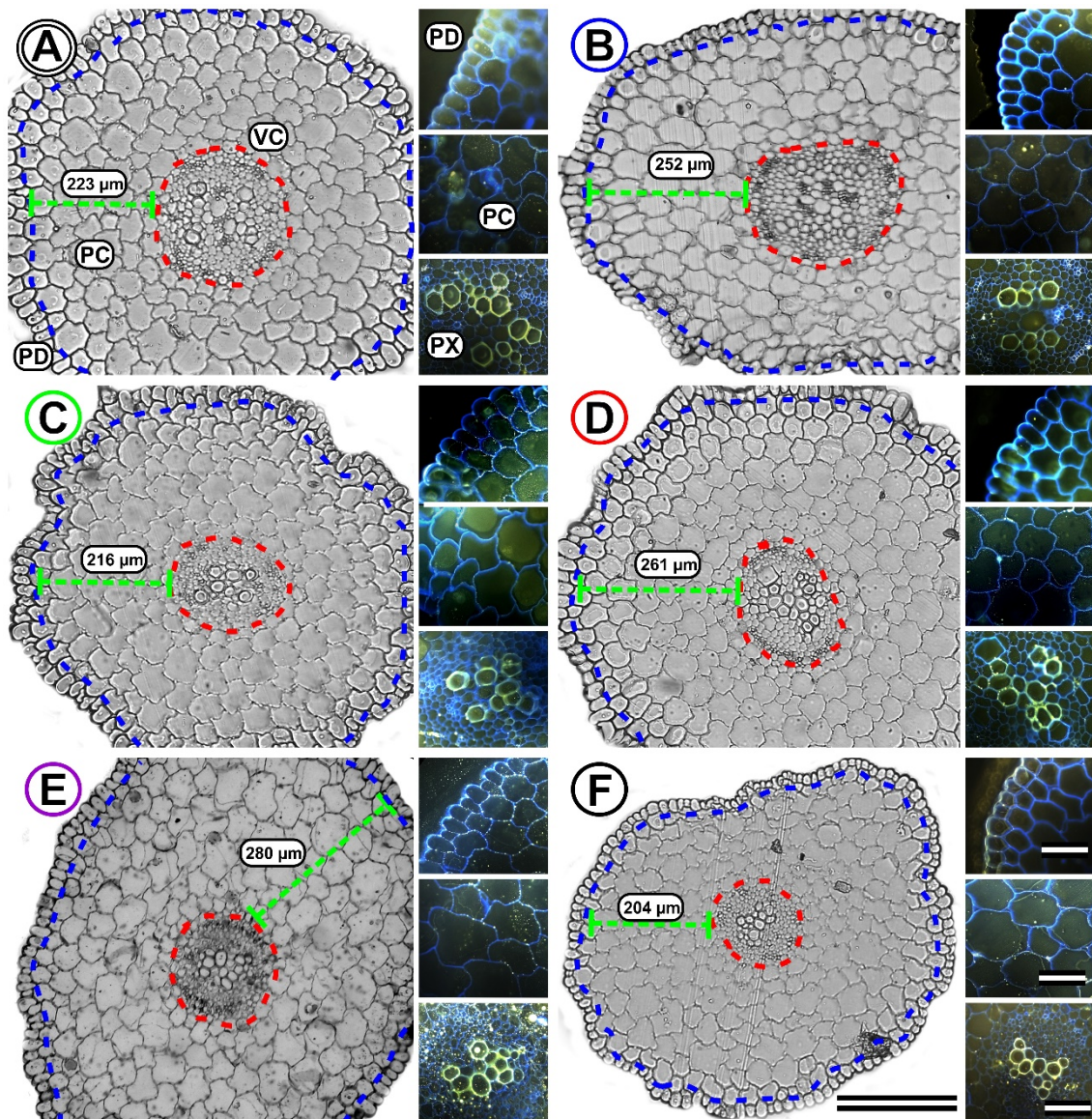
*Corresponding author: wcantunes@uem.br



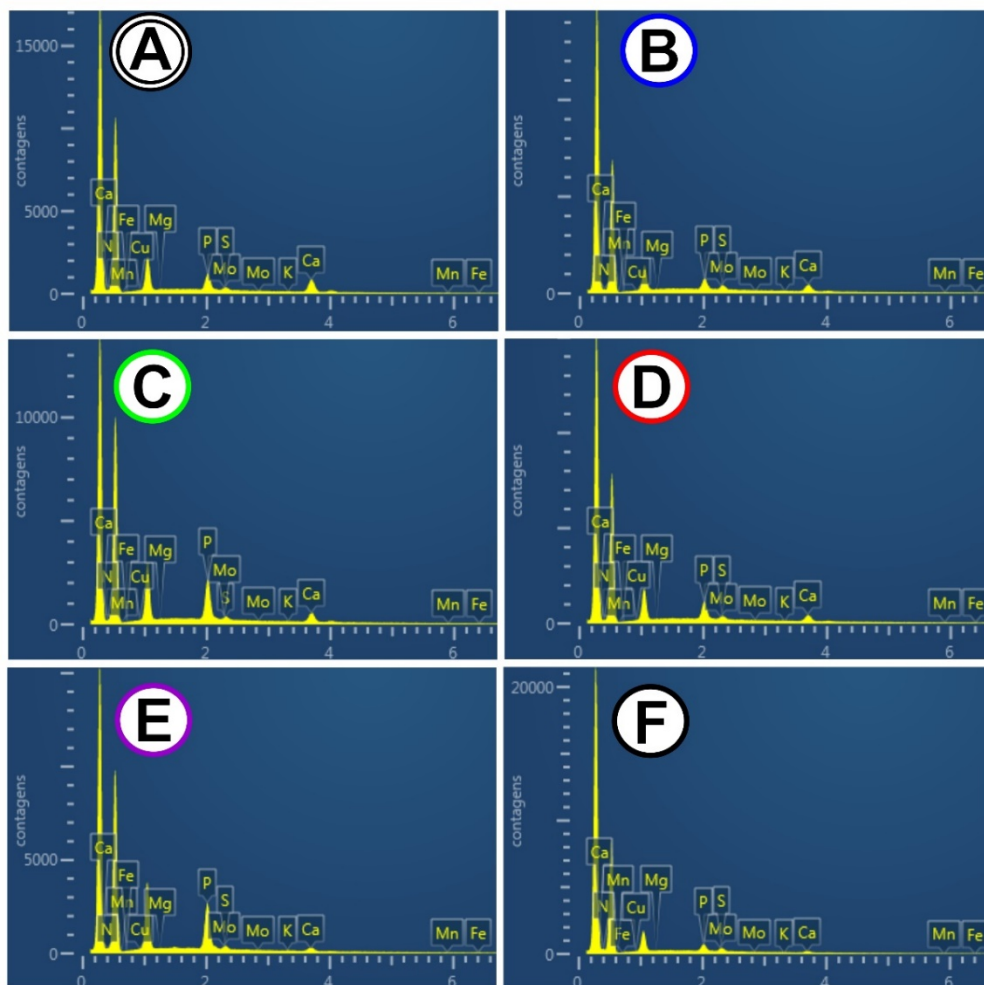
Supplementary Figure S1 – Light microscopy of a longitudinal section of tomato seedling hypocotyls grown under distinct light qualities (and dark) 10 days after the beginning of the treatments. Arrow indicate the limits of the single cortical parenchyma cell. (A) white light, (B) blue light, (C) green light, (D) red light, (E) far-red light, (F) dark. Scale bar = 200 μm .



Supplementary Figure S2 – Photosynthetic pigments of tomato seedlings grown under distinct light qualities and in the dark 10 days after the beginning of the treatments. (A) fresh weight basis. Inset, Anthocyanin contents. (B) seedling basis. The inset indicates the Chl *a/b* ratio. Chlorophyll *a* (Chl*a*), Chlorophyll *b* (Chl*b*), Chlorophyll total (Chl_{*a+b*}), Carotenoids (carotenoids+xanthophylls). Different letters over the bars indicate statistical differences between treatments by Duncan's test ($P < 0.05$). ($n=6 \pm SE$).

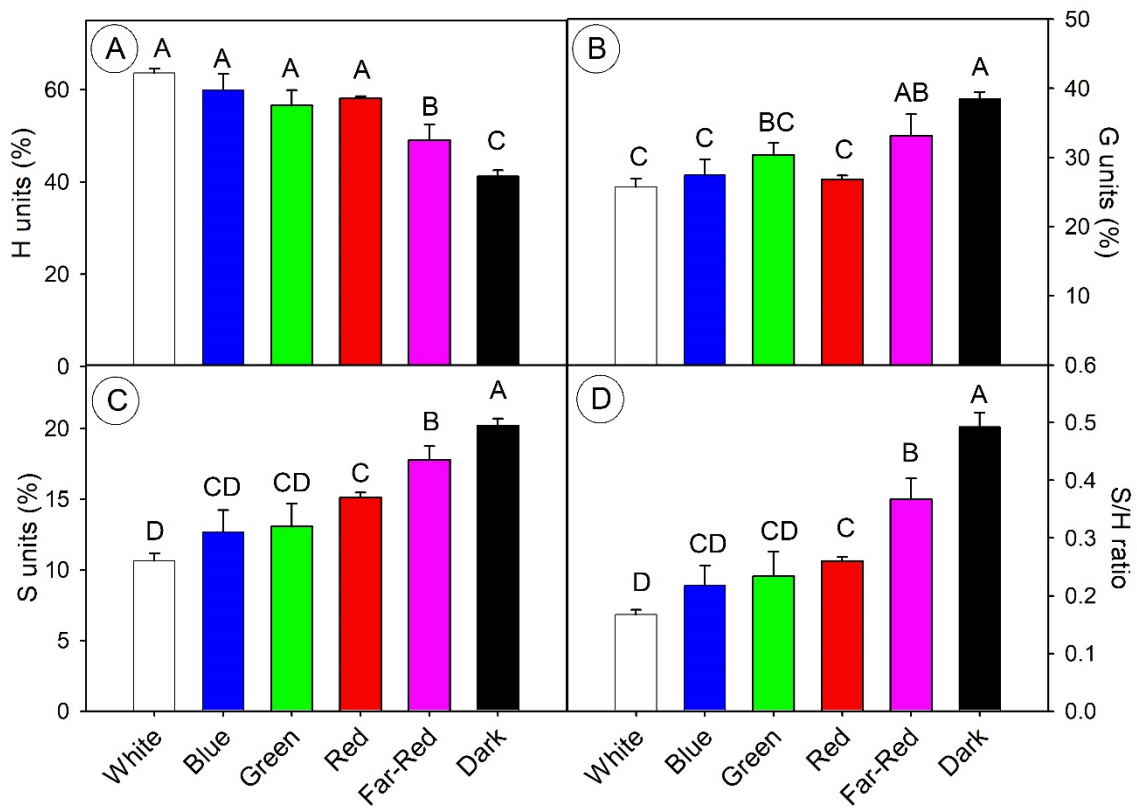


Supplementary Figure S3 – Cross section of the medial portion of tomato hypocotyls grown under distinct light qualities and in the dark 10 days after the beginning of the treatments. Left: light microscopy. Right: fluorescence microscopy highlighting protoderm, cortical parenchyma cells and xylem cells. (A) white light, (B) blue light, (C) green light, (D) red light, (E) far-red light, (F) dark. PD – protoderm, PC – parenchyma cells, PX – protoxylem, VC – vascular cylinder. The dashed blue line delimits the protoderm. The dashed green light indicates the cortical parenchyma thickness. The dashed red line delimits the vascular cylinder. Scale bar = 200 μm and inset 50 μm . Fluorescence slides were double stained by Calcofluor Bright White 28 (0.01%) for cellulose (blue) and Auramine O (0.01%) for lignin (yellow).

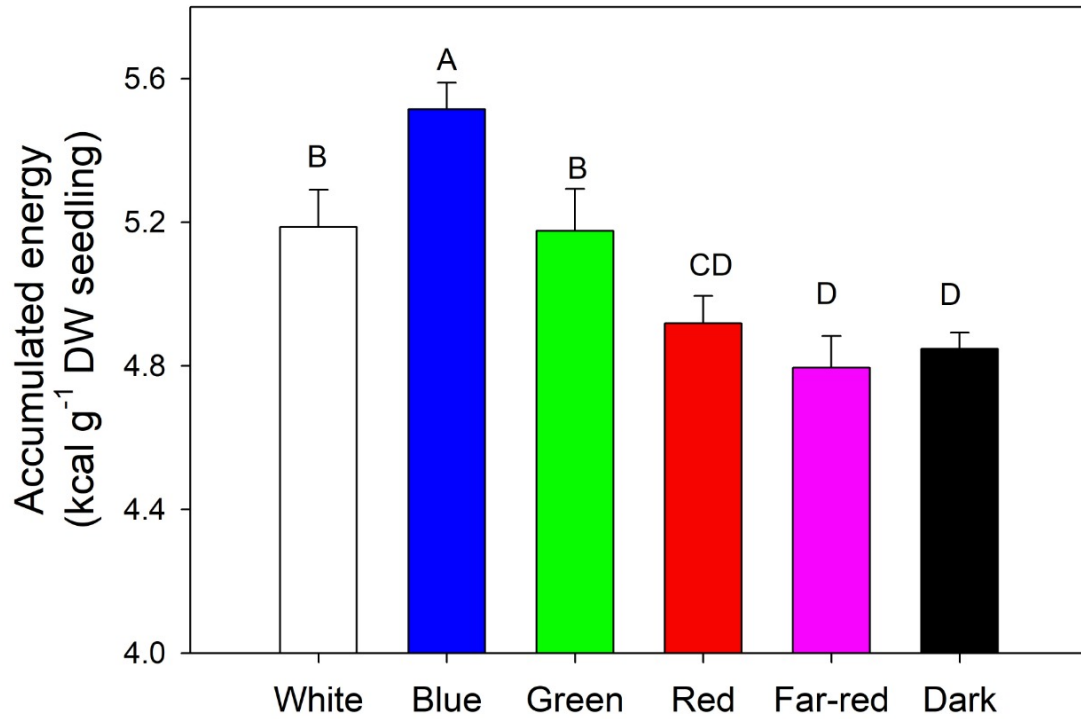


EDS element detect	White	Blue	Green	Red	Far-Red	Dark
P	37.4%	35.7%	61.1%	47.8%	71.7%	41.2%
S	8.6%	21.2%	8.8%	12.0%	11.2%	32.9%
Ca	45.5%	36.1%	24.1%	28.3%	10.3%	16.1%
Mg	5.4%	5.6%	4.4%	5.2%	4.3%	6.6%
K	0.6%	0.8%	0.4%	0.6%	0.9%	1.7%
Cu	0.0%	0.0%	0.6%	1.7%	0.4%	0.8%
Mn	0.0%	0.6%	0.0%	0.0%	0.0%	0.6%
Fe	0.3%	0.0%	0.7%	0.0%	1.1%	0.1%
N	0.0%	0.0%	0.0%	0.0%	0.0%	0.0%
Mo	2.3%	0.0%	0.0%	4.5%	0.0%	0.0%
Total	100.1%	100.0%	100.1%	100.1%	99.9%	100.0%

Supplementary Figure S4 –Energy-dispersive X-ray spectroscopy (EDS) of the elemental composition of tomato seedlings grown under distinct light qualities (and dark) 10 days after the beginning of the treatments. (A) white light, (B) blue light, (C) green light, (D) red light, (E) far-red light, (F) dark. (n=10).

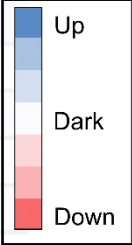


Supplementary Figure S5 – Lignin monomeric composition of tomato seedlings grown under distinct light qualities and in the dark 10 days after the beginning of the treatments. (A) *p*-hydroxyfenil (H units), (B) guayacyl (G units), (C) syringyl (S units) and (D) S/H ratio. Different letters over the bars indicate statistical differences between treatments by Duncan’s test ($P < 0.05$). ($n=6 \pm SE$).

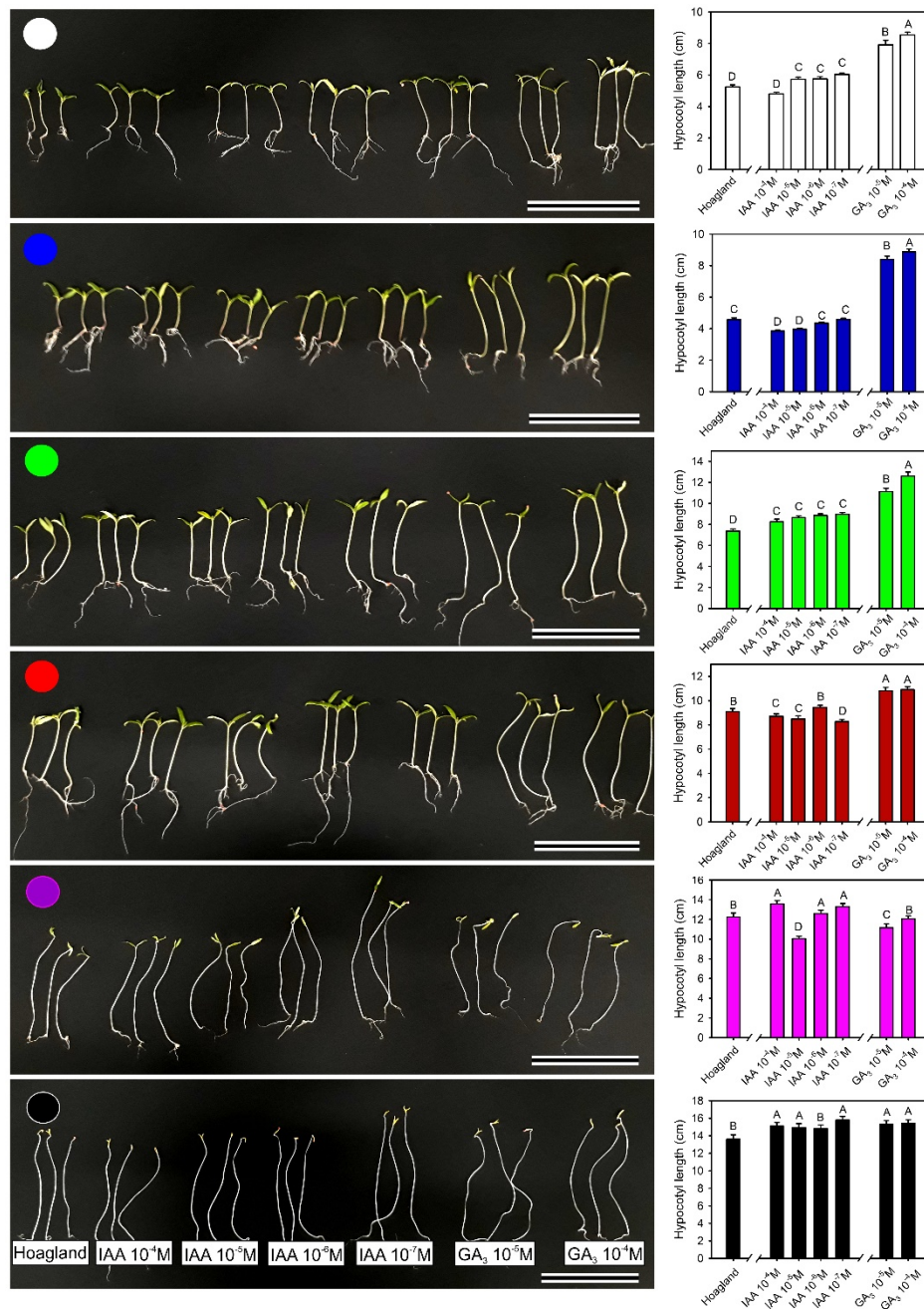


Supplementary Figure S6 – Calorimetric analysis of dried tomato seedlings grown under distinct light qualities and in the dark 10 days after the beginning of the treatments. Different letters over the bars indicate statistical differences between treatments by Duncan's test ($P < 0.05$). ($n=6 \pm SE$).

Profiling Hormones	White	Blue	Green	Red	Far-red	Dark
ABA	7.1%	69.9%	28.9%	56.5%	-7.5%	0
MEL	63.5%	183.9%	-12.2%	125.7%	92.3%	0
JA	10.5%	-17.5%	17.6%	11.6%	-10.2%	0
SA	-17.2%	28.3%	16.5%	-0.7%	19.8%	0
Z	475.6%	428.6%	241.1%	415.9%	157.3%	0
ZR	-75.5%	-37.7%	33.8%	6.9%	-17.7%	0
IPA	-8.7%	-42.5%	-53.4%	-17.6%	-9.1%	0
2iP	23.1%	127.8%	-78.3%	48.8%	28.8%	0
IAA	379.2%	625.7%	223.3%	243.7%	545.0%	0
GA ₁	68.8%	40.6%	-23.5%	33.5%	43.9%	0
GA ₃	118.3%	29.2%	-17.1%	320.3%	495.1%	0
GA ₄	5.9%	4.3%	11.9%	-6.3%	7.7%	0
GA ₇	82.9%	78.4%	70.2%	-15.9%	50.5%	0
GA _{TOTAL}	9.2%	4.7%	10.8%	-0.7%	13.5%	0



Supplementary Figure S7 – Heat map representing relative changes of hormonal contents in tomato seedlings grown under white, blue, green, red, far-red lights and in the dark. Data were normalized with reference to the mean response of dark treatment. Blue-to-red scale represent an upregulation to downregulation, respectively. The full data sets from these plant hormone profiling are available in the main text (Fig. 9). ABA: abscisic acid; MEL: melatonin; JA: jasmonic acid; SA: salicylic acid; Z: trans-zeatin; ZR: trans-zeatin riboside; IPA: isopentenyladenosine; 2iP: isopentenyladenine; IAA: indole-3-acetic acid and GAs (GA₁, GA₃, GA₄, GA₇ and GA_{Total}): gibberellins.



Supplementary Figure S8 – Representative image from tomato seedlings growing at distinct light qualities and (and dark) and treated with indol-3-acetic acid (IAA) or gibberellic acid (GA_3) 10 days after starting treatments. Up to down, seedlings growing under white light, blue light, green light, red light, far-red light, dark. Left-to-right: Hoagland solution, IAA 10^{-4} M, 10^{-5} M, 10^{-6} M, 10^{-7} M, GA_3 10^{-5} M, 10^{-4} M in Hoagland's solution. Scale bar = 10 cm. Graphs show hypocotyl length. Different letters over bars indicate statistical differences between treatments by Duncan's test ($P < 0.05$). ($n=20 \pm SE$).

CHAPTER 3

High Resolution Leaf Spectral Signature As A Tool For Foliar Pigment Estimation Displaying Potential For Species Differentiation



High resolution leaf spectral signature as a tool for foliar pigment estimation displaying potential for species differentiation

Renan Falcioni^{a,b,d}, Thaise Moriwaki^{a,d}, Mariana Pattaro^{a,d}, Renato Herrig Furlanetto^{c,d}, Marcos Rafael Nanni^{c,d}, Werner Camargos Antunes^{a,d,*}

^a Plant Ecophysiology Laboratory, Department of Biology, Brazil

^b Biochemistry of Plants Laboratory, Department of Biochemistry, Brazil

^c Group Applied to Soil Survey and Spatialization, Department of Agronomy, Brazil

^d State University of Maringá, Av. Colombo, 5790, Jd. Universitário, 87020-900, Maringá, Paraná, Brazil

ARTICLE INFO

Keywords:

Anatomy
High resolution spectral data
Light absorption
Optical leaf properties
Pigments
Species discrimination

ABSTRACT

Optical leaf profiles depend on foliar pigment type and content, as well as anatomical aspects and cellular ultrastructure, whose effects are shown in several species. Monocotyledon and Dicotyledon plants presenting natural pigment content variations and anatomical alterations were analyzed. Each plant species displays its own spectral signatures, which are, in turn, influenced by foliar pigment class (composition) and concentration, as well as anatomical and ultrastructural plant cell characteristics. Plants with no anthocyanin displayed increased reflectance and transmittance in the green spectral region (501–565 nm), while values decreased in the presence of anthocyanin. At wavelengths below 500 nm (350–500 nm), strong overlapping signatures of phenolics, carotenoids, chlorophylls, flavonoids and anthocyanins were observed. Using a partial least squares regression applied to 350–700 nm spectral data allowed for accurate estimations of different foliar pigment levels. In addition, a PCA and discriminant analysis were able to efficiently discriminate different species displaying spectra overlapping. The use of absorbance spectra only was able to discriminate species with 100 % confidence. Finally, a discussion on how different wavelengths are absorbed and on anatomical interference of light interaction in leaf profiles is presented.

1. Introduction

Leaf optical profiles (reflectance, absorbance and transmittance) depend on foliar pigment type and content (Gitelson and Solovchenko, 2018; Kume, 2018; Maas and Dunlap, 1989) as well as the structures in which the pigments are inserted (Hatier and Gould, 2007; Jacquemoud and Baret, 1990; Terashima et al., 2009; Vogelmann and Han, 2000; Xiao et al., 2016). Different models have been proposed to further the understanding of light and leaf interactions, both on the surface and in the mesophyll (Falcioni et al., 2017; Gitelson and Solovchenko, 2018; Kume, 2018; Maas and Dunlap, 1989; Moriwaki et al., 2019; Nishio, 2000; Terashima et al., 2009; Xiao et al., 2016). The main models explore the relationship between different pigment content variations and concentrations, as well as their organization at the structural level and specific leaf area (area/mass ratio) (Evans, 1986) and, consensually, emphasize the positive relationship between pigment content and leaf thickness in maximizing light absorption and decreasing reflectance and transmittance (Asner et al., 2008; Falcioni et al., 2017; Féret et al.,

2017, 2008; Jacquemoud and Baret, 1990; Kume, 2018). Some models indicate epidermal cells in the form of lenses, which allow for light focalization and maximum absorption by parenchyma cells (Bone et al., 1985). However, some studies discard this concept as being relevant for light absorption and argue that internal leaf characteristics are more expressive in their distribution along the vertical profile (Brodersen et al., 2008; Brodersen and Vogelmann, 2010, 2007; Xiao et al., 2016).

Maximizing light capture efficiency and use of available ambient light becomes possible when changes occur at the whole plant level (Niinemets, 2007), at the leaf levels (Falcioni et al., 2017) or at the chloroplast level (Moriwaki et al., 2019). Some of the most striking responses regarding leaf-level changes on optical property profiles are related to changes in foliar pigment content and their arrangement and organization, as well as mesophyll cell size and chloroplast and light absorption complex variations (Croce and Amerongen, 2014; Falcioni et al., 2017; Kume, 2018; Moriwaki et al., 2019; Nishio et al., 1993; Terashima et al., 2009; Xiao et al., 2016). In addition, the presence of extra-plastidial pigments on adaxial and abaxial epidermis, the

* Corresponding author at: State University of Maringá, Av. Colombo, 5790, Jd. Universitário, 87020-900, Maringá, Paraná, Brazil.
E-mail address: wcantunes@uem.br (W. Camargos Antunes).

<https://doi.org/10.1016/j.jplph.2020.153161>

Received 22 October 2019; Received in revised form 19 March 2020; Accepted 19 March 2020

Available online 18 April 2020

0176-1617/ © 2020 Elsevier GmbH. All rights reserved.

proportion of intercellular spaces, total leaf thickness and thylakoid stacking degree are variables that should also be included as key points in models to understand leaf light distribution and attenuation (Falcioni et al., 2017; Jacquemoud and Baret, 1990; Kume, 2018; Moriwaki et al., 2019; Sims and Gamon, 2002; Vogelmann et al., 1996; Xiao et al., 2016) and photosynthesis promotion in deeper leaf areas (Ichiro et al., 2016).

Chlorophylls as responsible for the initial steps of photosynthetic light reactions ordinary for all plants display two maximum absorption peaks, one in the blue range (430 and 453 nm, respectively for chlorophylls *a* and *b*), and another in the red range (642 and 662 nm, respectively for chlorophylls *b* and *a*) (Croce and Amerongen, 2014). In parallel, carotenoids present inflection in the blue absorption range (400–500 nm) with an overlap among chlorophylls regarding light absorption in this spectral range. New insights also consider that chlorophylls may contribute to absorbance in the green region (500–565 nm) and may modify optical leaf properties (Falcioni et al., 2017; Folta and Maruhnich, 2007; Moriwaki et al., 2019; Wang and Folta, 2013). Moriwaki et al. (2019) observed an increase in green absorption with increasing chlorophyll contents, but without significant increases in blue or red absorptions. On the other hand, pigments termed extra-plastidial (mainly vacuolar), such as anthocyanins (AnC) and flavonoids (Flv), as well as other phenolic compounds, display strong absorption in the green, blue, and ultraviolet/violet regions, respectively (Gitelson, 2011; Gitelson et al., 2017; Gould et al., 2018; Landi et al., 2015; Merzlyak et al., 2008) and, therefore, present another absorption spectra overlap point with chloroplast pigments (Gitelson, 2011; Hatier and Gould, 2007). Violet, red or purple leaf colors are characteristic of extra-plastidial pigments, which visually mask the green coloration of chlorophylls, as they are concentrated mainly, on the leaf epidermis and are reported as leaf profile light attenuators (Gitelson et al., 2017; Gould et al., 2018; Hatier et al., 2013). However, the interaction of these components with light penetration along the vertical leaf profile is still not well understood. In addition, extra-plastidial pigments strongly affect foliar reflectance patterns (Gitelson et al., 2009, 2001). Thus, we have developed new absorbance-based techniques applicable to cases where reflectance-based approaches fail (Gitelson and Solovchenko, 2018).

In recent years, the insertion of different Vegetation Indices (VI) and Normalized Difference Vegetation Indices (NDVIs) (Buchhorn et al., 2016; da Silva Junior et al., 2017) based on key wavelengths in the visible and near infrared range have been applied to the study and prediction of the amount of plant biomass on the terrestrial surface (Brocks and Bareth, 2018; Tilly et al., 2014), characterization and monitoring of agricultural crops (Fourty et al., 1996; Jacquemoud and Baret, 1990; Nanni et al., 2018), as well as of native species for environmental monitoring purposes (Asner et al., 2008; Gitelson et al., 2009). However, many of these indices are limited or comprise biased equations to estimate foliar pigment concentration, particularly in the presence of AnC and Flv when using VI technology. Moreover, some of these indices take into account only reflectance data (which are strongly influenced by the vacuolar pigments of the epidermis) and do not consider cellular structure organization and phenolic compound concentrations, which ultimately interfere with the absorption spectra, leading to failure in optical leaf pattern estimates, as well as estimates concerning chloroplast pigment contents.

A key point to understand optical leaf properties is the deconvolution of the total spectrum into fractions that contribute to light absorption. The inclusion of specific spectral bands or modeling using curves obtained by high-resolution hyperspectral sensors would provide important information on phenolic compounds, anthocyanins and flavonoids, as well as on components associated with foliar structural organization, in which mathematical models would become more sophisticated and closer to the *in vivo* reality, to the detriment of those obtained by multispectral images or virtually simulated in computational models (da Silva Junior et al., 2017; Féret et al., 2008; Gitelson,

2011; Gitelson et al., 2017; Gitelson and Solovchenko, 2018; Merzlyak et al., 2008; Xiao et al., 2016).

Hyperspectral sensors operate in hundreds of contiguous, narrow bands, providing more accurate and comprehensive information than their multispectral predecessors. When the obtained data are processed with multivariate discriminant analyses, such as proc DISCRIM and STEPDISC SAS (da Silva Junior et al., 2017), Successive Projection Algorithm (SPA) (Pan et al., 2015), Principal Component Analysis (PCA) (Gierlinger et al., 2012), Partial Redundancy Analysis (pRDA) (Ji et al., 2017), Linear Discriminant Analysis (LDA) or Partial Least Squares Regression (PLSR) (Nanni et al., 2018), it is possible to predict pigment concentration, nutritional status, discriminate species or estimate yields in the field (Blackburn, 2007; Calviño-Cancela and Martín-Herrero, 2016; Gitelson and Solovchenko, 2018; Gitelson and Merzlyak, 2004; Gitelson and Merzlyak, 1997; Nanni et al., 2018).

Based on the influence of morphological diversity and the diversity of the several foliar pigment compositions and concentrations, the deconvolution of reflectance, transmittance and leaf light absorption spectra in different Monocotyledon and Dicotyledon species were assessed. As these explain property alterations in the 350–2500 nm region, (with primary focus between 350–700 nm, based on the visible and photosynthetic region), the levels of *in vivo* pigments (chlorophylls, carotenoids, anthocyanins, flavonoids and total soluble phenolic compounds) were estimated based on the obtained spectra. Structural and ultrastructural changes were associated to spectral variations. The aim was to evaluate if data obtained by high resolution spectral sensors are able to discriminate pigment and cellular structure effects. This study demonstrates and advances the ability of this technique to solve complex problems concerning optical leaf properties and the use of routines in spectral curve discriminant models and multivariate analyses.

2. Material and methods

2.1. Plant material

Six species with natural leaf color variations were selected, varying in pigment class and content. Healthy *Megathyrsus maximus* Jacq. (known as Guinea grass and green panic grass), *Pennisetum purpureum* Schumach. (purple elephant grass), *Philodendron* sp. (L.), *Tradescantia pallida* cv. purpurea (Rose) D.R.Hunt. (purple-heart), *Cordyline fruticosa* (L.) A. Chev. (black-mystique) and *Cordyline fruticosa* (L.) A. Chev. (florida-red) leaves were selected in a way to include wide pigment and anatomy variations of Monocotyledon and Dicotyledon species (Fig. 1). Young and healthy expanded leaves from each species were collected from the Botanical Garden of the State University of Maringá, in Brazil, during autumn.

2.2. Leaf pigments

The following procedure allowing for the simultaneous quantification of total chlorophyll (Chl), carotenoids (Car), anthocyanins (AnC) and flavonoids (Flv) in leaf extracts, as described by Gitelson et al. (2017) and Gitelson and Solovchenko (2018). Leaf segments (2 cm²) were ground in chloroform-methanol (2:1, v/v) in the presence of CaCO₃. After complete extraction, distilled water (20 % of the total extract volume) was added. Extracts were centrifuged at 3200 rpm for 15 min until phase separation.

Total Chl and Car concentration were spectrophotometrically quantified in the lower (chloroform) phase, following (Wellburn, 1994). The upper (water-methanol) phase was used for total Flv quantification, determined spectrophotometrically at λ_{358} nm using a molar absorption coefficient of $\epsilon_{358} = 25.4 \text{ mM}^{-1} \text{ cm}^{-1}$, following (Gitelson et al., 2017). After Flv determinations, the water-methanol phase was acidified with HCl (final HCl concentration of 0.1 %) and used for AnC quantification at λ_{530} nm applying an absorption coefficient of $\epsilon_{530} = 30 \text{ mM}^{-1} \text{ cm}^{-1}$ (Gitelson et al., 2017; Gitelson and

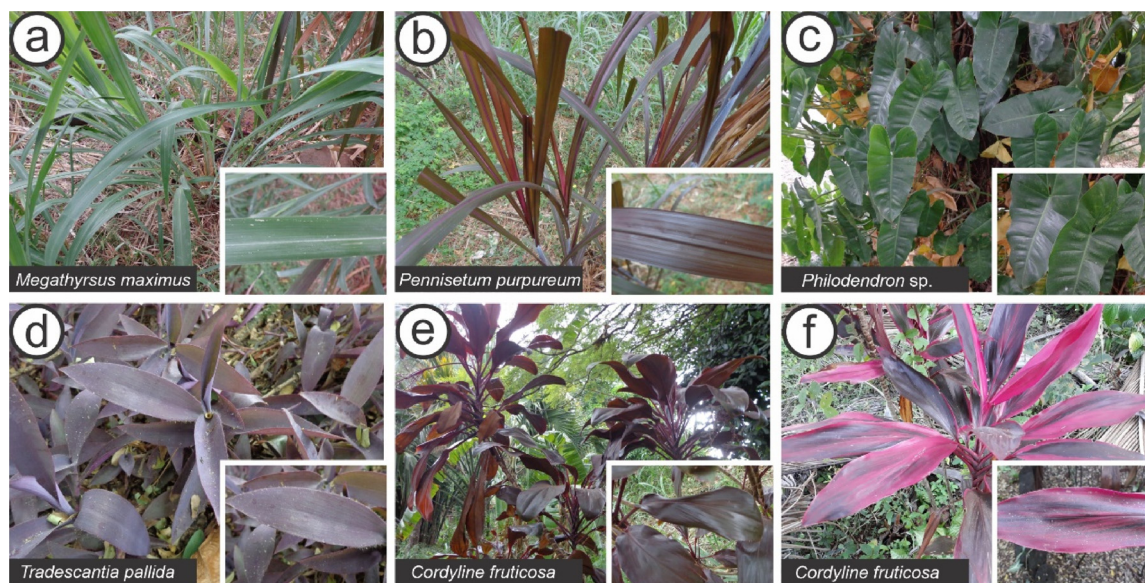


Fig. 1. Representative images of the plants assessed in this study, displaying significant morphological and pigment variations. Inset, close up of the leaves. (a) *Megathyrsus maximus* Jacq., green leaf, Monocotyledoneae, (b) *Pennisetum purpureum* Schumach., purple leaf, Monocotyledoneae, (c) *Philodendron* sp. (L.), green leaf, Dicotyledoneae, (d) *Tradescantia pallida* (Rose) D.R.Hunt., purple leaf, Dicotyledoneae, (e) *Cordyline fruticosa* (L.) A. Chev. (black-mystique), purple leaf, Monocotyledoneae and (f) *Cordyline fruticosa* (L.) A. Chev. (florida-red), pink with purple spots, Monocotyledoneae. (For interpretation of the references to colour in the Figure, the reader is referred to the web version of this article).

Solovchenko, 2018). Spectral scans were performed on a Lambda 1050 UV/VIS/NIR Spectrophotometer (PerkinElmer, Inc., Massachusetts, USA). Chl, Car, AnC and Flv concentrations were expressed both as area and dry weight units. To do this, a similar leaf sample were collected and dried at 70 °C for 48 h to express concentrations on a dry weight basis.

2.3. Total soluble phenolic compound quantification

Total soluble phenol (PhC) quantification was carried out according to Ragaee (2006), with modifications. Briefly, 100 mg of fresh leaves were crushed in 80 % (v/v) methanol. The methanolic extracts were centrifuged at 15,000 rpm for 60 s. Phenolic quantification was initiated by the addition of 85 µL of methanolic extract, 85 µL of the Folin-Ciocalteu reagent (1 M), 170 µL of Na₂CO₃ (3.56 M) and 830 µL of deionized water. The samples remained in the dark for 40 min and were then centrifuged for 30 s at 15,000 rpm followed by analysis on a spectrophotometer at λ725 nm. The equivalent PhC concentration was determined using gallic acid as reference, $Y = 87.651x + 1.6515$; $r^2 = 0.993$.

2.4. Optical microscopy analysis

Cross sections of fresh leaves (hand cut) were used for histological studies, particularly where chloroplast (green) and extra-plastidial (pink-purple) pigments are distributed. Leaf segments (2 cm²) of the medial region were fixed with Karnovsky's solution (Karnovsky, 1965) and stored at 4 °C until processing. Subsequently, the fixed samples were dehydrated in an increasing ethanol series [50, 70, 80, 90 and 100 % (three times)] and infiltrated with methyl-methacrylate (Leica Histo-resin®) (Souza et al., 2016). Block sectioning was performed on a rotation microtome (Eikonol, São Paulo, BRA) and the sections (8µm) were then dyed with Toluidine Blue in acetate buffer pH 4.7. The images were obtained on a Leica ICC50 light microscope (Leica Company, Wetzlar, DEU). Histochemical and anatomical characteristics for leaves, mesophyll and parenchyma cells, epidermis of the adaxial and abaxial faces and free intercellular spaces were analyzed using the ImageJ software (<https://imagej.nih.gov/ij>).

2.5. Transmission electron microscopy

Transversal sections leaf samples were fixed in modified Karnovsky's solution (Karnovsky, 1965) for transmission electron microscopy (TEM) analysis. Karnovsky's solution was composed by TEM-grade 2.5 % glutaraldehyde and 2 % paraformaldehyde in 0.05 M cacodylate buffer (pH 7.2) and post-fixed for 1 h with 1 % osmium tetroxide. The samples were then contrasted in bloc with 0.5 % uranyl acetate overnight, dehydrated in an acetone concentration series [30, 50, 70, 80, 90 and 100 % (three time)], infiltrated and then polymerized into Spurr low viscosity epoxy resin. Sections (70 nm thick, Diamond Knife) were obtained using an ultramicrotome MTX Power-tome X (Boeckeler Instruments RMC Products, Egham, UK) and contrasted with 3 % uranyl acetate and lead citrate. Analyses were performed using a transmission electron microscopy JEOL JEM 1400 (Leica Microsystems Inc., Illinois, USA) in 80 kV. More details in (Falcioni et al., 2018; Moriwaki et al., 2019).

2.6. Optical leaf properties

Reflectance (R) and transmittance (T) were measured directly using two coupled spectroradiometers (ASD Inc; FieldSpec 3 Jr., Colorado, USA), collimated and calibrated with a standard Spectralon® dish as the 100 % reflectance reference immediately before use, following manufacture instructions to ensure identical calibration. An ASD spectroradiometer light beam plant probe was coupled to another probe at the opposite leaf surface with the light off, in order to simultaneously measure leaf reflectance and transmittance (350–2500 nm), respectively. The probes were positioned attached to leaf lamina by a slight pressure through the rubber end, to avoid light leaking. The equipment was programmed to perform 50 readings for each sample, thereby generating an average spectral curve. All light emitted by one probe should be reflected and detected by the same probe (R), absorbed or transmitted through the leaf lamina and, finally, detected by the opposite probe (T), where light absorption (A) was estimated as $[A = 1 - (R + T)]$ (Falcioni et al., 2017). This experimental procedure ensures the simultaneous measurements of both R and T. Also, this approach is considered a unidimensional system. Light source is

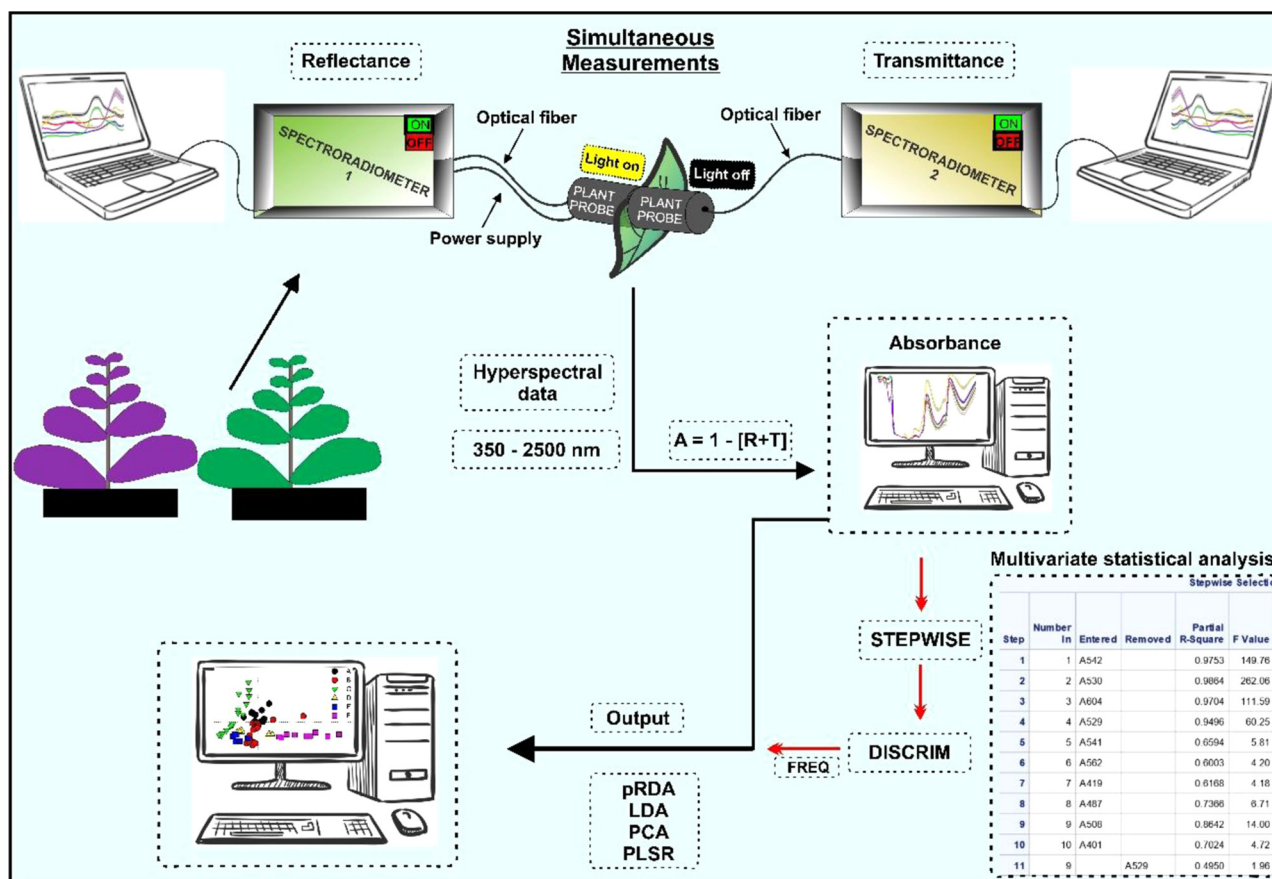


Fig. 2. Representative schematic of the analysis method applying high resolution (350-2500 nm) hyperspectral sensors using two calibrated and collimated spectroradiometers to obtain simultaneous reflectance and transmittance data. The absorbance data were calculated by equation $[A = 1 - (R + T)]$. Spectral curve of reflectance or transmittance data can be obtained with ~ 10 s for each leaf sample. In addition, multivariate analyses were performed to select the most significant wavelengths based on the proc STEPDISC routines, by STEPWISE regressor variables selection (wavelength - nm) and obtaining the discriminant models by the proc DISCRIM procedure, with simulation of the validation models of the wavelengths selected through the proc FREQ (red row show these process). Multivariate statistical can be directly applied for analysis, calibration and development models by Partial Redundancy Analysis (pRDA), Linear Discriminant Analysis (LDA), Principal Component Analysis (PCA), Partial Least Squares Regression (PLSR) or others multivariate analyses. The outputs were used for species discrimination and pigment content estimation based on hyperspectral data. (For interpretation of the references to colour in the Figure, the reader is referred to the web version of this article).

orthogonal to the leaf lamina. In addition, this procedure was carried out in order to measure R from adaxial leaf surface and inverted to measure R from the abaxial leaf surface. A simple measurement and statistical analysis scheme are displayed in Fig. 2.

2.7. Univariate statistical analysis

The data (pigments and anatomy) were submitted to a One-Way ANOVA for mean comparisons. Statistical significances were considered at $P < 0.05$ (Zar, 2010). Duncan's test was applied to compare data means, also at $P < 0.05$. Pearson's correlation test was also applied when applicable. All univariate statistical analyses were performed using the Statistica 10® software (Statsoft Inc., Oklahoma, USA). All graphs were prepared using the Sigma Plot 10.0® (Systat, California, USA) software package.

2.8. Multivariate statistical analysis

2.8.1. Reflectance, transmittance and absorbance spectral deconvolution

Initially, a statistical analysis of the spectral curves by a principal component analysis (PCA) was performed using the The Unscrambler X 10.4® software (Camo Software, Oslo, NOK). The degree of explanation is attributed using the first two components (PC1 and PC2) prior to obtaining Fisher's discriminant linear models. The discriminant

functions were obtained using the proc STEPDISC algorithm, applying the STEPWISE method available in the Statistical Analysis System® software (SAS Institute, Inc. North Carolina, USA). Wavelengths were selected according to Lambda Wilk's value and following likelihood criteria and partial F-value input. A 5% criterion for input and 10 % for output were applied as error probabilities.

The wavelengths that best explained the differences were subjected to a discriminant analysis using the proc DISCRIM routine available in the SAS® software, in order to create predictive models through linear combinations of predictor variables (wavelengths). The obtained models were then simulated through the proc FREQ using 70 % of the spectral curves and tested with the 30 % remaining curves. This procedure was tested 50 times in a randomized mode, independently, in order to predict the chance of success based (and error) on the selected spectral bands. Thus, only wavelengths able to discriminate all plants were selected (da Silva Junior et al., 2017).

2.8.2. Partial Least Squares Regression (PLSR) analysis of reflectance and absorbance curves

For the model construction, the data were divided into two groups, the first set consisting of 30 samples used for calibration and cross-validation and a second group composed of 25 independent samples used for external prediction of the PLSR model. Thus, the biochemical data of foliar pigments quantified as total chlorophylls (Chl a + b),

carotenoids (Car), anthocyanins (AnC), flavonoids (Flv) and phenolic compounds (PhC) were compared to the spectral curves. Each variable (pigment) was treated as an independent variable. The multivariate calibration models were developed by a Partial Least Square Regression (PLSR) using the The Unscrambler X version 10.4 software (Camo Software, Oslo, NOK). The algorithm for model inputs was NIPALS and output outlier limits were defined by Leverage's type and analyzed by the Leverage and Hotelling's T^2 (limit in 5%). The predictive ability of the calibrations models was evaluated by calculating the coefficients of determination (R^2) and the root mean square error (RMSEC for calibration, RMSECV for cross-validation and RMSEP for prediction). The leaves-one-out cross validation method was used as a preliminary form of attribute prediction. In parallel, an independent predictor based on an unknown dataset was also used. Following Minasny and McBratney (2013), $R^2 > 0.75$ values are considered as displaying excellent prediction capacity, R^2 values between 0.75 and 0.5 are considered good, and $R^2 < 0.5$, low. Additionally, the ratio of performance to deviation (RPD) was calculated by equation $[RPD = \frac{1}{\sqrt{1-R^2}}]$ with R^2 calculated (R^2C), cross-validation (R^2CV) or predicted (R^2P) for the calculation, and applied as a useful indicator of the expected accuracy of PLS predictions. Additionally, for a quality analytical performance, RPD must be at least 3 for agricultural applications, while RPDs between 2 and 3 are considered both good, 1.5–2 as medium and lower than 1.5, as poor (Nanni et al., 2018). β -coefficients, $Y = \beta_0 + \beta_1\lambda_1 + \dots + \beta_n\lambda_n + \varepsilon$, for leaf pigments obtained with hyperspectral data for reflectance and absorbance curves (350 at 700 nm) are displayed.

3. Results

3.1. Chloroplast and extra-plastidial pigment contents

When exploring genetic diversity, "green" and "purple" leaves (Fig. 1) displayed variations in chloroplast (Chl and Car) (Fig. 3a) and extra-plastidial pigment contents (AnC, Flv and PhC) ($P < 0.05$) (Fig. 3b-c and 4c inset) expressed both as area (Fig. 4) and mass (Fig. S1). Chl and Car contents were higher in *Philodendron* sp., *T. pallida* and *C. fruticosa* black-mystique (1170 to 1380 mg m^{-2}) and lower in *P. purpureum* and *C. fruticosa* florida-red (532 and 517 mg m^{-2} , respectively) ($P < 0.05$) (Fig. 4a).

AnC levels were always higher for purple plants ($P < 0.05$, above 50 up to 162 nmol cm^{-2}), in relation to green plants (Fig. 4b), however similar between *P. purpureum* and *C. fruticosa* florida-red ($P > 0.05$) when expressed as mass unit (Fig. S1). It was possible to detect AnC in green plants, however at extremely low values (2.3 – 4.8 nmol cm^{-2}) (Fig. 4b). Correlated with AnC ($r = 0.76$; $P < 0.05$), flavonoid levels were higher ($P < 0.05$) in purple species (233 – 728 nmol cm^{-2}) and lower in green plants (30 – 100 nmol cm^{-2}) (Fig. 4c). PhC contents in leaves were not related to Flv or AnC accumulation (Fig. 4c inset).

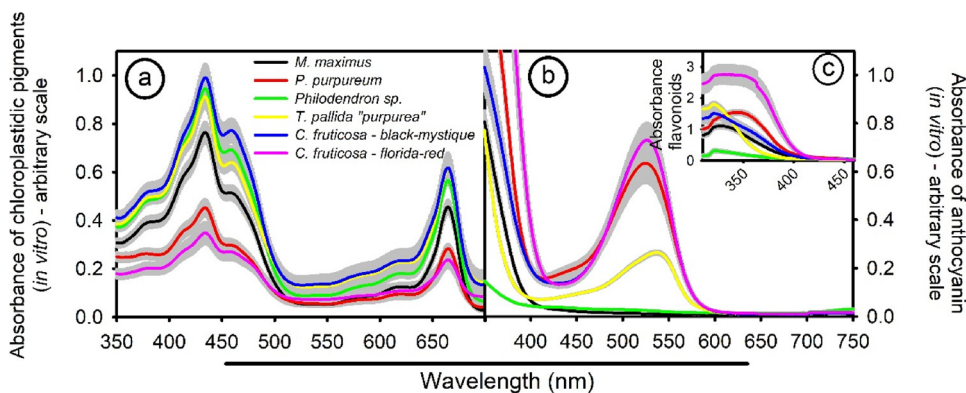


Fig. 3. (a) Spectral absorbance curve of total photosynthetic pigments (350–700 nm), (b) anthocyanins (350–750 nm) and (c) flavonoids (300–460 nm) (*in vitro*) in leaves belonging to different species. Each repetition was produced by taking the means of measurements calculated for five different leaves. ($n = 5 \pm \text{SE}$). These curves are obtained per unit leaf. The standard error is shown in grey.

3.2. Leaf anatomy

Philodendron sp. evidenced homogeneous and compact palisade parenchyma, albeit with large spaces in the lacunar parenchyma towards the abaxial face (Fig. 5c). *T. pallida* exhibited anthocyanins (AnC) arranged on both the adaxial and abaxial surfaces, with a thick hypodermis, formed by 1–3 cell layers and the presence of both palisade and spongy parenchyma (Fig. 5d). The anthocyanins in *C. fruticosa* black-mystique are arranged in the adaxial and abaxial epidermis. This species also presents a homogeneous chlorophyll parenchyma comprising isodiametric cells in the half facing the adaxial face and flattened in the lower half facing the abaxial face (Fig. 5e). *C. fruticosa* florida-red presented a homogeneous parenchyma, with scarce intercellular spaces, constituted by isodiametric cells and exposed anthocyanins in both epidermal faces. No typical chlorophyll parenchyma was found, although scattered spots containing chlorophyll were present (Fig. 5f).

T. pallida demonstrated increased leaf thickness, associated with increases in the adaxial and abaxial epidermis (Figs. 5 and S2; inset). On the other hand, *Philodendron* sp. and *C. fruticosa* black-mystique showed similar leaf thickness ($P > 0.05$). Typical plants with C4 photosynthetic metabolism, *M. maximus* and *P. purpureum* presented lower leaf and parenchyma cells (mesophyll cells and bundle sheath cells) thickness ($P < 0.05$), but similar adaxial and abaxial epidermis thickness ($P > 0.05$) (Fig. 5a-b and Fig. S2a-d).

3.3. Mesophyll (chlorenchyma) cell ultrastructure

Rounded to flat chloroplasts were observed in all species, in some cases also containing starch (Fig. 6). In *C. fruticosa* florida-red, parenchyma cells were mostly absent from chloroplasts, but when present, were associated with underdeveloped thylakoids, and low electro-density lamella and stroma (Fig. 6f inset). The presence of electro-density points in the vacuoles were evidenced in AnC-accumulating plants (Fig. 6f). Higher thylakoid stacking and electro-density was evidenced in *Philodendron* sp. among all assessed species (Fig. 6c), which may be associated to higher pigment, protein and lipid contents (Fig. 6). Structures called plastoglobules were present in all species (Fig. 6, arrow). Visually, no evidence of cell wall changes was observed based on electro-density and thickness patterns (Fig. 6).

3.4. Optical leaf properties

In most species, the abaxial epidermis presented higher reflectance indices than the adaxial epidermis (Fig. 7a-b and S3) reaching 89 % and 61 % higher values than the adaxial surface in *Philodendron* sp. and *Tradescantia pallida*, respectively. In contrast, *P. purpureum*, that displays dorsiventral symmetry, presented similar reflectance levels on both surfaces (Fig. 7a-b and S3). Plants with no AnC displayed increased reflectance and transmittance in the green spectral region

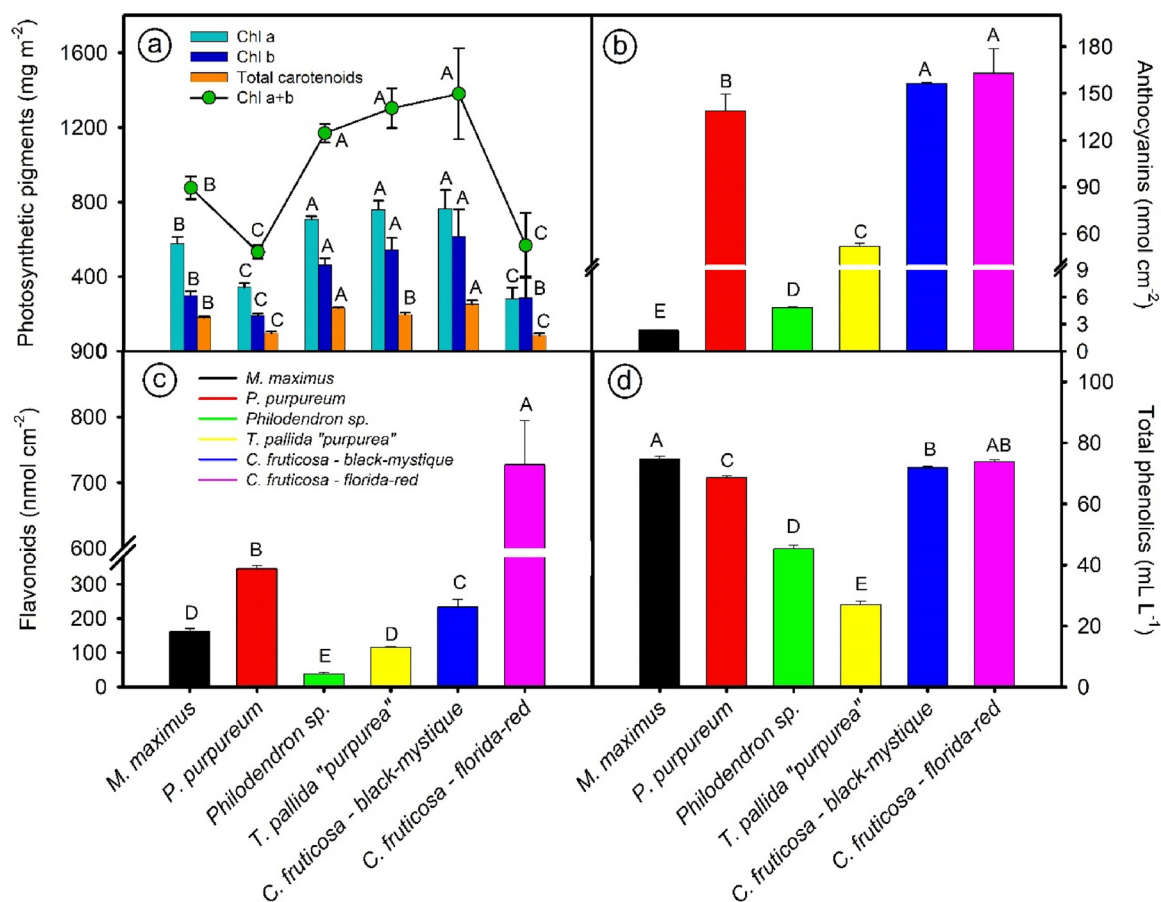


Fig. 4. Plastidial (photosynthetic) and extra-plastidial (mainly vacuolar) pigment contents expressed by leaf area unit. (a) chlorophyll a (Chla), chlorophyll b (Chlb), chlorophylls a + b (Chl total), total carotenoids (Car); (b) anthocyanins (AnC), and (c) flavonoids (Flv) and (d) total soluble phenolics equivalent to gallic acid from six species displaying naturally varying pigment contents. Different letters over dots or bars indicate statistical differences between plants (Duncan's test; $P < 0.05$). ($n = 5 \pm SE$).

(501–565 nm) (Fig. 7a-d), while values decreased in the presence of AnC (Fig. 7a-d).

The absorption curves are inversely proportional to the reflectance and transmittance curves ($P < 0.05$) between 501 and 565 nm, with maxima between 530 and 550 nm (Fig. 7e-f). Therefore, *T. pallida* and *C. fruticosa* (black-mystique and florida-red) exhibit increases over 90 % in green (501–565 nm) to yellow (566–590 nm) absorption ($P < 0.05$) (Fig. 7e-f). On the other hand, leaf absorption curves were different ($P < 0.05$) between *P. purpureum* and *C. fruticosa* (black-mystique and florida-red), although both exhibit similar anthocyanin levels (Fig. 3b and 7e-f). The region formed by UV-A (350–400 nm), violet (401–439 nm) and blue (440–485 nm) bands displayed small but significant differences ($P < 0.05$) between species (Fig. 7). It is emphasized that at wavelengths less than 500 nm an intense competition occurs between carotenoids, chlorophylls, flavonoids and soluble phenolic compounds that directly influence leaf profile light interactions (Fig. 7 and 8).

In the near-infrared region (700–1300 nm), reflectance of up to 50 % of the incident light and absorbance with a maximum of 18 % at 700 nm and with progressive decreases up to 1058 nm reaching values close to zero for all species were observed (Fig. 8a-b and e-f). On the other hand, in the short-wave infrared region (1300–2500 nm), reflectance decreases and absorbance increases were noted (Fig. 8a-b and 8e-f), in particular for *T. pallida* (Fig. 8).

3.5. Principal Components Analysis as a tool for species discrimination

Principal component analyses (350–700 nm) indicate the

formation of distinct clusters between species through the analysis of reflectance, transmittance and absorbance data (Fig. 9). The first two components explained over 98 % of the total data variance obtained for reflectance, transmittance or absorbance (Fig. 9a-f). The total explanation percentage of PC1 was above 86 % and 54 % for the adaxial (Fig. 9a, c and e) and abaxial (Fig. 9b, d and f) surfaces, respectively. The transmittance data presented clusters overlap between two species, explained in 11 % by PC2 (Fig. 9c-d). The clusters formed by the reflected light and absorbed light were completely separated from each other, with complete absence of overlap and values over 80 % established by the PC1 for the adaxial surfaces (Fig. 9a-b and e-f). Higher degrees of total variance explanations were achieved by absorbed light. In addition, absorption data were also associated to the PCA highest precision and accuracy (Fig. 9f).

3.6. Deconvolution of the most significant spectra and spectral bands

Spectra deconvolution (400–700 nm) by the STEPDISC method selected 36 wavelengths (10 for reflectance, 8 for transmittance and 18 for absorbance), all significant based on the partial R^2 , F-value and average squared canonical correlation criteria (Table S1), covering from the blue (400–480 nm) and red (600–660 nm) regions, but mainly in the green/yellow region of (500–600 nm) (Table S1).

Based on the wavelengths selected by the proc STEPDISC (SAS model) (Table S1), the discriminant models generated with the sample calibration of the spectral curves and defined by the contingency coefficients ($R^2 = 0.9129$), were validated with independent samples in the discriminant models generated for reflectance, transmittance and

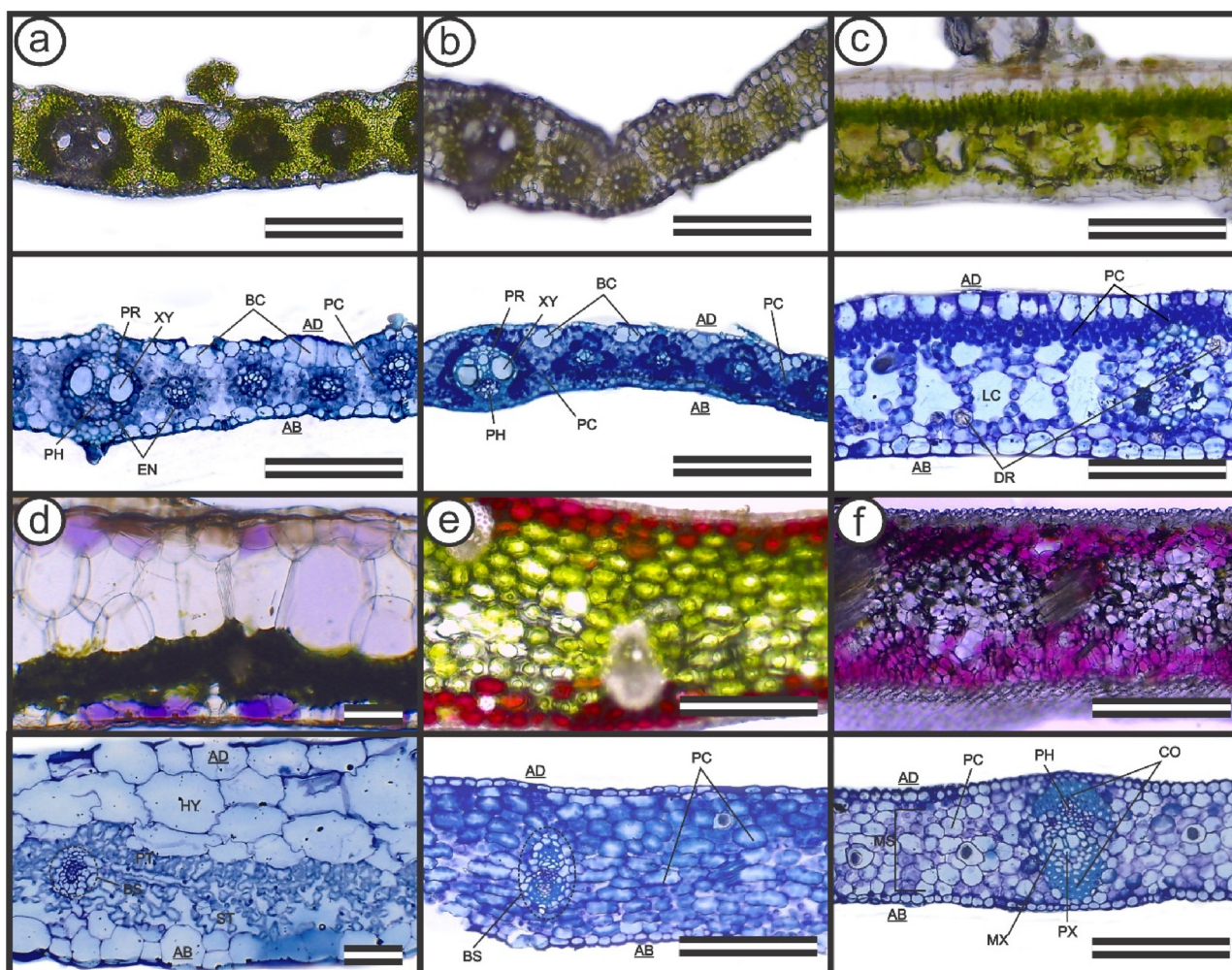


Fig. 5. Light microscopy of fresh leaf cross -sections (hand cut, up) and histoiresin-fixed (below) of representative leaves from (a) *Megathyrsus maximus*, (b) *Pennisetum purpureum*, (c) *Philodendron* sp., (d) *Tradescantia pallida*, (e) *Cordyline fruticosa* (black-mystique) and (f) *Cordyline fruticosa* (florida-red). AB = abaxial epidermis, AD = adaxial epidermis, BC = bulliform cell, BS = bundle sheath cell, CO = collenchyma, DR = druse, EN = endoderm, HY = hypoderm, LC = lacune (large air space), MS = mesophyll, MX = metaxylem, PC = parenchyma cell, PH = phloem, PR = pericycle, PT = palisade tissue, PX = protoxylem ST = spongy tissue, XY = xylem. Scale bar = 200 μ m. (For interpretation of the references to colour in the Figure, the reader is referred to the web version of this article).

light absorption, with very high significance ($P < 0.001$). The constructed and validated models correctly classified total reflectance (92.71 %; $R^2 = 0.890$), transmittance (90.26 %; $R^2 = 0.893$) and absorbance (88.34 %; $R^2 = 0.888$) data (Table 1 and 2). The data indicate very low classification errors among green-green, purple-green or even purple-purple species (Table 2). It should be noted that only absorbance data were able to completely distinguish (100 % accuracy) between *Philodendron* sp. and *Tradescantia pallida* (Table 2, green row).

3.7. Estimation of foliar pigments contents by the PLSR method

The models estimated by a Partial Least Square Regression (PLSR) in response to reflectance and light absorption spectral curves (350–700 nm) for leaf pigments (total chlorophylls, carotenoids, anthocyanins, flavonoids and phenolic compounds) were considered good to excellent, assessed by the lower root mean square error (RMSE) values, the coefficients of determination (R^2) and the ratio of performance to deviation (RPD) (Fig. 10 and S3). In sum, the models presented high pigment content prediction capacity, despite high spectral interference of one group of compounds with another group under diverse anatomical effects over spectral curves. In addition, internal validation by the leave-in-out method (evaluated by RMSEC) and compared with the root mean square error of cross-validation (RMSECV) presented extremely

low values (excellent results) associated with R^2x , in particular for anthocyanins (AnC) (RMSEC = 0.016 and RMSEP = 0.037), flavonoids (Flv) (RMSEC = 0.059 and RMSEP = 0.096) and phenolic compounds (PhC) (RMSEC = 0.001 and RMSEP = 0.001) (Fig. 10e–j). In the model validation estimated by the root mean square error of prediction (RMSEP) obtained by external analyses, the data confirm the quality by fitting RMSEC (Fig. 10), i.e., these data presented excellent predictive abilities as obtained by hyperspectral sensors, using both reflectance and absorbance curves (Fig. 7 and S4). These results were consistent with those from the PCA and STEPDISC method analyses (Fig. 9, S4 and Tables 1,2, S1).

4. Discussion

4.1. Interaction between anatomical structures on spectral signatures

Spectral signatures are influenced by foliar pigment class (composition) and concentration, as well as anatomical and ultrastructural plant cell characteristics. A thinner mesophyll or leaf containing many cell spaces, correlated to greater amounts of air spaces and gaps next to cellular agglomerates (Fig. 7a–c), such as in *M. maximus* and *Philodendron* sp., revealed higher transmittance values (Fig. 8c–d), which may have contributed to lower light attenuation in the gaps and higher light

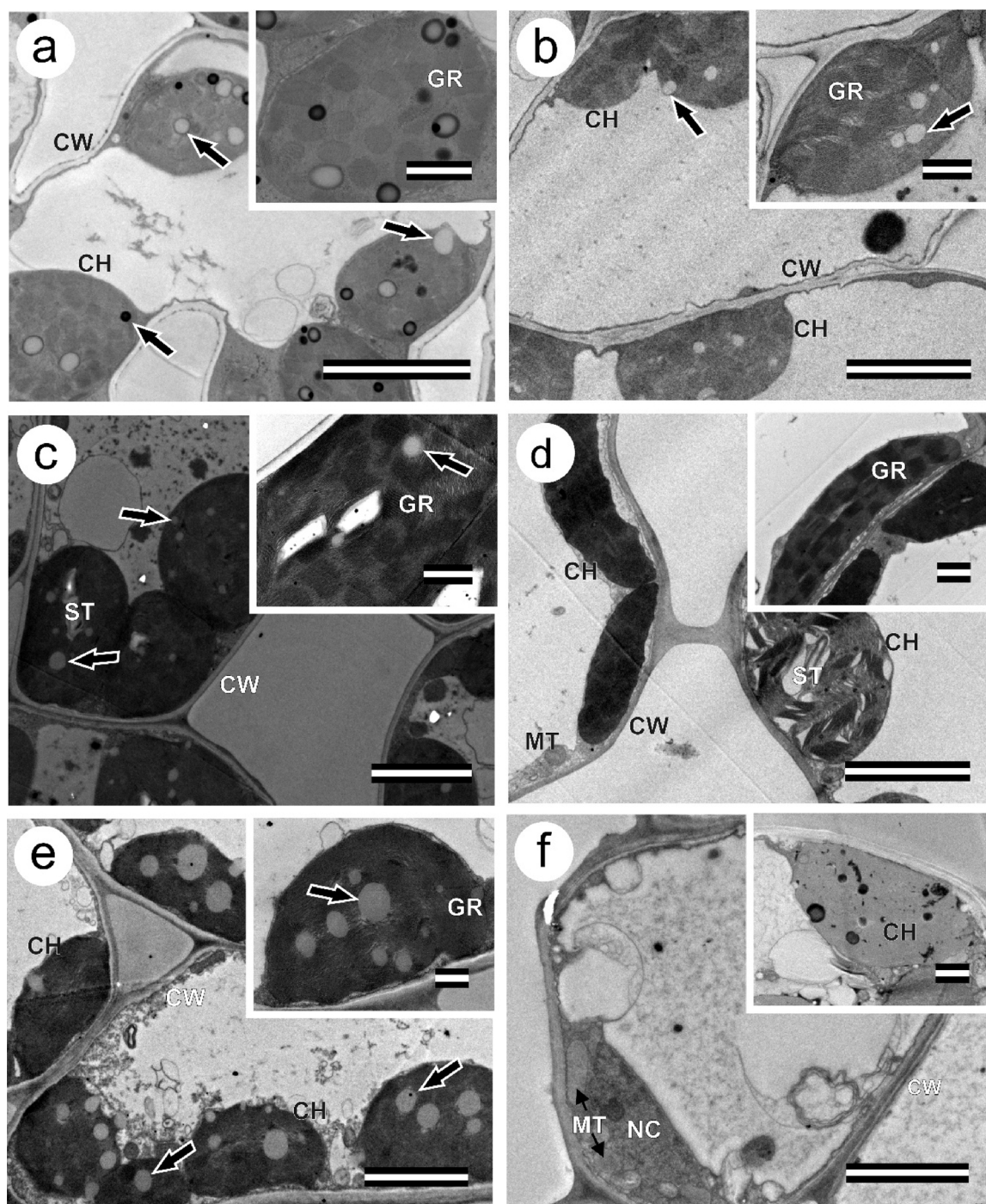


Fig. 6. Chlorenchyma cell ultrastructure viewed by transmission electron microscopy (TEM). (a) *Megathyrsus maximus*, (b) *Pennisetum purpureum* (c) *Philodendron* sp., (d) *Tradescantia pallida*, (e) *Cordyline fruticosa* (black-mystique), (f) *Cordyline fruticosa* (florida-red). Arrow = plastoglobules inside chloroplast, NC = nucleus, CH = chloroplast, CW = cell wall, GR = granum, ML = middle lamella, MT = mitochondria, ST = starch. Scale bar = 4 μ m and inset 1 μ m. (For interpretation of the references to colour in the Figure, the reader is referred to the web version of this article).

absorption in cell agglomerates (Gates et al., 1965). Similarly, thinner tobacco leaves display higher transmittance values compared to thicker leaves (Falcioni et al., 2017). However, thicker leaves with similar photosynthetic pigment contents compared to thinner leaves display greater green absorptivity (Falcioni et al., 2017) indicating that the green light should be absorbed at greater leaf tissue depths (Vogelmann and Han, 2000), significant for lacunar parenchyma photosynthesis (Evans and Vogelmann, 2003). These data reinforce the idea that leaf anatomy can affect optical patterns regardless of pigment content. The intrinsic ability of plants to perceive the environment (Wada et al.,

2005) and alter optical leaf properties have been demonstrated in response to light levels, nitrogen fertilization (Moriwaki et al., 2019), anthocyanin (Hatier et al., 2013) and flavonoid levels (Gitelson and Solovchenko, 2018), hormone content (Falcioni et al., 2017) and saline stress (Carter and Knapp, 2001). Also, as demonstrated herein, variations in soluble phenol content levels (Fig. 4c, inset, Fig. 10i–j and S1) significantly alter absorption patterns from 350 to 500 nm.

Pigments significantly affect spectral leaf patterns, although the interferences of the cell wall and extra-plastidial components on absorption patterns between 400–700 nm appear to be minimal (Baldini

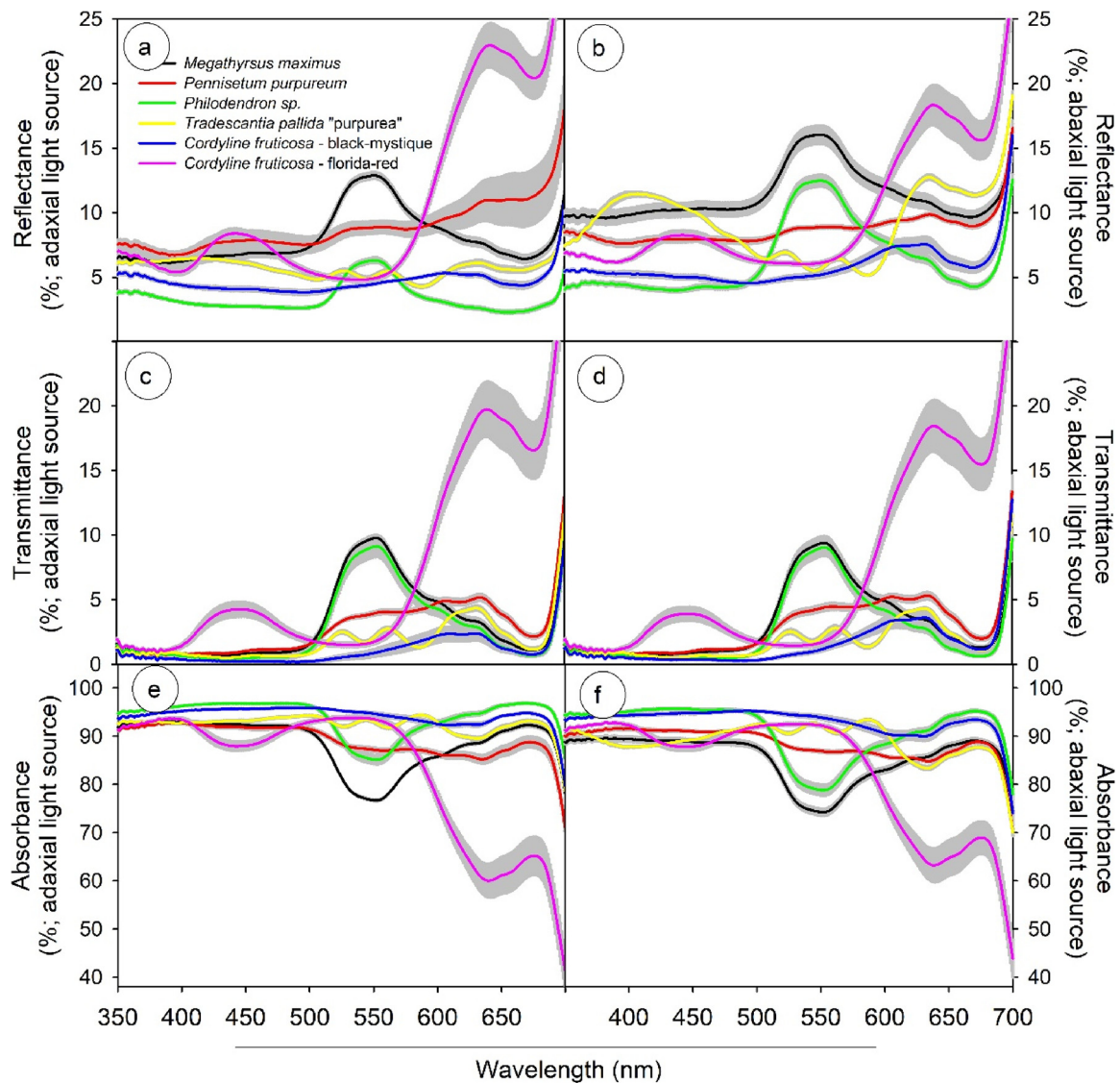


Fig. 7. Leaf spectral curves (*in vivo*) from 350 to 700 nm from fully expanded leaves belonging to different species. (a and b) reflectance, (c and d) transmittance and (e and f) absorbance. (a, c and e) adaxial light source and (b, d and f) abaxial light source. A light beam from a plant probe was coupled to another probe aligned on opposite surface with the light off, in order to simultaneously measure leaf reflectance and transmittance (350–700 nm). This procedure was repeated on both surfaces. Each repetition was produced by taking the mean measurements calculated from two different leaves from same plant. ($n = 5 \pm SE$). The standard error is shown in grey.

et al., 1997; Gates et al., 1965; Jacquemoud and Baret, 1990; Latimer, 1958; Maas and Dunlap, 1989; Ustin et al., 2001). Cellular structures such as cell walls, cytoplasmic content and organelles like mitochondria and chloroplasts, when devoid of any type of pigment, exhibit over 95 % incident light absorption reduction concerning the leaf profile in relation to the visible region (Fig. 8e–f) (Gates et al., 1965; Latimer, 1958). The absorbed light of 500–1300 nm in albino leaves is minimal, as reported by Baldini et al. (1997) and Maas and Dunlap (1989). Despite low absorptivity, transmittance is not extremely high (Fig. 8). As an example, the 1058 nm wavelength approaches zero absorption, but T is not close to 100 % following the Beer-Lambert law. Spectral bands in the near-infrared are capable of interacting inside the mesophyll and undergo internal scattering (Gates et al., 1965; Latimer, 1958; Ustin et al., 2001) so that the incident light is detected equitably in the sensors in either the reflectance or transmittance position, with values around 50 % for each (Fig. 8a–d). Leaves with a more compact mesophyll and a greater number of cell layers generally presented higher reflectance values, such as *Cordyline* species (Fig. 7e–f and 8a–b).

In the short-wave infrared (1300–2500 nm) a strong interference

of leaf thickness were observed (Jacquemoud and Baret, 1990; Kume, 2018). These effects are most evident in tissues containing cells with large vacuoles and high water content as evidenced by light and TEM microscopy and clearly noticeable in thicker *T. pallida* purpurea leaves compared to thinner *C. fruticosa* leaves. A high correlation ($r = 0.91$; $P < 0.001$) was noted between leaf thickness and absorbance at 1440 nm (peak at the water absorbance band). There is no evidence that Flv and AnC can interfere in the absorbance in this spectral range, according to spectral pigments and foliar curves (Fig. 4c, 5 d, 6 e–f) (Gates et al., 1965; Latimer, 1958).

Hypodermis cells (atypical cell) with large vacuoles and high water content (Fig. 5d) weakly contribute to the absorption of electromagnetic radiation (except in the presence of AnC and Flv) in the visible range, as reported by Solovchenko (2010), and strongly related to changes in the light refractive index in the transition from the hypodermis to the palisade parenchyma, immediately below, with a relatively higher proportion of air spaces. This refractive index change induces higher rates of specular and diffuse reflectance in the air-water transition (Latimer, 1958; Solovchenko, 2010; Ustin et al., 2001). This

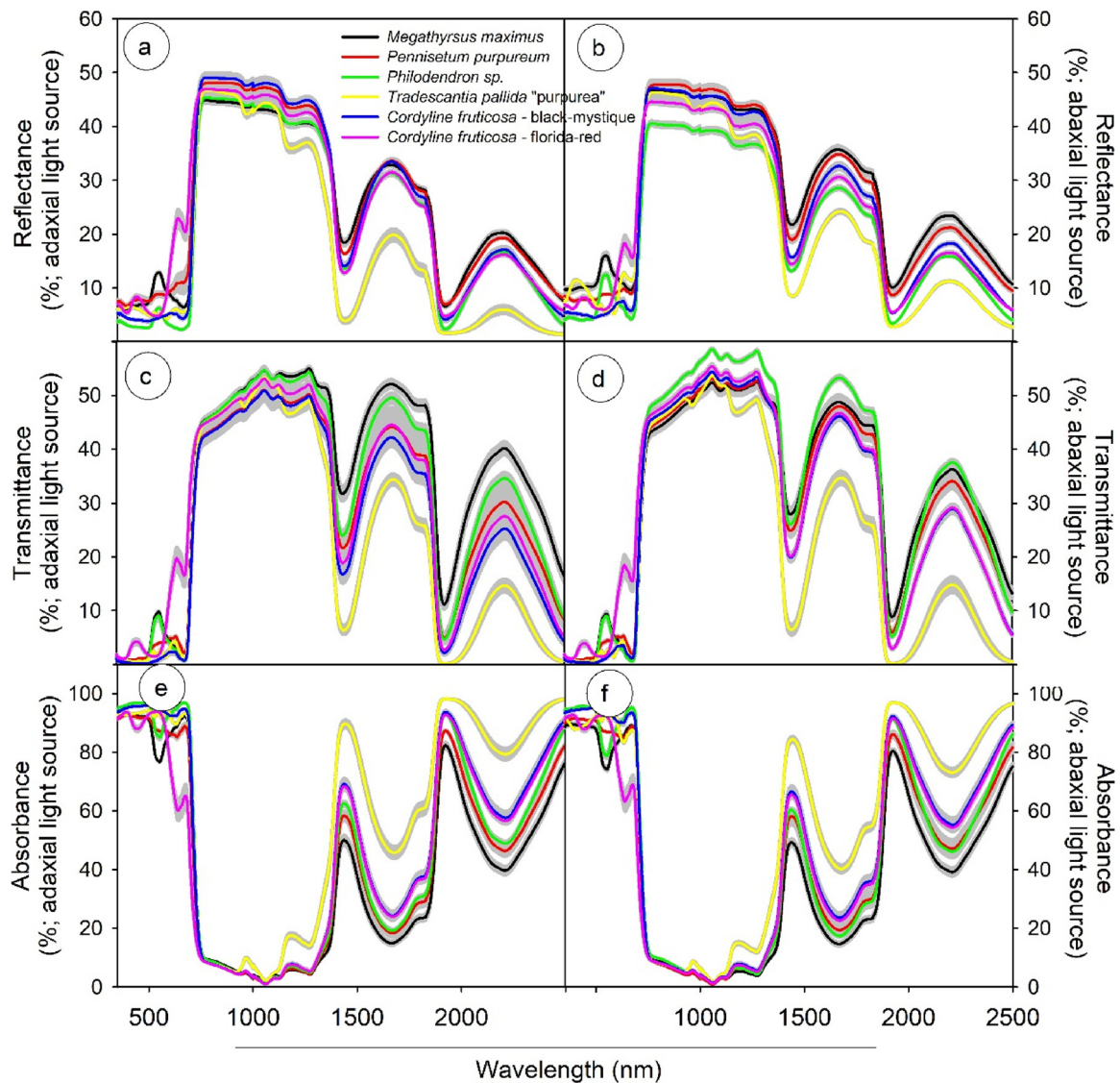


Fig. 8. Spectral leaf absorbance curves (*in vivo*) from 350 to 2500 nm of healthy fully expanded leaves belonging to different species. (a and b) reflectance, (c and d) transmittance and (E and F) absorbance. (a, c and e) adaxial light source and (b, d and f) abaxial light source. Each repetition was produced by taking the means of the measurements calculated from two different leaves from same plant. ($n = 5 \pm SE$). The standard error is shown in grey.

anatomical characteristic can explain the high scattering and light absorption rates in the photosynthetically active range in the palisade parenchyma below when the light is impinging on the adaxial position, but also higher reflectance indices of the adaxial epidermis in relation to the abaxial epidermis in *T. pallida* and *Philodendron sp.* when the light is in the abaxial to adaxial direction (inverted).

4.2. Pigments disposition in various structures

Variations in the size, organization and arrangement of the cells present in the leaf mesophyll influence optical patterns, particularly with regard to absorbance (Fig. 7 and 8). Plants that contain similar pigment content, such as anthocyanins or chlorophylls (Fig. 4a-b), presented distinct spectral profile patterns across the visible region (Fig. 7). Therefore, spectral variations are related to variations in internal cellular structure (Fig. 6) (Féret et al., 2017; Ustin et al., 2001; Xiao et al., 2016). Low pigmented spaces are present between each *P. purpureum* vascular bundle, allowing for freely transmitted light, while such spaces are absent in *C. fruticosa* (florida-red), increasing absorbance particularly in the green band associated to the presence of AnC, but not Flv (Fig. 3).

The presence of AnC is directly correlated with increased green light absorbance in *T. pallida* (Fig. 5c–d e 6e–f). In *Philodendron sp.* (which does not accumulate AnC; Fig. 4) it is observed that the high absorptivity in the green region is due exclusively to chlorophylls, whereas in *T. pallida* an overlapping of different pigment classes leads to a total effect on the spectral curve. The individual interferences of chlorophylls and anthocyanins could be statistically separated by the discriminant analysis using 351 points from 350–700 nm (instead of "fixed" models), in which a greater contribution of bands between 500 and 600 nm is noted for the separation (Tables 1,2 and S1).

By the Beer-Lambert law, a proportionality in absorbance relative to the absorbance peak of a certain substance is expected if the pigment were evenly distributed within the cell (Terashima et al., 2009). It is noted that *in vivo* pigments are compartmentalized in different organelles (e.g., chloroplast and vacuole, mainly), whose *in vivo* concentrations are greater in relation to the distribution in an *in vitro* solution. As evidenced by Moriwaki et al. (2019), nitrogen supplementation in tomato plants resulted in increases in chlorophyll content and increased green light absorption, but not blue or red (Moriwaki et al., 2019). This phenomenon emphasizes absorption saturation in the peaks and linearity in lower absorptivity bands. The

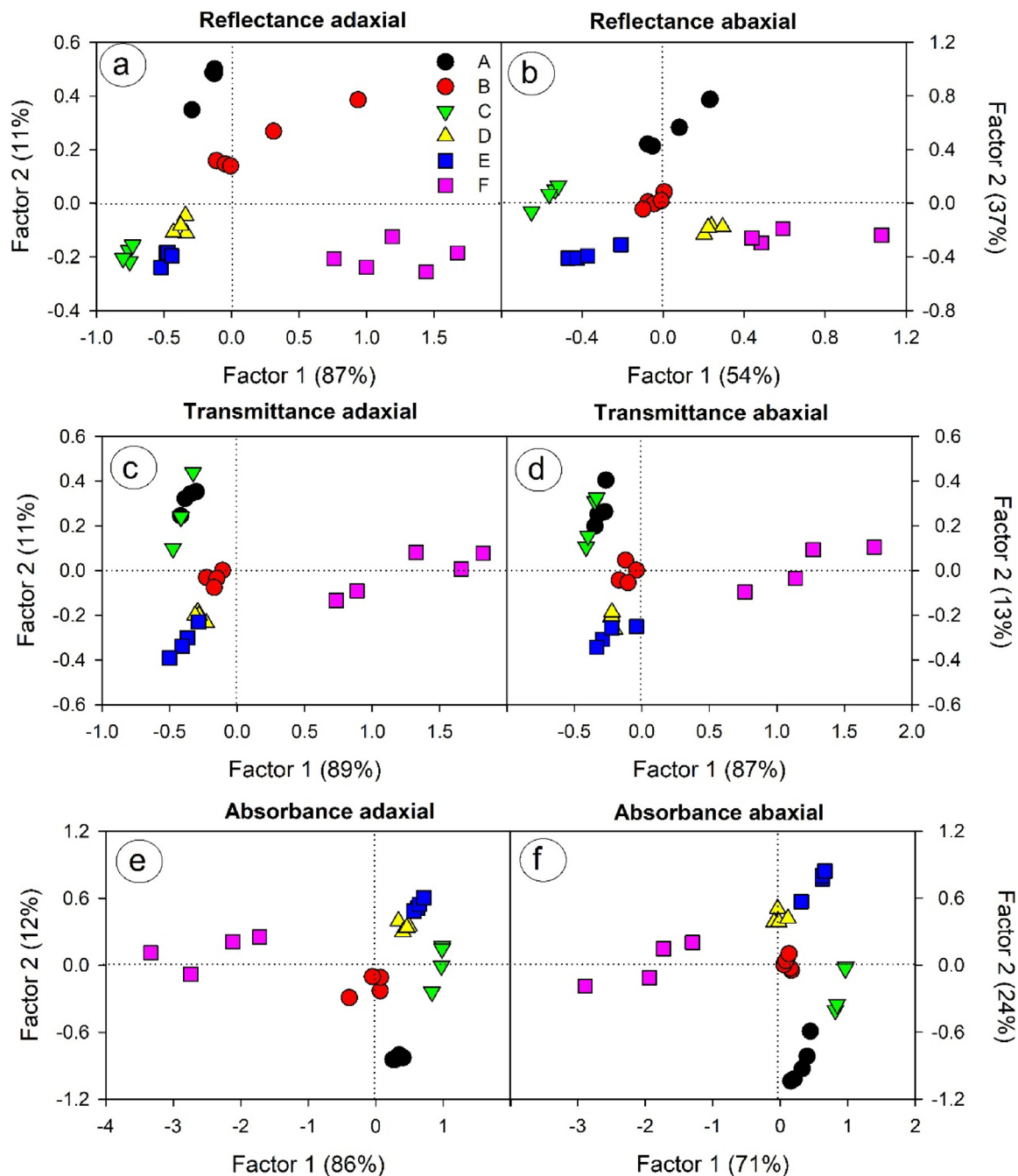


Fig. 9. Principal component analysis (PCA) of spectral curves from different species. (a and b) reflectance, (c and d) transmittance and (e and f) absorbance. Measurements obtained from the adaxial (a,c and e) or abaxial (b, d and f) surfaces. (n = 6).

Table 1

Stepwise discriminant output for wavelengths, indicating error frequency and acceptance by models comprising reflectance, transmittance and absorbance data.

Measurements	Model test	Frequency (number)	Percentage (%)
Reflectance	Error	27	7.28
	Accept	344	92.71
	Total	371	100
Transmittance	Error	38	9.74
	Accept	352	90.26
	Total	390	100
Absorbance	Error	45	11.66
	Accept	341	88.34
	Total	386	100

higher green absorptivity is related to thylakoids richly stacked in chloroplasts and presenting strong electron-densities when visualized by TEM (Moriwaki et al., 2019) and as demonstrated herein in *Phylodendron* sp. and *T. pallida* chloroplasts (Fig. 6c–d).

TEM images aid in the understanding of spectral curves. TEM reveals electron-dense (and possibly light-absorbing) points and characteristic only in the vacuoles of plants containing AnC (Fig. 6). Therefore, it is evident that different elements (pigments and structure) must be integrated in order to understand spectral leaf properties (Falcioni et al., 2017; Féret et al., 2017; Fourty et al., 1996; Hatier and Gould, 2007; Kume, 2018; Moriwaki et al., 2019; Vogelmann, 1993; Xiao et al., 2016). Thus, for the understanding of *in vivo* responses, the inclusion of different spectral and anatomical analysis methods are relevant (Xiao et al., 2016).

Table 2

Output from the DISCRIM analysis using selected reflectance, transmittance and absorbance data wavelengths, indicating the error percentage and acceptance based on the model estimated using 70 % of data selected randomly among species. Green is the highest accept value and red, the highest error % from discriminating between species by model. FQ = frequency and ST = estimate.

Measurements	Species	Simulations	A	B	C	D	E	F	Total
Reflectance	<i>M. maximus</i>	FQ	50	2	4	0	1	0	57
		ST	87.72	3.51	7.02	0	1.75	0	100
	<i>P. purpureum</i>	FQ	1	59	0	1	2	0	63
		ST	1.59	93.65	0	1.59	3.17	0	100
	<i>Philodendron</i> sp.	FQ	1	0	57	0	0	0	58
		ST	1.72	0	98.28	0	0	0	100
	<i>T. pallida</i>	FQ	0	4	0	64	4	2	74
		ST	0	5.41	0	86.49	5.41	2.7	100
	<i>C. fruticosa</i> (black- mystique)	FQ	0	4	0	0	47	0	51
		ST	0	7.84	0	0	92.16	0	100
	<i>C. fruticosa</i> (florida-red)	FQ	0	0	0	0	1	67	68
		ST	0	0	0	0	1.47	98.53	100
Total		-	-	-	-	-	-	-	371
Transmittance	<i>M. maximus</i>	FQ	53	0	6	0	0	0	59
		ST	89.83	0	10.17	0	0	0	100
	<i>P. purpureum</i>	FQ	0	61	0	0	4	1	66
		ST	0	92.42	0	0	6.06	1.52	100
	<i>Philodendron</i> sp.	FQ	10	0	65	0	1	0	76
		ST	13.16	0	85.53	0	1.32	0	100
	<i>T. pallida</i>	FQ	0	0	1	64	0	0	65
		ST	0	0	1.54	98.46	0	0	100
	<i>C. fruticosa</i> (black- mystique)	FQ	0	3	0	0	45	7	55
		ST	0	5.45	0	0	81.82	12.73	100
	<i>C. fruticosa</i> (florida-red)	FQ	0	2	0	0	3	64	69
		ST	0	2.9	0	0	4.35	92.75	100
Total		-	-	-	-	-	-	-	390
Absorbance	<i>M. maximus</i>	FQ	58	6	6	1	7	0	78
		ST	74.36	7.69	7.69	1.28	8.97	0	100
	<i>P. purpureum</i>	FQ	2	50	2	0	3	0	57
		ST	3.51	87.72	3.51	0	5.26	0	100
	<i>Philodendron</i> sp.	FQ	0	0	78	0	0	0	78
		ST	0	0	100	0	0	0	100
	<i>T. pallida</i>	FQ	0	0	0	56	0	0	56
		FQ	0	0	0	100	0	0	100
	<i>C. fruticosa</i> (black- mystique)	ST	0	1	0	3	51	0	55
		FQ	0	1.82	0	5.45	92.73	0	100
	<i>C. fruticosa</i> (florida-red)	ST	1	4	1	5	3	48	62
		FQ	1.61	6.45	1.61	8.06	4.84	77.42	100
Total		-	-	-	-	-	-	-	386

4.3. Spectral signature deconvolution

The plant spectra of the screened pigments are also greatly influenced by scattering (multiple internal reflection/refraction), which arises from the complex morphology of plant cell tissues and causes considerable increases in the effective radiation absorption within plant tissues (Butler and Norris, 1960; Solovchenko, 2010; Vogelmann, 1993). Thus, light absorbed by pigment molecules convert the lowest-energy (ground) state to an excited state. This event should occur, if and only if, the light diffuses throughout the leaf profile and undergoes numerous internal scattering until reaching the target molecule (Sun et al., 1998; Xiao et al., 2016). On the other hand, this energy can be readily reflected or transmitted if this transfer is not favorable (Brodersen and Vogelmann, 2010; Gates et al., 1965). The ability to identify specific electromagnetic spectrum bands is manifested as a result of this exchange (Gates et al., 1965; Nanni et al., 2018). Thus, spectra deconvolution becomes a powerful tool in predicting foliar pigment concentrations (Fig. 10 and S3), but also in species

characterization and identification (Fig. 9, Tables 1 and 2) (Féret et al., 2017, 2008; Sims and Gamon, 2002), in particular, for plants displaying similar pigment contents (Chl, Car, AnC, Flv and PhC) (Figs. 2 and 3) or strong overlap of some spectral bands (Fig. 7). The applied multivariate approach enables the separation/quantification that univariate analyses are unable to promote, possibly by inter-correlation variable structure.

Species identification and pigment content estimation was more accurate when using absorbance data (Fig. 10) compared to reflectance data (Fig. S4). High resolution sensors are able to generate enough accurate data that allows for distinction between substances that absorb in the same spectral region through a PLSR analysis. It is noteworthy that absorbed light data are, in a way, "unbiased" from the effects promoted by the epidermis and anatomical and ultrastructural aspects, as well as leaf thickness. Thus, this technique applying multiple coupled sensors allows for the development of more accurate models. For example, the obtained predictability for PhC was above 99 % ($R^2C = 0.996$ and $RMSEP = 0.001$) (Fig. 10j), and the ability to distinguish chlorophyll effects within the interferences promoted by AnC and Flv

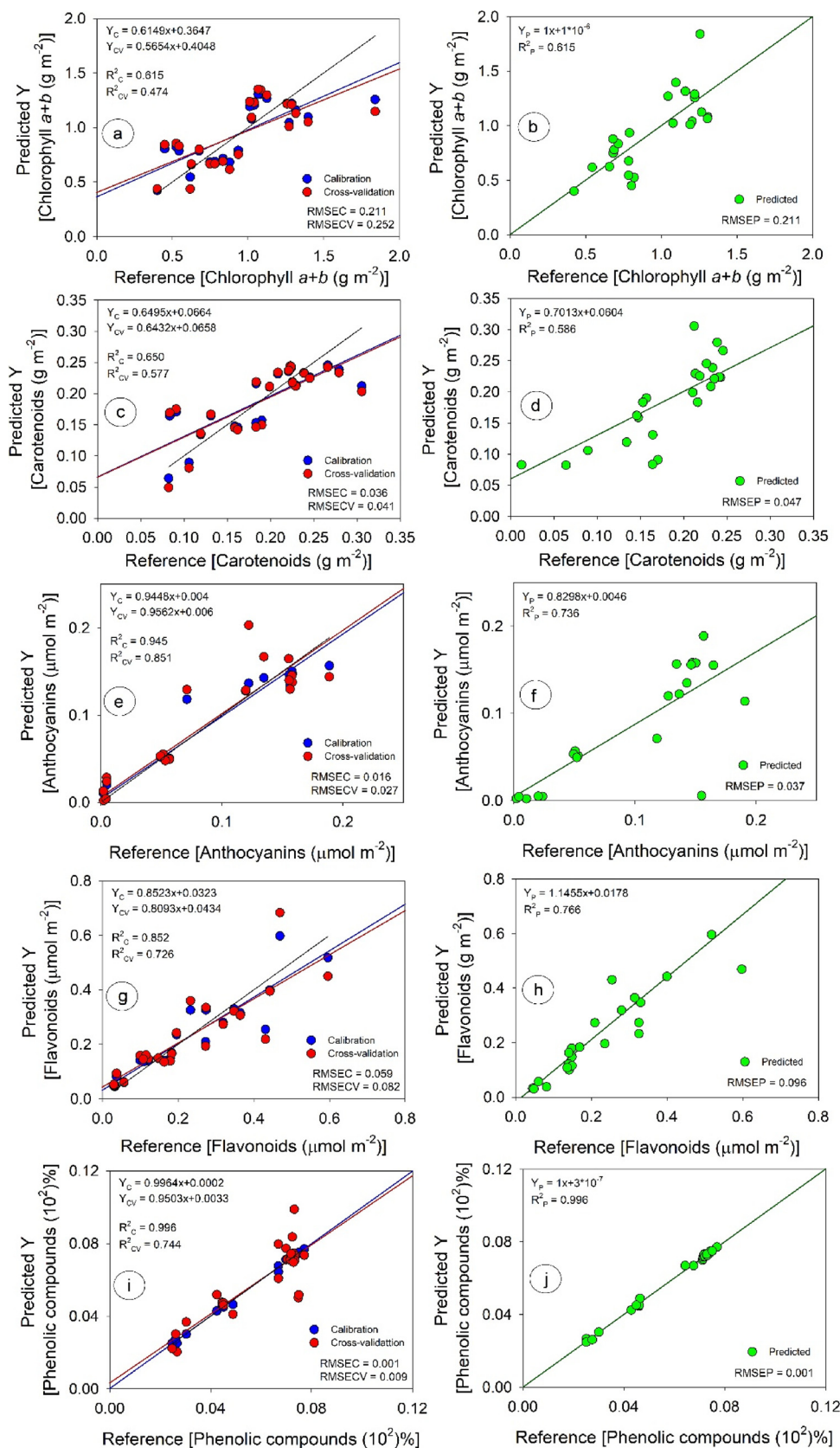


Fig. 10. Scatter-plot of the models based on absorbance curves (350–700 nm) obtained from spectroradiometer data. Relationship between leaf pigments measurements (blue dots) in the laboratory and predicted contents estimated by hyperspectral curves associated with the PLSR technique using cross-validation (red dots). A prediction (green dots) using an independent sample coupling to calibrated models. (a–b) chlorophyll a + b (Chl a + b), (c–d) carotenoids (Car), (e–f) anthocyanins (AnC), (g–h) flavonoids (Flv) and (i–j) phenolic compounds (PhC). Statistical analysis for leaf pigments in (a, c, e, g and i) calibration (blue points) and cross-validation (red points). (b, d, f, h and j) prediction (green points). Determination coefficient calibration (R^2C), root mean square error calibration (RMSEC), linear equation calibration (YC), determination coefficient cross-validation (R^2CV), root mean square error for cross-validation (RMSECV), linear equation cross-calibration (YCV), determination coefficient prediction (R^2P), root mean square error for prediction (RMSEP), linear equation prediction (YP). Residual prediction deviation (RPD) was calculated by $[RPD = \frac{1}{\sqrt{1-R^2x}}]$, where x represents the determination coefficient (R^2x). Regression calibration line (blue line), regression cross-validation line (red line), regression prediction (green line) and line 1:1 (black solid line). 30 samples were used for calibration (blue dots) and cross-validation (red dots) set of an independent 25 samples (green dots) were used for the test set. (For interpretation of the references to colour in the Figure, the reader is referred to the web version of this article).

was also observed, in addition to allowing for near-zero estimation of extra-chloroplastidic pigments in non-accumulating species. In the presence of high flavonoid and anthocyanin contents, chlorophyll content estimates were less accurate than in other studies or even using

the vegetation indices calibrated for green leaves and not for purple leaves. We highlight that flavonoids and anthocyanins accumulate on the leaf epidermis and lead to pink or purple leaf color (Fig. 1). Chlorophylls are present in parenchyma cells located in internal parts

(middle) of the leaves, as indicated in Fig. 5. The compounds are not evenly distributed on the leaf lamina in either case.

4.4. Multivariate statistics

The results indicate that the use of spectral responses allows for the distinction between plant species (Fig. 9, Tables 1 and 2), by PCA and discriminant analyses. Multivariate techniques have been previously applied to characterize and separate different species (Asner et al., 2008; Calviño-Cancela and Martín-Herrero, 2016; Moura et al., 2016). Using PCA analyses for the discrimination of green and red lettuces, Moura et al. (2016) attributed 75 % of explanation to the first two components (Moura et al., 2016). At the same time, lettuce plants with polyphenol content variations were differentiated with explanations of 93.4 % using the first two factors (Llorach et al., 2008). Combining PCA and LDA (linear discriminant analysis) techniques for reflectance data aiming to classify vegetation cover in native Antarctic species, Calviño-Cancela and Martín-Herrero (2016) explained 99.4 % of the data variation and obtained discriminant indices scores of 92 %, by analyzing of spectral bands from UV–A to the visible spectrum (Calviño-Cancela and Martín-Herrero, 2016). In an unprecedented way, Gitelson et al. (2017) and Gitelson and Solovchenko (2018), demonstrated that techniques to estimate anthocyanin (AnC) and flavonoid (Flv) concentrations obtained with transmittance data (T) in an integrating sphere spectrophotometer (350–800 nm) obtained excellent RMSE results, with data transformation into absorbance performed by applying (AnC) $[A = -\ln(T)]$. T and R measurements using integrating spheres are not simultaneously, and if a sample positioning is not perfect, only a few millimeters from a reflecting surface, a fraction of the transmitted light fails to strike the integrating surface, causing a considerable chance of error (Merzlyak et al., 2002). This problem can be easily solved by coupling two sensors. Our data show that better results are achieved with absorbance data (Fig. 9, Tables 1 and 2). In addition, the estimated models were able to predict pigment concentrations (Chl, Car, AnC, Flv and PhC) by using absorption curves. PLSR analyses using absorbance data displayed similar or higher correlations (Fig. 9 and S4) compared to those described in other studies (Ferri et al., 2004; Guo et al., 2018; Llorach et al., 2008).

4.5. Absorbance spectra advantages

Acquisition of spectra by high resolution sensors and analyzed by curve deconvolution associated to PLSR (Nanni et al., 2018) and other multivariate analyzes (Jolliffe, 2002), derive more robust and reliable models, as evidenced by the RMSE values and related to the use of contiguous bands, to the detriment of the use of IR that take advantage of specific wavelengths. The flexibility of choosing between different spectral bands by a discriminant analysis associated to the high precision and accuracy of high-resolution spectral data allows for species discrimination and pigment concentration estimations (Fig. S4). Although reflectance spectra remain highly popular due to their quick and remote way of obtaining agricultural monitoring (Llorach et al., 2008; Nanni et al., 2018), and environmental (Calviño-Cancela and Martín-Herrero, 2016) data, the real understanding of optical leaf profile absorption properties *in vivo* should be observed by absorbance spectra deconvolution or directly measured at the cell level with the use of microscopes coupled to spectroradiometers (Hatier et al., 2013; Hatier and Gould, 2007). On the other hand, new techniques such as the simultaneous measurements of the adaxial and abaxial faces with spectroradiometers, according to the pioneering works of Falcioni et al. (2017) and Moriwaki et al. (2019) and also employed herein (Fig. 2), reaffirm the idea of more robust data in the understanding of the optical leaf profile. The results presented herein open up the possibility for the use of absorbance spectral curves, with reaches up to 100 %, obtained by deconvolution by multivariate statistical routines (Table 2).

The current vegetation indices (da Silva Junior et al., 2017)

obtained by means of images captured by multispectral sensors (Zhu et al., 2017), despite providing quick monitoring and displaying over acquisition costs (Pan et al., 2015), may result in biased and low reliability models (Lebourgeois et al., 2008). One of the main reasons is the limited resolution and quality of the sensors, associated to technical restrictions in distinguishing subtle differences of analyzed objects. On the other hand, hyperspectral sensors (currently 0.7–3 nm) ensure high capacity and resolution information and data. Thus, the use of simultaneous hyperspectral sensors not only to monitor (Nanni et al., 2018), differentiate (Gitelson, 2011) (Fig. 9) or predict foliar pigment concentration but also to ensure a better understanding of the interactions promoted by light throughout the leaf profile may be applied (Figs. 7 and 8).

The reports by Blackburn (2007) and Gitelson and Solovchenko (2018) placed the development of more accurate techniques and methods to estimate pigment contents and to improve the understanding of light interaction in the leaf profile under "future" perspectives. Thus, the present study advances and demonstrates a fast, accurate and improved way to do this with the use of high resolution absorbance curves as a methodological alternative to increase the robustness, comprehensiveness and scope optical leaf property studies (Blackburn, 2007; Gitelson and Solovchenko, 2018; Huang et al., 2015; Ling et al., 2019).

5. Conclusions

The results reported herein provide support for absorbance spectra analysis by robust statistical tools, in order to perform accurate and accurate inferences on optical leaf properties, understand light interaction in relation to different levels of foliar pigments and distinguish the influence of cell organization and arrangement and their effective contribution to the leaf profile in different species. In addition, the inclusion of anatomical data is useful in understanding the unique characteristics of spectral curves in plants displaying similar foliar pigment levels. The multivariate statistical analysis allowed not only for the prediction and estimation of different foliar pigment levels, but also the discrimination of different species displaying spectra overlaps. Thus, the simultaneous measurements by the coupling of two sensors allowed for quick, accurate and non-destructive measures of the interactions between more significant spectral bands concerning optical leaf properties.

Author contributions

RF, WCA, designed the experiment, performed analyses, and wrote the manuscript. TM, MP, RHF and MRN performed analyses and reviewed the manuscript.

CRediT authorship contribution statement

Renan Falcioni: Conceptualization, Methodology, Investigation, Formal analysis, Funding acquisition, Writing - review & editing. **Thaise Moriwaki:** Conceptualization, Methodology, Investigation, Formal analysis, Writing - review & editing. **Mariana Pattaro:** Formal analysis, Writing - review & editing. **Renato Herrig Furlanetto:** Formal analysis, Methodology, Software, Writing - review & editing. **Marcos Rafael Nanni:** Formal analysis, Methodology, Software, Writing - review & editing, Funding acquisition. **Werner Camargos Antunes:** Conceptualization, Methodology, Investigation, Formal analysis, Writing - review & editing, Funding acquisition.

Declaration of Competing Interest

The authors declare that they have no conflict of interest.

Acknowledgments

This study was partially funded by the National Council of Technological and Scientific Development – CNPq, Coordenação de Aperfeiçoamento de Pessoal de Nível Superior (CAPES), Financiadora de Estudos e Projetos (FINEP) and Fundação Araucária – Paraná, Brazil. Scholarships granted by the Brazilian Government (Renan Falcioni and Mariana Pattaro – CNPq) and (Thaise Moriwaki and Renato Herrig Furlanetto – CAPES) are gratefully acknowledged. The author would like to thank COMCAP–UEM for the spectroradiometer, microscopy use, and professional support to the analysis and Prof. Luiz A. Souza (State University of Maringá) for his review on anatomical descriptions. Scholarships granted by the Brazilian Government to Renan Falcioni (CNPq-GD 142218/2017-0) are gratefully acknowledged. The authors would also like to thank the anonymous reviewers for their valuable considerations concerning this manuscript.

Appendix A. Supplementary data

Supplementary material related to this article can be found, in the online version, at doi:<https://doi.org/10.1016/j.jplph.2020.153161>.

References

- Asner, G.P., Jones, M.O., Martin, R.E., Knapp, D.E., Hughes, R.F., 2008. Remote sensing of native and invasive species in Hawaiian forests. *Remote Sens. Environ.* 112, 1912–1926.
- Baldini, E., Facini, O., Nerozzi, F., Arboree, C., 1997. Leaf characteristics and optical properties of different woody species. *Trees* 12, 73–81.
- Blackburn, G.A., 2007. Hyperspectral remote sensing of plant pigments. *J. Exp. Bot.* 58, 855–867.
- Bone, R.A., Lee, D.W., Norman, J.M., 1985. Epidermal cells functioning as lenses in leaves of tropical rain-forest shade plants. *Appl. Opt.* 24, 1408–1412.
- Brooks, S., Bareth, G., 2018. Estimating barley biomass with crop surface models from oblique RGB imagery. *Remote Sens.* 10, 01–16.
- Brodersen, C.R., Vogelmann, T.C., 2007. Do epidermal lens cells facilitate the absorbance of diffuse light? *Am. J. Bot.* 94, 1061–1066.
- Brodersen, C.R., Vogelmann, T.C., 2010. Do changes in light direction affect absorption profiles in leaves? *Funct. Plant Biol.* 37, 403–412.
- Brodersen, C.R., Vogelmann, T.C., Williams, W.E., Gorton, H.L., 2008. A new paradigm in leaf-level photosynthesis: direct and diffuse lights are not equal. *Plant Cell Environ.* 31, 159–164.
- Buchhorn, M., Reynolds, M.K., Walker, D.A., 2016. Influence of BRDF on NDVI and biomass estimations of Alaska Arctic tundra. *Environ. Res. Lett.* 11, 1–13.
- Butler, W.L., Norris, K.H., 1960. The spectrophotometry of dense light-scattering material. *Arch. Biochem. Biophys.* 87, 31–40.
- Calviño-Cancela, M., Martín-Herrero, J., 2016. Spectral discrimination of vegetation classes in ice-free areas of Antarctica. *Remote Sens.* 8, 1–15.
- Carter, G.A., Knapp, A.K., 2001. Leaf optical properties in higher plants: linking spectral characteristics to stress and chlorophyll concentration. *Am. J. Bot.* 88, 677–684.
- Croce, R., Amerongen, H., Van, 2014. Natural strategies for photosynthetic light harvesting. *Nat. Chem. Biol.* 10, 492–501.
- da Silva Junior, C.A., Nanni, M.R., Teodoro, P.E., Silva, G.F.C., 2017. Vegetation indices for discrimination of soybean areas: a new approach. *Agron. J.* 109, 1331–1343.
- Evans, J.R., 1986. A quantitative analysis of light distribution between the two photosystems, considering variation in both the relative amounts of the chlorophyll-protein complexes and the spectral quality of light. *Photobiochem. Photobiophys.* 10, 135–147.
- Evans, J.R., Vogelmann, T.C., 2003. Profiles of ¹⁴C fixation through spinach leaves in relation to light absorption and photosynthetic capacity. *Plant Cell Environ.* 26, 547–560.
- Falcioni, R., Moriwaki, T., Bonato, C.M., de Souza, L.A., Nanni, M.R., Antunes, W.C., 2017. Distinct growth light and gibberellin regimes alter leaf anatomy and reveal their influence on leaf optical properties. *Environ. Exp. Bot.* 140, 86–95.
- Falcioni, R., Moriwaki, T., Benedito, E., Bonato, C.M., de Souza, L.A., Antunes, W.C., 2018. Increased gibberellin levels enhance the performance of light capture efficiency in tobacco plants and promote dry matter accumulation. *Theor. Exp. Plant Physiol.* 30, 235–250.
- Féret, J.B., François, C., Asner, G.P., Gitelson, A.A., Martin, R.E., Bidet, L.P.R., Ustin, S.L., le Maire, G., Jacquemoud, S., 2008. PROSPECT-4 and 5: advances in the leaf optical properties model separating photosynthetic pigments. *Remote Sens. Environ.* 112, 3030–3043.
- Féret, J.B., Gitelson, A.A., Noble, S.D., Jacquemoud, S., 2017. PROSPECT-D: towards modeling leaf optical properties through a complete lifecycle. *Remote Sens. Environ.* 193, 204–215.
- Ferri, C.P., Formaggio, A.R., Schiavinato, M.A., 2004. Narrow band spectral indexes for chlorophyll determination in soybean canopies [Glycine max (L.) Merrill]. *Brazilian J. Plant Physiol.* 16, 131–136.
- Folta, K.M., Maruhnich, S.A., 2007. Green light: a signal to slow down or stop. *J. Exp. Bot.* 58, 3099–3111.
- Fourty, T., Baret, F., Jacquemoud, S., Schmuck, G., Verdebout, J., 1996. Leaf optical properties with explicit description of its biochemical composition: direct and inverse problems. *Remote Sens. Environ.* 56, 104–117.
- Gates, D.M., Keegan, H.J., Schleter, J.C., Weidner, V.R., 1965. Spectral properties of plants. *Appl. Opt.* 4, 11–20.
- Gierlinger, N., Keplinger, T., Harrington, M., 2012. Imaging of plant cell walls by confocal Raman microscopy. *Nat. Protoc.* 7, 1694–1708.
- Gitelson, A., 2011. Nondestructive estimation of foliar pigments (chlorophylls, carotenoids, and anthocyanins) contents: evaluating a semi-analytical three-band model. In: Thenkabail, P.S., Lyon, J.G., Huete, A. (Eds.), *Hyperspectral Remote Sensing of Vegetation*. CRC Press, New York, pp. 782.
- Gitelson, A.A., Merzlyak, M.N., 2004. Non-destructive assessment of chlorophyll, carotenoid and anthocyanin content in higher plant leaves: principles and algorithms. *J. Plant Physiol.* 160, 271–282.
- Gitelson, A.A., Merzlyak, M.N., 1997. Remote estimation of chlorophyll content in higher plant leaves. *Int. J. Remote Sens.* 18, 2691–2697.
- Gitelson, A., Solovchenko, A., 2018. Non-invasive quantification of foliar pigments: possibilities and limitations of reflectance- and absorbance-based approaches. *J. Photochem. Photobiol. B, Biol.* 178, 537–544.
- Gitelson, A.A., Merzlyak, M.N., Chivkunova, O.B., 2001. Optical properties and non-destructive estimation of anthocyanin content in plant leaves. *Photochem. Photobiol.* 74, 38.
- Gitelson, A.A., Chivkunova, O.B., Merzlyak, M.N., 2009. Nondestructive estimation of anthocyanins and chlorophylls in anthocyanic leaves. *Am. J. Bot.* 96, 1861–1868.
- Gitelson, A., Chivkunova, O., Zhigalova, T., Solovchenko, A., 2017. In situ optical properties of foliar flavonoids: implication for non-destructive estimation of flavonoid content. *J. Plant Physiol.* 218, 258–264.
- Gould, K.S., Jay-Allemand, C., Logan, B.A., Baissac, Y., Bidet, L.P.R., 2018. When are foliar anthocyanins useful to plants? Re-evaluation of the photoprotection hypothesis using *Arabidopsis thaliana* mutants that differ in anthocyanin accumulation. *Environ. Exp. Bot.* 154, 11–22.
- Guo, T., Tan, C., Li, Q., Cui, G., Li, H., 2018. Estimating leaf chlorophyll content in tobacco based on various canopy hyperspectral parameters. *J. Ambient Intell. Humaniz. Comput.* 1–09.
- Hatier, J.H.B., Gould, K.S., 2007. Black coloration in leaves of *Ophiopogon planiscapus* “Nigrescens”. Leaf optics, chromaticity, and internal light gradients. *Funct. Plant Biol.* 34, 130–138.
- Hatier, J.H.B., Clearwater, M.J., Gould, K.S., 2013. The functional significance of black-pigmented leaves: Photosynthesis, photoprotection and productivity in *Ophiopogon planiscapus* “Nigrescens”. *PLoS One* 8, 1–13.
- Huang, J., Wei, Chen, Zhang, Y., Blackburn, G.A., Wang, X., Wei, Chuanwen, Wang, J., 2015. Meta-analysis of the detection of plant pigment concentrations using hyperspectral remotely sensed data. *PLoS One* 10, 1–26.
- Ichiro, T., Hiroki, O., Takashi, F., Riichi, O., 2016. Light environment within a leaf. II. Progress in the past one-third century. *J. Plant Res.* 129, 353–363.
- Jacquemoud, S., Baret, F., 1990. PROSPECT: a model of leaf optical properties spectra. *Remote Sens. Environ.* 34, 75–91.
- Ji, M., Deng, J., Yao, B., Chen, R., Fan, Z., Guan, J., Li, X., Wu, F., Niklas, K.J., 2017. Ecogeographical variation of 12 morphological traits within *Pinus tabulaeformis*: the effects of environmental factors and demographic histories. *J. Plant Ecol.* 10, 386–396.
- Jolliffe, I.T., 2002. *Principal Component Analysis*, 2nd ed. Springer, USA, New York.
- Karnovsky, M.J., 1965. A formaldehyde-glutaraldehyde fixative of high osmolarity for use in electron microscopy. *J. Cell Biol.* 27, 137A.
- Kume, A., 2018. Importance of the green color, absorption gradient, and spectral absorption of chloroplasts for the radiative energy balance of leaves. *J. Plant Res.* 131, 501–514.
- Landi, M., Tattini, M., Gould, K.S., 2015. Multiple functional roles of anthocyanins in plant-environment interactions. *Environ. Exp. Bot.* 119, 4–17.
- Latimer, P., 1958. Apparent shifts of absorption bands of cell suspensions and selective light scattering. *Science* 127 (80-), 29–30.
- Lebourgeois, V., Bégué, A., Labbé, S., Mallavan, B., 2008. Can commercial digital cameras be used as multispectral. *Sensors* 8, 7300–7322.
- Ling, B., Goodin, D.G., Raynor, E.J., Joern, A., 2019. Hyperspectral analysis of leaf pigments and nutritional elements in tallgrass prairie vegetation. *Front. Plant Sci.* 10, 1–13.
- Lorach, R., Martínez-Sánchez, A., Tomás-Barberán, F.A., Gil, M.I., Ferreres, F., 2008. Characterisation of polyphenols and antioxidant properties of five lettuce varieties and escarole. *Food Chem.* 108, 1028–1038.
- Maas, S.J., Dunlap, J.R., 1989. Reflectance, transmittance, and absorbance of light by normal, etiolated, and albino corn leaves. *Agron. J.* 81, 105.
- Merzlyak, M.N., Chivkunova, O.B., Melø, T.B., Naqvi, K.R., 2002. Does a leaf absorb radiation in the near infrared (780–900 nm) region? A new approach to quantifying optical reflection, absorption and transmission of leaves. *Photosynth. Res.* 72, 263–270.
- Merzlyak, M.N., Chivkunova, O.B., Solovchenko, A.E., Naqvi, K.R., 2008. Light absorption by anthocyanins in juvenile, stressed, and senescing leaves. *J. Exp. Bot.* 59, 3903–3911.
- Minasny, B., McBratney, A.B., 2013. Digital mapping of soil carbon. *Adv. Agron.* 3, 4.
- Moriwaki, T., Falcioni, R., Tanaka, F.A.O., Cardoso, K.A.K., Souza, L.A., Benedito, E., Nanni, M.R., Bonato, C.M., Antunes, W.C., 2019. Nitrogen-improved photosynthesis quantum yield is driven by increased thylakoid density, enhancing green light absorption. *Plant Sci.* 278, 1–11.
- Moura, L.O., Lopes, Dde C., Steidle-Neto, A.J., Ferraz, Lde C.L., Lanamar, Cde A., Martins,

- L.M., 2016. Evaluation of techniques for automatic classification of lettuce based on spectral reflectance. *Food Anal. Methods* 9, 1799–1806.
- Nanni, M.R., Cezar, E., Silva Junior, C.Ada, Silva, G.F.C., da Silva Gualberto, A.A., 2018. Partial least squares regression (PLSR) associated with spectral response to predict soil attributes in transitional lithologies. *Arch. Agron. Soil Sci.* 64, 682–695.
- Niinemets, Ü., 2007. Photosynthesis and resource distribution through plant canopies. *Plant Cell Environ.* 30, 1052–1071.
- Nishio, J.N., 2000. Why are higher plants green? Evolution of the higher plant photosynthetic pigment complement. *Plant Cell Environ.* 23, 539–548.
- Nishio, J., Sun, J., Vogelmann, T., 1993. Carbon fixation gradients across spinach leaves do not follow internal light gradients. *Plant Cell* 5, 953–961.
- Pan, W.J., Wang, X., Deng, Y.R., Li, J.H., Chen, W., Chiang, J.Y., Yang, J.B., Zheng, L., 2015. Nondestructive and intuitive determination of circadian chlorophyll rhythms in soybean leaves using multispectral imaging. *Sci. Rep.* 5, 1–13.
- Ragaee, S., 2006. Antioxidant activity and nutrient composition of selected cereals for food use. *Food Chem.* 98, 32–38.
- Sims, D.A., Gamon, J.A., 2002. Relationships between leaf pigment content and spectral reflectance across a wide range of species, leaf structures and developmental stages. *Remote Sens. Environ.* 81, 337–354.
- Solovchenko, A., 2010. *Photoprotection in Plants: Optical Screening-based Mechanisms*, 1st ed. Springer, Berlin Heidelberg, Berlin.
- Souza, L.A., Rosa, S.M., Moscheta, I.S., Mourão, K.S.M., Rodella, R.A., Rocha, D.C., Lolis, M.I.G.A., 2016. *Morfologia E Anatomia Vegetal: Técnicas E Práticas*, 3rd ed. Editora UEPG, Ponta Grossa.
- Sun, J., Nishio, J.N., Vogelmann, T.C., 1998. Green light drives CO₂ fixation deep within leaves. *Plant Cell Physiol.* 39, 1020–1026.
- Terashima, I., Fujita, T., Inoue, T., Chow, W.S., Oguchi, R., 2009. Green light drives leaf photosynthesis more efficiently than red light in strong white light: revisiting the enigmatic question of why leaves are green. *Plant Cell Physiol.* 50, 684–697.
- Tilly, N., Hoffmeister, D., Cao, Q., Huang, S., Lenz-Wiedemann, V., Miao, Y., Bareth, G., 2014. Multitemporal crop surface models: accurate plant height measurement and biomass estimation with terrestrial laser scanning in paddy rice. *J. Appl. Remote Sens.* 8, 083671.
- Ustin, S.L., Jacquemoud, S., Govaerts, Y., 2001. Simulation of photon transport in a three-dimensional leaf: implications for photosynthesis. *Plant Cell Environ.* 24, 1095–1103.
- Vogelmann, T.C., 1993. Plant tissue optics. *Annu. Rev. Plant Physiol. Plant Mol. Biol.* 44, 231–251.
- Vogelmann, T.C., Han, T., 2000. Measurement of gradients of absorbed light in spinach leaves from chlorophyll fluorescence profiles. *Plant Cell Environ.* 23, 1303–1311.
- Vogelmann, T.C., Bornman, J.F., Yates, D.J., 1996. Focusing of light by leaf epidermal cells. *Physiol. Plant.* 98, 43–56.
- Wada, M., Shimazaki, K., Iino, M., 2005. *Light Sensing in Plants*, 1st ed. Springer, Japan, Japan.
- Wang, Y., Folta, K.M., 2013. Contributions of green light to plant growth and development. *Am. J. Bot.* 100, 70–78.
- Wellburn, A.R., 1994. The spectral determination of chlorophylls a and b, as well as total Carotenoids, using various solvents with spectrophotometers of different resolution. *J. Plant Physiol.* 144, 307–313.
- Xiao, Y., Tholen, D., Zhu, X.G., 2016. The influence of leaf anatomy on the internal light environment and photosynthetic electron transport rate: exploration with a new leaf ray tracing model. *J. Exp. Bot.* 67, 6021–6035.
- Zar, J.H., 2010. *Biostatistical Analysis*, 5th ed. Pearson Education, Upper Saddle River - New Jersey.
- Zhu, H., Chu, B., Zhang, C., Liu, F., Jiang, L., He, Y., 2017. Hyperspectral imaging for presymptomatic detection of tobacco disease with successive projections algorithm and machine-learning classifiers. *Sci. Rep.* 7, 1–12.

Supplemental material

Title: High resolution leaf spectral signature as a tool for foliar pigment estimation displaying potential for species differentiation

Renan Falcioni ^{1,2,4}, Thaise Moriwaki ^{1,4}, Mariana Pattaro ^{1,4}, Renato Herrig Furlanetto ^{3,4}, Marcos Rafael Nanni ^{3,4}, Werner Camargos Antunes ^{1,4*}

¹Plant Ecophysiology Laboratory. Department of Biology.

²Biochemistry of Plants Laboratory. Department of Biochemistry.

³Group Applied to Soil Survey and Spatialization. Department of Agronomy.

⁴State University of Maringá. Av. Colombo, 5790, Jd. Universitário, Maringá-Paraná-Brazil, Zip code: 87020-900.

*Correspondence: Werner Camargos Antunes; wcantunes@uem.br; Phone: +55 44 30115290 (W.C.A)

Table S1 Stepwise discriminant output for selected leaf reflectance, transmittance and absorbance wavelengths in six plant species

Type analysis	Step	Wavelength selected (nm)	Partial R ²	F Value	Average squared canonical correlation
Reflectance	1	546	0.984	216.830	0.197
	2	603	0.984	209.590	0.391
	3	528	0.976	127.890	0.585
	4	525	0.944	50.540	0.773
	5	484	0.815	12.360	0.890
	6	515	0.810	11.080	0.898
	7	529	0.555	3.240	0.916
	8	521	0.524	2.860	0.915
	9	513	0.676	5.410	0.924
	10	528	0.583	3.350	0.953
Transmittance	1	543	0.966	108.410	0.193
	2	528	0.988	290.080	0.384
	3	601	0.928	44.050	0.554
	4	521	0.870	21.440	0.708
	5	513	0.882	22.330	0.797
	6	507	0.812	12.130	0.813
	7	533	0.631	4.440	0.888
	8	520	0.510	2.500	0.903
Absorbance	1	542	0.975	149.760	0.195
	2	530	0.986	262.060	0.391
	3	604	0.970	111.590	0.582
	4	529	0.950	60.250	0.771
	5	541	0.659	5.810	0.797
	6	562	0.600	4.200	0.849
	7	419	0.617	4.180	0.853
	8	487	0.737	6.710	0.857
	9	508	0.864	14.000	0.888
	10	401	0.702	4.720	0.890
	11	545	0.698	4.610	0.883
	12	443	0.651	3.360	0.890
	13	649	0.837	8.210	0.958
	14	656	0.927	20.210	0.970
	15	655	0.871	9.460	0.992
	16	606	0.881	8.890	0.993
	17	602	0.913	10.480	0.994
	18	564	0.980	38.920	0.994

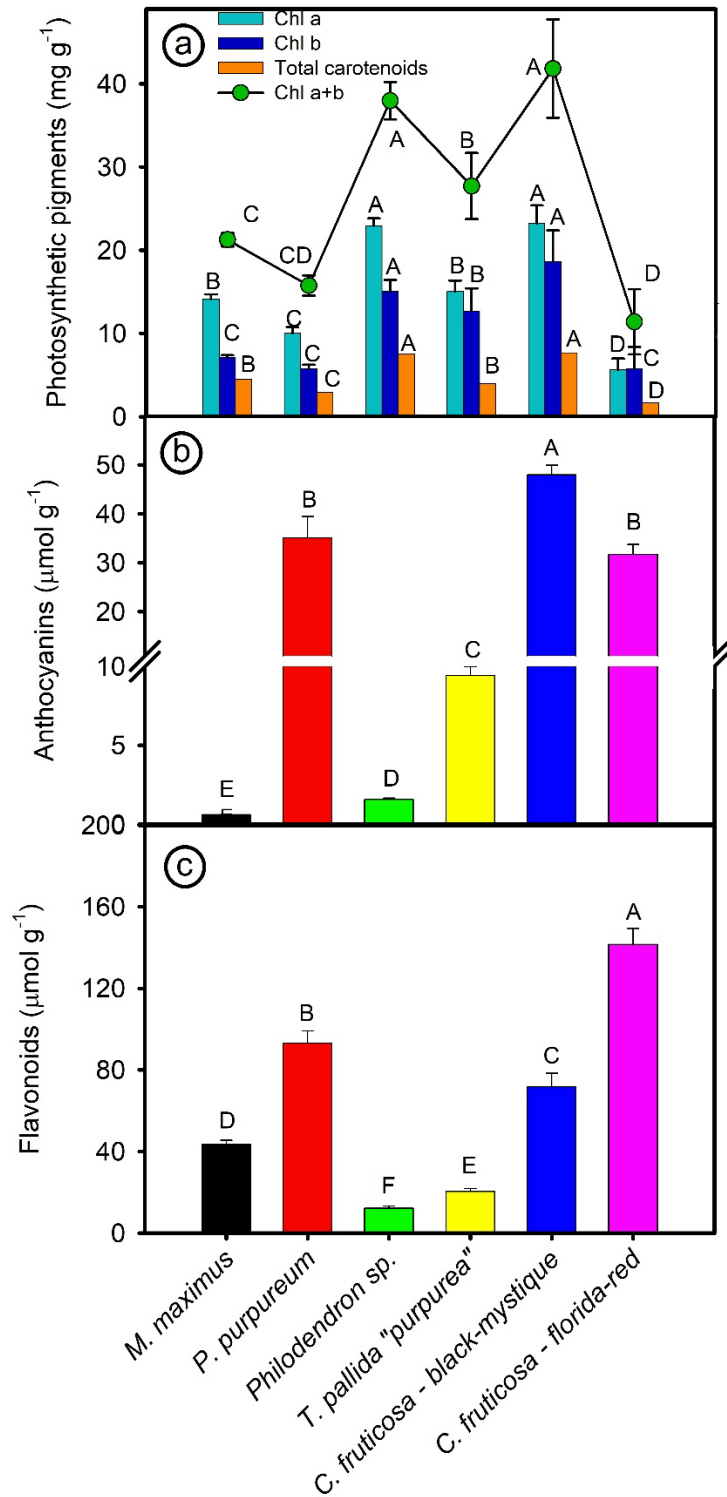


Fig. S1 Chloroplastidic (photosynthetic) and extra-chloroplastidic (mainly vacuolar) pigment contents expressed per dry leaf weight. **(a)** chlorophyll *a* (Chl*a*), chlorophyll *b* (Chl*b*), chlorophylls *a+b* (Chl total), total carotenoids (Car), **(b)** anthocyanin (AnC) and **(c)** flavonoids (Flv) from six species with naturally varying pigment contents. Different letters over dots or bars point to statistical differences among species (Duncan's test; $P < 0.05$). ($n=5 \pm SE$)

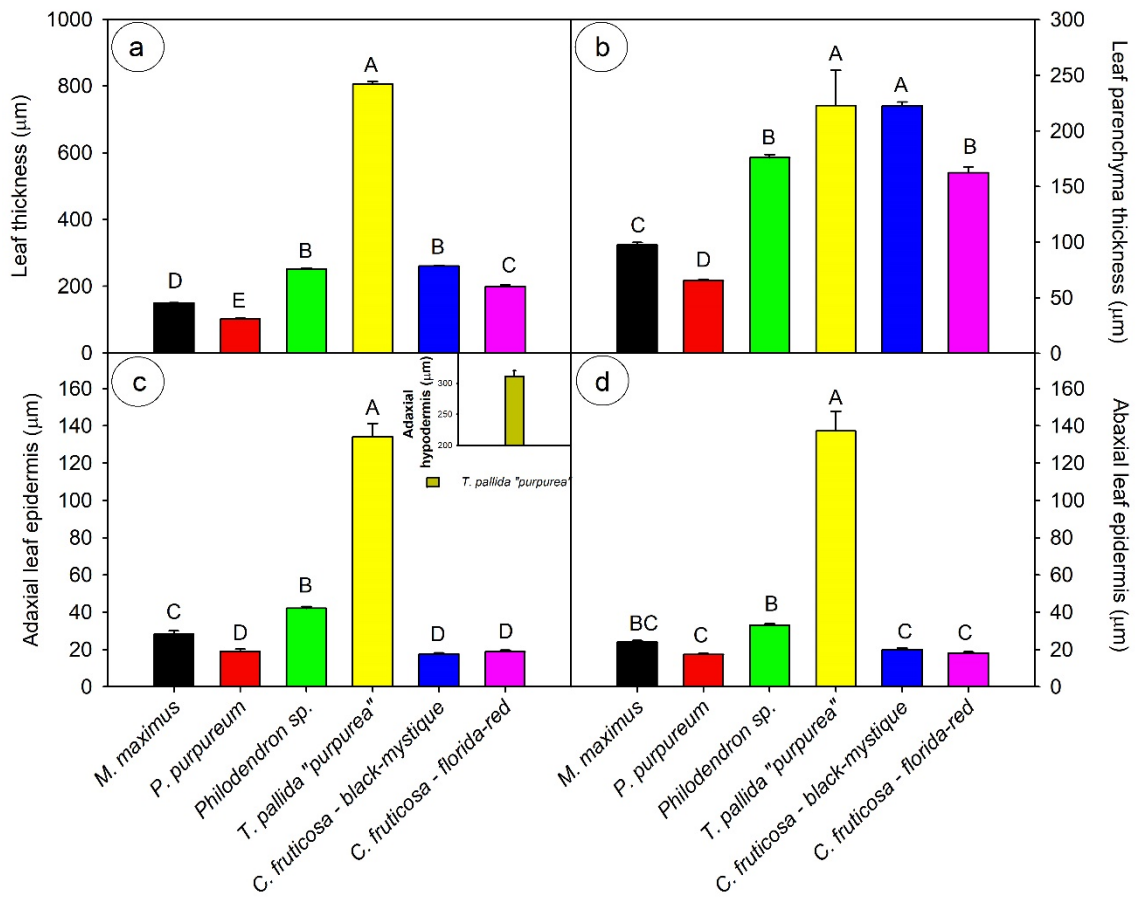


Fig. S2 (a) Leaf thickness, (b) leaf parenchyma thickness, (c) adaxial leaf epidermis, (d) abaxial leaf epidermis from different species. Inset, adaxial thickness of hypodermis in *T. pallida*. Different letters over bars points to statistical differences among species (Duncan's test; P < 0.05). (n=5±SE)

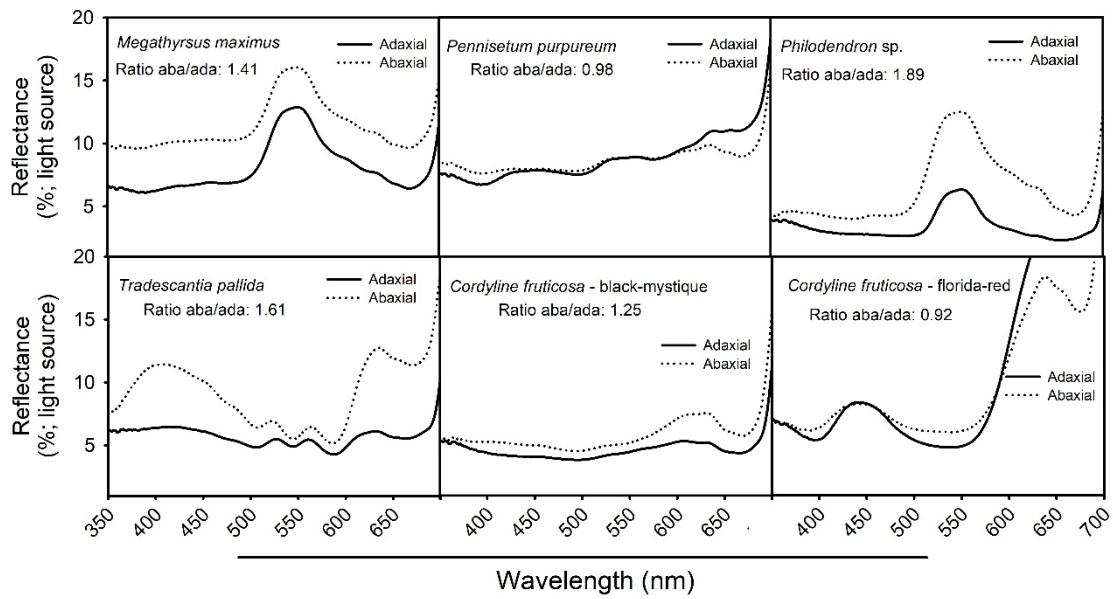


Fig. S3 Leaf spectral reflectance (*in vivo*) from 350 to 700 nm from adaxial light source and abaxial light source from fully expanded leaves belonging to different species. The average ratio of abaxial to adaxial reflectances is also described. Each repetition was produced by taking the mean measurements calculated from two different leaves from same plant. (n=5). The standard error was omitted for clarity

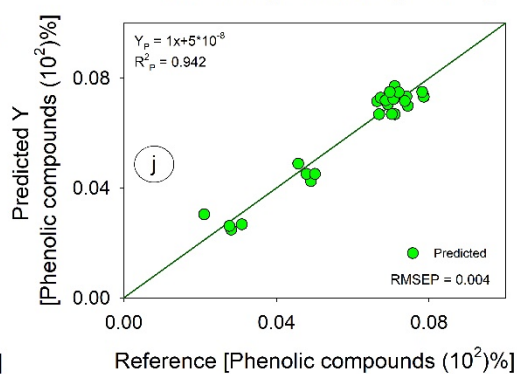
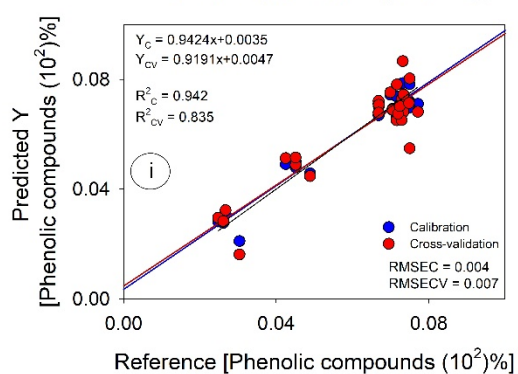
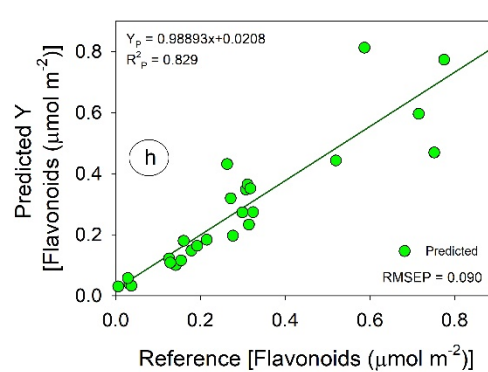
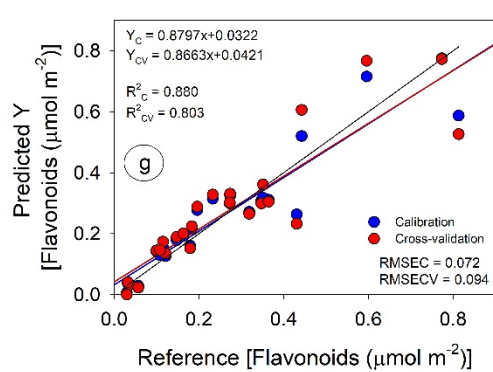
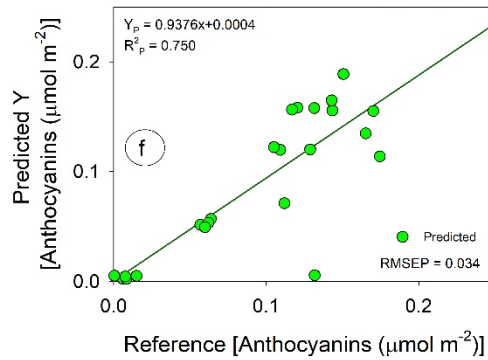
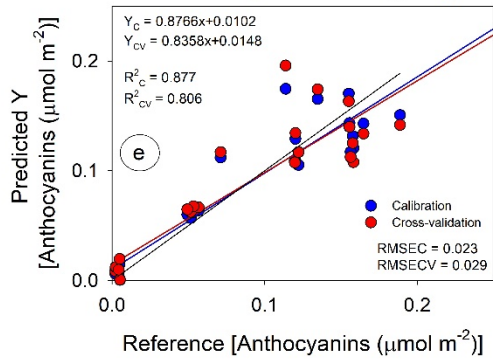
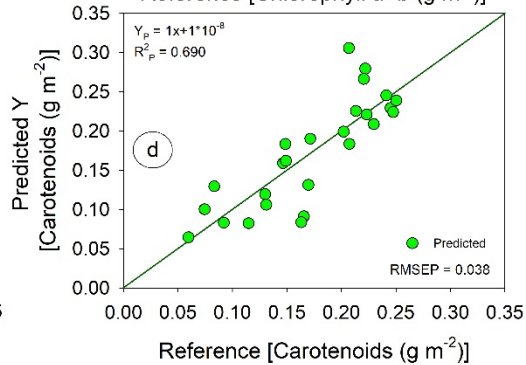
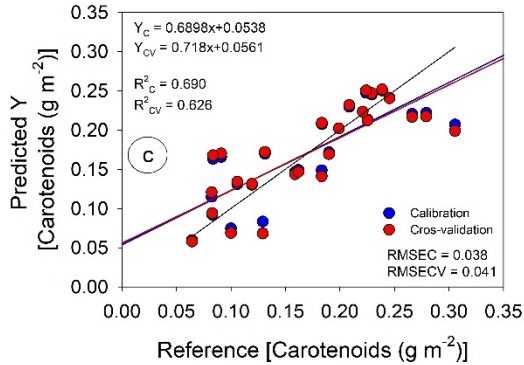
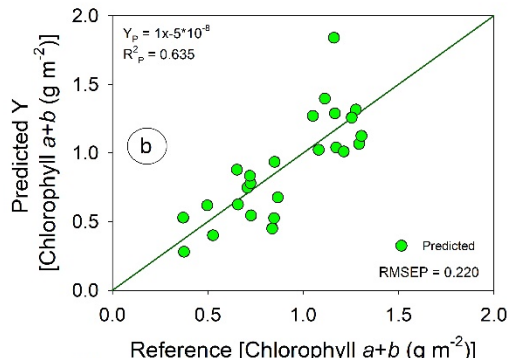
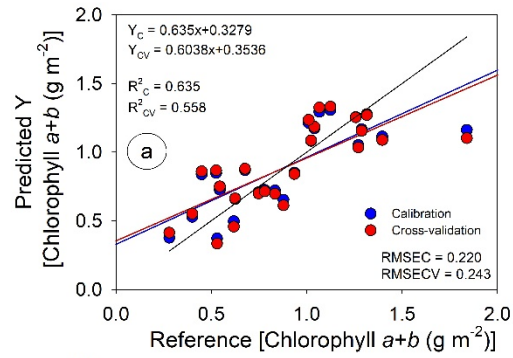


Fig. S4 Scatter-plot of models based on reflectance curves (350–700 nm) obtained from spectroradiometer data. Relationship between leaf pigments measurements (blue dots) in laboratory and predicted contents estimated by hyperspectral curves associated with the PLSR technique using cross-validation (red dots). A prediction (green dots) using independent sample coupling to calibrated models. **(a-b)** chlorophyll *a+b* (Chl *a+b*), **(c-d)** carotenoids (Car), **(e-f)** anthocyanins (AnC), **(g-h)** flavonoids (Flv) and **(i-j)** phenolic compounds (PhC). Statistical analysis for leaf pigments in **(a, c, e, g and i)** calibration (blue points) and cross-validation (red points). **(b, d, f, h and j)** prediction (green points). Determination coefficient calibration (R^2_C), root mean square error calibration (RMSEC), linear equation calibration (Y_C), determination coefficient cross-validation (R^2_{CV}), root mean square error for cross-validation (RMSECV), linear equation cross-calibration (Y_{CV}), determination coefficient prediction (R^2_P), root mean square error for prediction (RMSEP), linear equation prediction (Y_P). Residual prediction deviation (RPD) has been calculated by $[RPD = \frac{1}{\sqrt{1-R^2_x}}]$, where x represents the determination coefficient (R^2_x). Regression calibration line (blue line), regression cross-validation line (red line), regression prediction (green line) and line 1:1 (black solid line). 30 samples were used for calibration (blue dots) and cross-validation (red dots) set of an independent 25 samples (green dots) were used for the test set